ROYAL BELGIAN INSTITUTE OF NATURAL SCIENCES
OPERATIONAL DIRECTORATE NATURAL ENVIRONMENT
Suspended Matter and Seabed Modelling and Monitoring team

WESTDIEP AQUACULTURE MONITORING:

Understanding and monitoring the effects of an offshore mussel, oyster and seaweed aquaculture farm on the seabed and suspended sediments composition and dynamics off the coast of Nieuwpoort, Belgium

ACTIVITY REPORT 2022

PREPARED BY **LOUISE DELHAYE** – JANUARY 2024

CONTENTS

LIST OF FIGURES

LIST OF TABLES

1. INTRODUCTION

In a context of increasing demand for food and decreasing resources availability, aquaculture emerges as a promising green industry, contributing to the blue revolution (Cabre et al., 2021; O'Donncha et al 2017). In view of the large issue of overexploitation of marine and water resources, while 89% of wild fish stocks are being overfished, farming of finfish, shellfish and seaweed has been viewed as a shortfall-filling alternative and has largely increased in the past years (Cabre et al., 2021; Duarte et al., 2009; FAO, 2016). With an annual growth rate of 5.8% since 2001, aquaculture is one of the fastest growing industries (FAO, 2018).

Mussel aquaculture, in particular, is considered to be one of the least impactful food production method as it usually grows native shellfish species which take their nutrients directly from the environment, decreasing the turbidity of the water in the process (Avdelas et al., 2021). This property makes them interesting solutions for eutrophication management (Cabre et al., 2021), one of the most concerning threat to coastal environment. However, as highlighted by Bergström (2014), these mitigation impacts might be unpredictable and not as straightforward as expected.

Although this topic is still debated, mussel aquacultures are also potential tools for carbon absorption (Avdelas et al., 2021). The carbon footprint of longline mussel aquacultures was calculated to be much lower than other agricultural practices (SARF, 2012; FAO, 2014). In Italy, the first certificates of carbon credits for carbon uptake are already being delivered, opening a new market where the higher impacts businesses can buy "green" certificates (Avdelas et al., 2021).

Mussels constitute a healthy source of food for consumption, further raising the attention that is being drawn to it. Not only is it a low fat, low calories food but it is also an excellent source of sodium, selenium, vitamin B12, zinc and foliate (FAO, 2014). In addition to that, mussel aquaculture also presents the advantage of not requiring any medication or anti-fouling, and it has not been associated with amplification of pathogens that may infect wild stocks (Avdelas et al., 2021).

In 2016, the shellfish industry produced over 17 T of molluscs, mussels contributing to 8% of it (FAO, 2018), the vast majority of them (94%) come from aquaculture. While China constitutes the largest producer of mussel from aquaculture (FAO, 2018), the production of mussels in Europe has reached a peak in the 1950s (with a yearly production of 600 000 T) and then decreased to 480 000 T in 2016 (Avdelas et al., 2021).

This decrease can be explained by the challenges and pressures that the mussel industry is facing, e.g. unreliable seed availability (high interannual variability), poor water quality and pollution, biotoxins and toxic algal blooms. In Europe, one of the challenges is the pressure and competition with the external market, forcing the producers to sell at reduced prizes (Avdelas et al., 2021). As most sheltered spaces are being used, there is now the constraint to find available space for the installation of mussel farms. This is pushing the aquacultures to go more offshore and to develop new technologies in order to remain competitive (FAO, 2014), this is particularly true for mussel aquacultures which are more extensive than other seafarms and need a fast access to a port as well as a high local productivity combined with a limited predation on the mussels (Avdelas et al., 2021). Offshore aquacultures will have the challenge to adapt to the consequences of climate change, e.g. more intense and more extreme weather events, higher seed mortality, possibly more algal blooms as well as ocean acidification (Avdelas et al., 2021).

To encourage the creation of shellfish aquacultures in spite of the challenges that the sector is facing, many incentives are being created such as the Baltic EcoMussel (FAO, 2014). But while the enthusiasm for the sustainability of mussel farms seems to be growing, the potential impacts of such aquacultures, especially the more extensive offshore ones, should not be overlooked. These impacts include effects on currents, sedimentation, light, removal of plankton and nutrients, organic enrichment of seabed via pseudo-faeces reducing biodiversity and abundance. These potential impacts can be balanced with local environmental benefits (Avdelas et al., 2021) such as creating structures that are shelters, and the reduction of eutrophication through filter-feeding.

Long-established consumer, Belgium is the only main consuming country in Europe that is not also a main producer (FAO, 2014). In 2022, a new innovative longline offshore mussel aquaculture was installed by the Colruyt Group off the coast of Nieuwpoort. It is expected to produce 600 tons of mussels by 2025, and in a second and third phases, it is also expected to produce oysters and seaweed, mainly aimed at the Belgian internal market. In order to ensure that this aquaculture farm doesn't have negative impacts on the environment, its development is accompanied by a comprehensive monitoring program focusing on several aspects (i.e. fauna and flora, marine mammals, birds, benthos, microplastics, hydrodynamics and sedimentology). The latter aspect is the focus of this report.

1.1. THE WESTDIEP AQUACULTURE PROJECT

Codevco, as part of the Colruyt Group, is developing a nearshore longline shellfish aquaculture off the coast of Nieuwpoort with the objective to sell products of the North Sea on a commercial scale. This project is taking place in Zone C (Westdiep), a zone dedicated to commercial and industrial activities following the Belgian marine spatial plan for 2020-2026.

The project is expected to last 30 years and will be developed in three phases:

- Phase I (2022-2025): Installation of 25% of the aquaculture, with an estimated annual production of 600 tons of mussels and the installation of two plots of oysters at the end of this phase.
- Phase II (2025-2028): Installation of 50% of the aquaculture, with an estimated annual production of 1200 tons of mussels, 24 tons of oysters and 55 tons of seaweed.
- Phase III (2028-2052): Full exploitation of the aquaculture, with an estimated annual production of 2400 tons of mussels, 82 tons of oysters and 110 tons of seaweed.

For this aquaculture, the long-line technique is used. The installation is divided into two parts: the primary structure (screw anchors, main lines and large corner buoys) is designed to remain in the water for a long time, while the secondary structure (small buoys, weights, droppers) will be reinstalled after each harvest. As shown in Figure 1.1, the main line (100-120 m) is connected on each side to a screw anchor using anchor lines and is kept at a constant distance from the surface using buoys. A total of 1400 screw anchors will be anchored in the seabed, protruding about 50 cm. These screw anchors have a maximum length of 5.5 m and a maximum diameter of 0.8 m. The structure is always installed parallel to the current. The secondary structure (whether for mussels, oysters or seaweed cultivation) is then attached to this primary backbone. A plot consists of five main lines placed 20 m apart. Once fully developed, the aquaculture will cover an area of 4.54 km² and will consist of 120 mussel plots, 10 oyster plots and 10 seaweed plots (Figure 1.2).

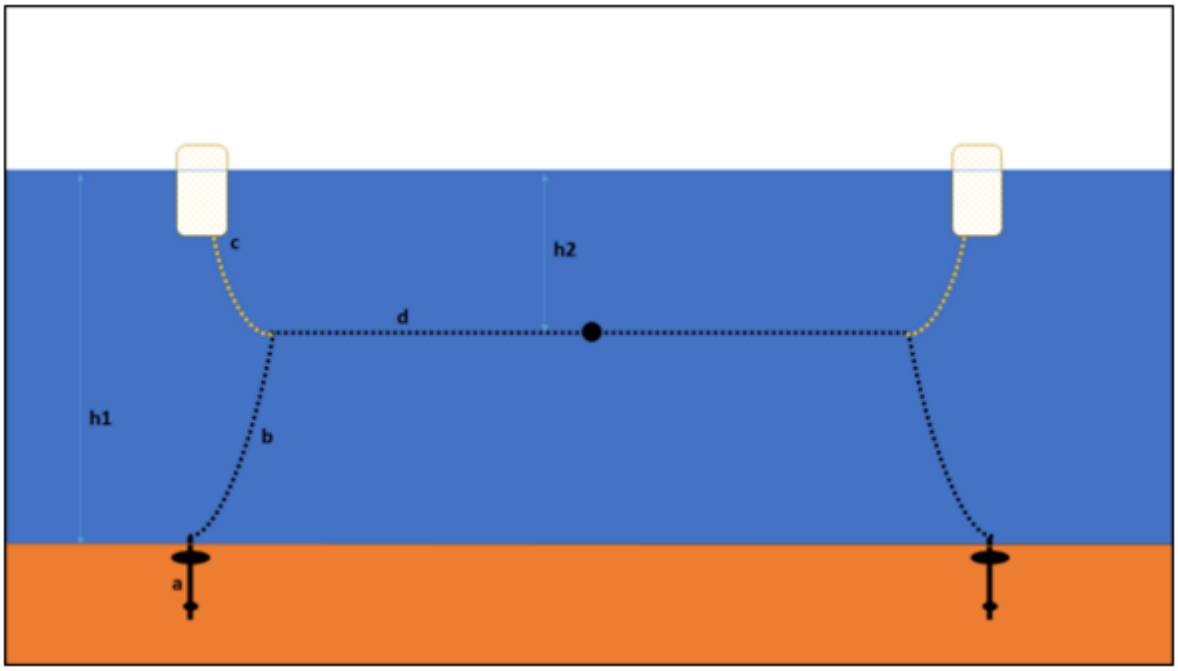

Figure 1.1. Schematic representation of main line with anchorage for mussels farming. Legend: a: screw anchor, b: anchor rope, c: corner buoy, d: main line. Source: IMDC, 2020.

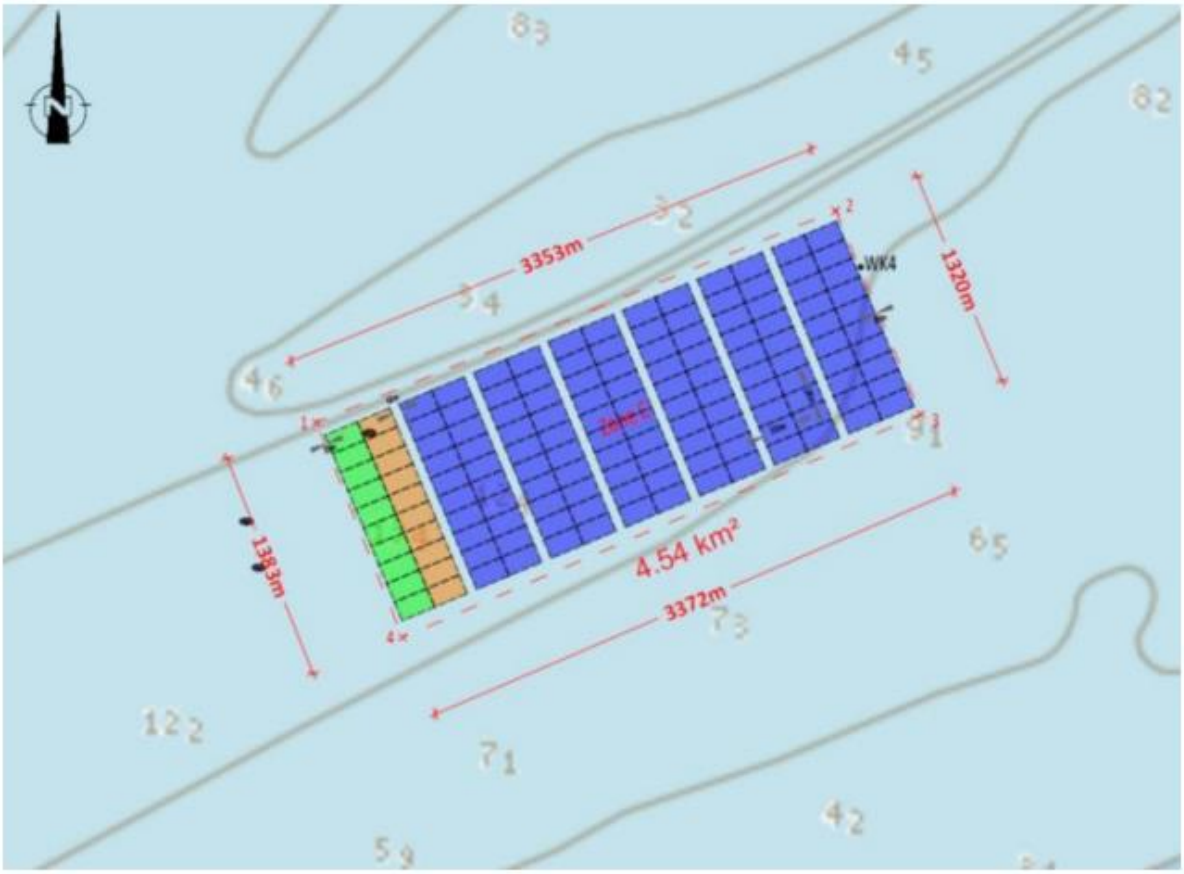

Figure 1.2. Representation of the fully developed aquaculture. Source: IMDC, 2020.

Mussel cultivation depends on the natural settlement of spats. These are present in the water depending on its temperature and concentration in nutrients. There are therefore two main periods:

April-May and October-November. These spats will attach to the empty lines and the mussels can be harvested from June to December. Unlike mussel spats, oysters and seaweeds will be grown from purchased juveniles and seeds.

1.2. RESEARCH OBJECTIVES OF THE SEDIMENTOLOGY PART OF THE MONITORING

Following the Marine Strategy Framework Directive (MSFD), the research objectives of the sedimentology part of the Westdiep aquaculture monitoring project are divided into two main targets (impacts on the seabed integrity (1) and impacts on hydrographical conditions (2)), each of which is subdivided into smaller research tasks or hypothesis (Table 1.1). The first, corresponding to descriptor 6 of the MSFD, aims at ensuring that the seabed conserves the structure and functions of its ecosystem. This means that no major changes in the bathymetry, composition, roughness, substrate type or seabed connectivity should occur that would adversely impact benthic ecosystems. The second target corresponds to descriptor 7 and aims at ensuring that no alteration of the hydrographical conditions will impact marine ecosystems. This includes changes in salinity, temperature, hydrodynamics, turbidity and suspended particulate matter (SPM) content.

Table 1.1. Description of the research targets and tasks (hypothesis) of the Codevco sedimentological monitoring.

TARGET 1: MONITORING IMPACTS ON THE SEABED INTEGRITY	
TASK.1.A	**ASSESSING MORPHOLOGICAL CHANGES** Despite the large number of screw anchors, it was assumed in the environmental impact assessment that the physical disturbance of the seabed would be minimal and limited to 0.02% of the farm's surface area (IMDC, 2020). Coastal sandbanks are dynamic features, but the aquaculture farm is located in a relatively stable area. However, this does not rule out possible erosion (e.g., scouring) or sedimentation (e.g., smothering) processes around the concession.
TASK.1.B	**ASSESSING CHANGES IN SEABED COMPOSITION** The deposition of shells as well as faeces and pseudo-faeces is likely to alter the composition of the seabed. Indeed, under certain conditions, faeces and pseudofaeces will be dispersed throughout the BPNS and have a limited impact, but it is also possible that, during neap tides for instance, they may settle more rapidly and deposit in certain places on the bottom, therefore changing the seabed composition. As a consequence, the content in organic matter is expected to increase. In addition to that, the deposition of shells will likely increase the calcium carbonate content in the surface sediments.
TASK.1.C	**ASSESSING CHANGES IN SEABED ROUGHNESS & TYPE** As mentioned above, the presence of the aquaculture will likely results in an increased deposition of shells, which can have an impact on the structure of the seabed, as well as faeces and pseudo-faeces, which, by trapping clay and silt particles, will in turn increase the fine fraction in the sediments below or in the vicinity of the aquaculture farm.
TARGET 2: MONITORING IMPACTS ON THE HYDROGRAPHICAL CONDITIONS	
TASK.2.A	**ASSESSING CHANGES IN HYDRODYNAMICS AND SEDIMENT TRANSPORT** As a result of changing currents and waves, it is possible that near-bed sediment transport would change. This is impossible to estimate without a good assessment of hydrodynamical changes. The main uncertainty is whether the drop lines will generate a turbulence strong enough to interact with the seabed, and cause mixing throughout the water column. If this is the case, then a limited increase in turbidity may occur.
TASK.2.B	**ASSESSING CHANGES IN THE TURBIDITY AND SPM CONCENTRATION IN THE WATER COLUMN** Due to the filtrating action of mussels, a reduction in the turbidity of the water column can be expected. It is estimated that 240 million liters of water per hour will be filtered when the mussels and oysters reach maturity. However, this diminution might be counterbalanced by the production of faeces and pseudo-faeces generated by the aquaculture farm. Considering a concentration of matter in suspension of 21 mg/l (concentration near Nieuwpoort), 5000 kg of SPM would be filtered out of the water column per hour (IMDC, 2020) while the faeces and pseudofaeces production would be of about 2500 kg. Due to likely limited bottom disturbances and slightly changing sediment transport, it can be assumed that turbidity will not change significantly. The modelling study of BMM (2005) indicated a possible increase of 2.4 mg/l due to faeces and pseudo-faeces, but this study took place within the area of maximum turbidity, closer to the coast compared to this study site.
TASK.2.C	**ASSESSING CHANGES IN PARTICLE SIZE AND COMPOSITION IN THE WATER COLUMN** It is expected that the mussels will filter small mineral particles from the water (< 10 µm) that are captured in the production of larger faeces and pseudofaeces (500-3000 µm). This might result in a change in the size of the particles in suspension, but also the type with more flocs and less isolated fine sediment particles. The aquaculture farm might also affect the number and species of plankton ad larvae present in the area.

1.3. OBJECTIVES OF THIS REPORT

The aim of this report is to relate the activities carried out in 2022 by the Suspended Matter and Seabed Monitoring and Modelling (SUMO) team as well as to present the preliminary results of the sedimentological monitoring of the Westdiep aquaculture farm. In addition to this, this report intends to describe the Westdiep environment as observed in 2022 in as much detail as possible, in order to better understand it and to facilitate the monitoring in the coming years.

2. MATERIALS & METHODS

2.1. STUDY AREA

The area (Zone C) in which the aquaculture is being installed is located about 4 km off the coast of Nieuwpoort, south of the Nieuwpoort sandbank (Figure 2.1), part of the Coastal Banks system. Considered to be in a "dynamic equilibrium", they are stable geomorphological features which have experienced only slight changes within their area over the past two centuries (Van Cauwenberghe, 1971; Mathys, 2010). Despite strong tidal currents and storm events, the silt and sand only migrates little from one sandbank to another (Van Cauwenberghe, 1971) but their crest would be slowly growing while the channels between the banks are deepening. Erosion of the Nieuwpoort bank would be mainly occurring on its seaward side while a slight sedimentation would occur on its landward side (Janssens et al., 2011). Other sandbanks in the area would, however, be subject to more changes as highlighted by Mathys et al. (2010) and Lapaty et al. (2019), including the Smal bank on the South-West (Figure 2.1). The seabed of the Westdiep area, south of the Nieuwpoort bank, is classified as sandy to silty sand (class A5.2 following the EUNIS classification) with a clay/silt percentage between 2.5 to 5% (up to 10% at some locations) and a median diameter of 100-200 µm (Van Lancker et al., 2007). Sediment transport in the project area is similar to that of the region and is towards the North-East, in line with the dominant tidal current (Lapaty et al., 2019; IMDC, 2020). Ieperian clay from the Kortrijk formation can be found under the surficial layer of quaternary sand (Le Bot et al., 2003). Depths in the project zone are ranging from -9 to -15 m LAT based on data collected in 2017 and 2018 by the Flemish Hydrography.

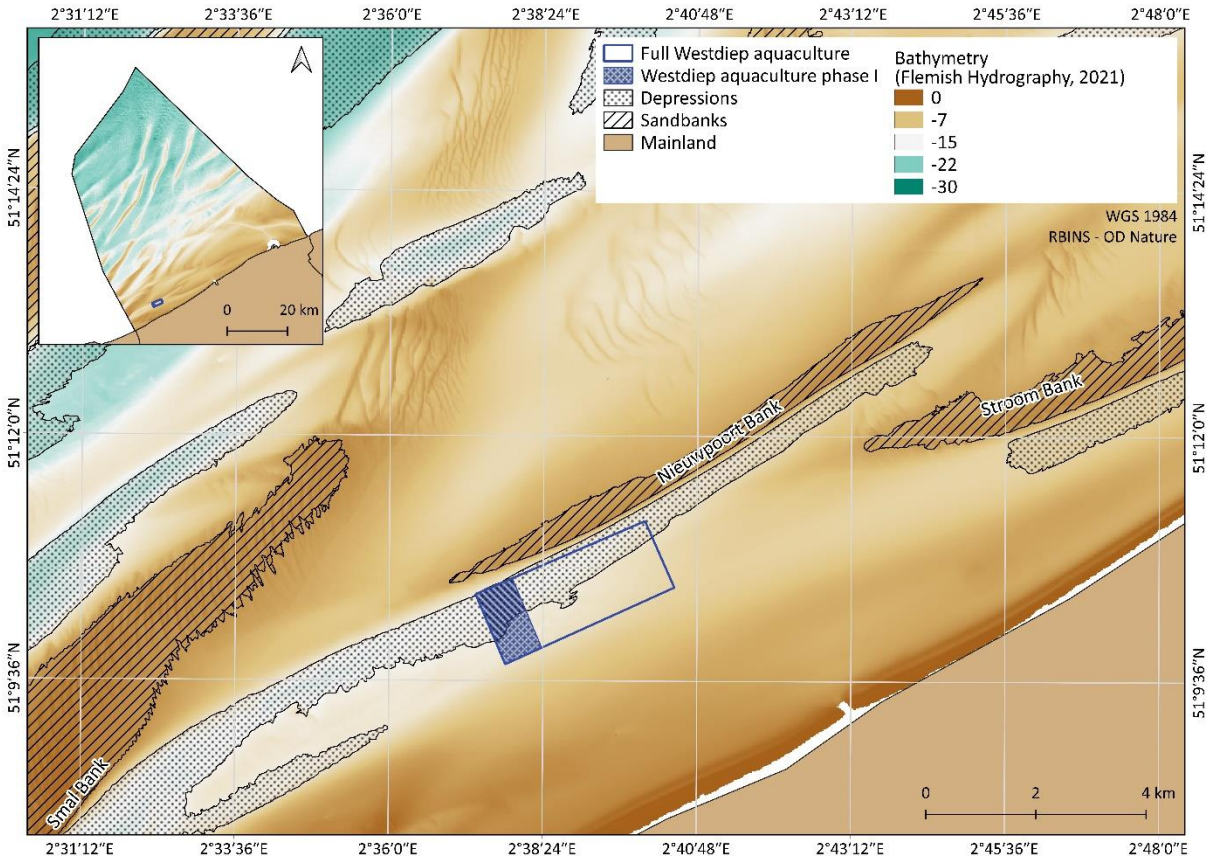

Figure 2.1. Location of the Westdiep aquaculture farm in the geomorphological context of the Belgian part of the North Sea.

With currents being dominated by tidal action, maximum current velocities are reached during high tide and range between 0.8 and 1 m/s in the project area (Lanckneus et al., 2001).

Although Belgian coastal waters are known to be highly eutrophic due to the large input of nutrients from rivers, the Westdiep area would be located just outside of the coastal turbidity maximum zone where concentrations of suspended matter are ranging between 20 mg/l at the surface and 4000 mg/l near the seabed (Lauwaert et al., 2016). The environmental impact assessment reports that the area would be comparable to the monitoring station W03 and would have an average dissolved inorganic nitrogen (DIN) concentration of 40.29 µmol/l for 2000-2005 and of 36.5 µmol/l for the period 2007-2018 (IMDC, 2020). At the surface, the SPM concentration in winter is about twice as high as in summer and is estimated at 31 mg/l based on measurement data from the Belgian Marine Data Centre (BMDC). Smaller flocs and lower settling velocities occur in winter compared to summer (Fettweis et al., 2015). Transport of sediment comes from SW (Lanckneus et al., 2001).

According to data measured at Nieuwpoort (Meetnet Vlaamse Banken[1]) in 2022, the wind speed was ranging from 0.2 m/s (12/01/2022) to 30.6 m/s (18/02/2022) with an average of 6.4 m/s. The predominant wind direction was North-East and South-South-West (Figure 2.2), which is in accordance with the southwest dominant winds reported in the environmental impact assessment (IMDC, 2020). Like for the rest of the Belgian part of the North Sea, winds coming from the North generate high waves. De Roo et al. (2016, as cited in IMDC, 2020) reported that the wave height in Zone C is in general less than 1 m with periods of 3 to 4 seconds but can go up to 5 m under specific conditions. In 2022, data from the Meetnet Vlaamse Banken showed a mean wave height of 59 cm (from 0.07 m on 18/04/2022 to 3.6 m on 01/04/2022) and an average period of 3.5 s (from 2 s on 31/10/2022 to 7 s on 31/03/2022) (Figure 2.3). These data are measured a few kilometers closer to the shore compared to the Westdiep zone so small differences are likely to occur.

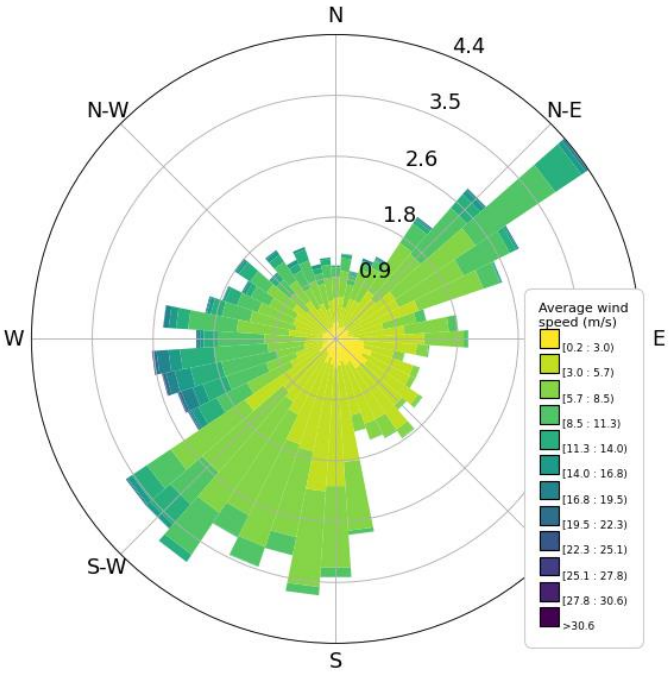

Figure 2.2. Wind speed and direction for 2022.

[1] https://meetnetvlaamsebanken.be/

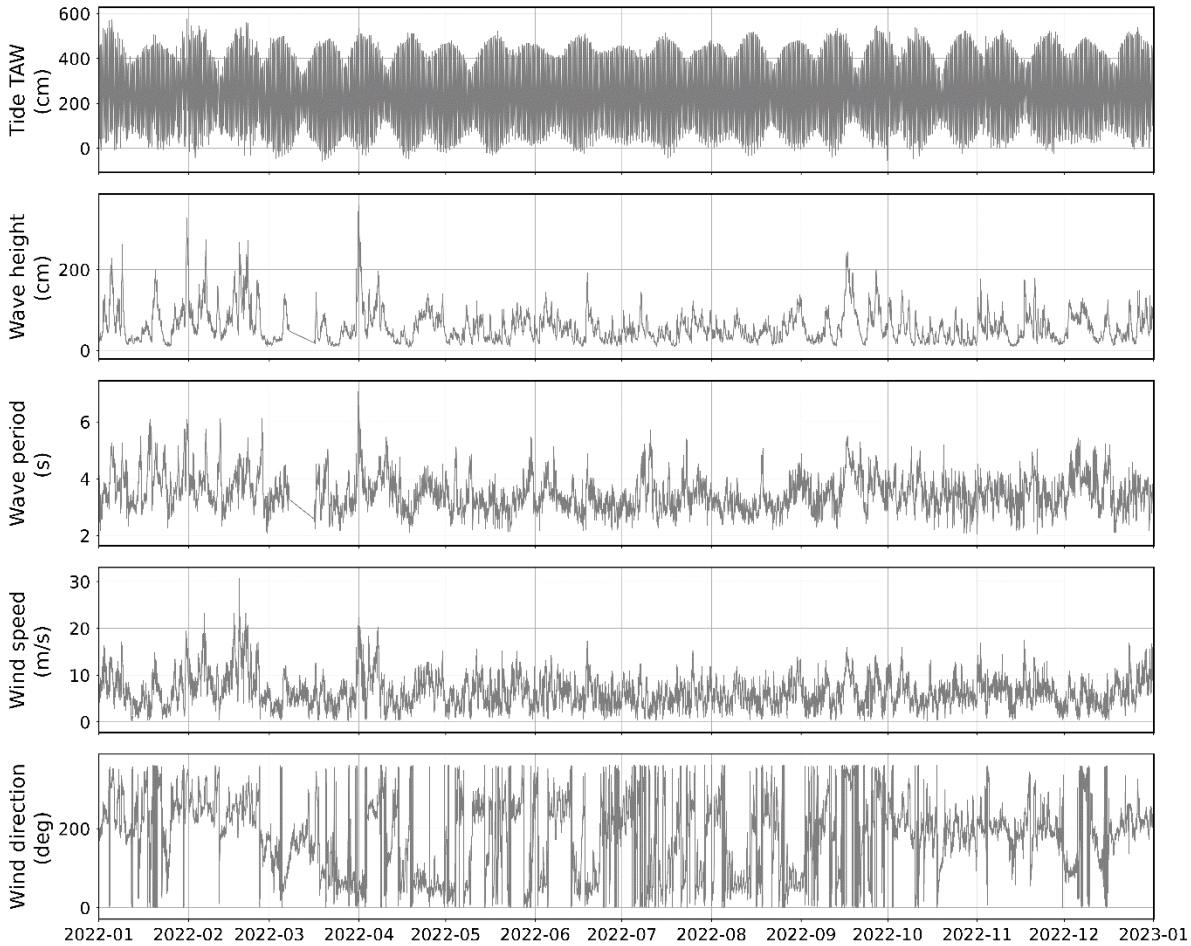

Figure 2.3. Tides, wave height and period, wind speed and direction at Nieuwpoort in 2022.

2.2. OVERVIEW OF THE ACTIVITIES

The measurement schedule of 2022 and an overview of the different instruments that were used for this monitoring are provided in Table 2.1 and Table 2.2 below. Sediment samples were taken at six locations with a box core and six multibeam transects were surveyed East of the aquaculture farm. In addition to that, two cycles of water measurements were performed in August and December, the first tripod was successfully deployed for 6 weeks and ten satellite images from Landsat 8 could be used.

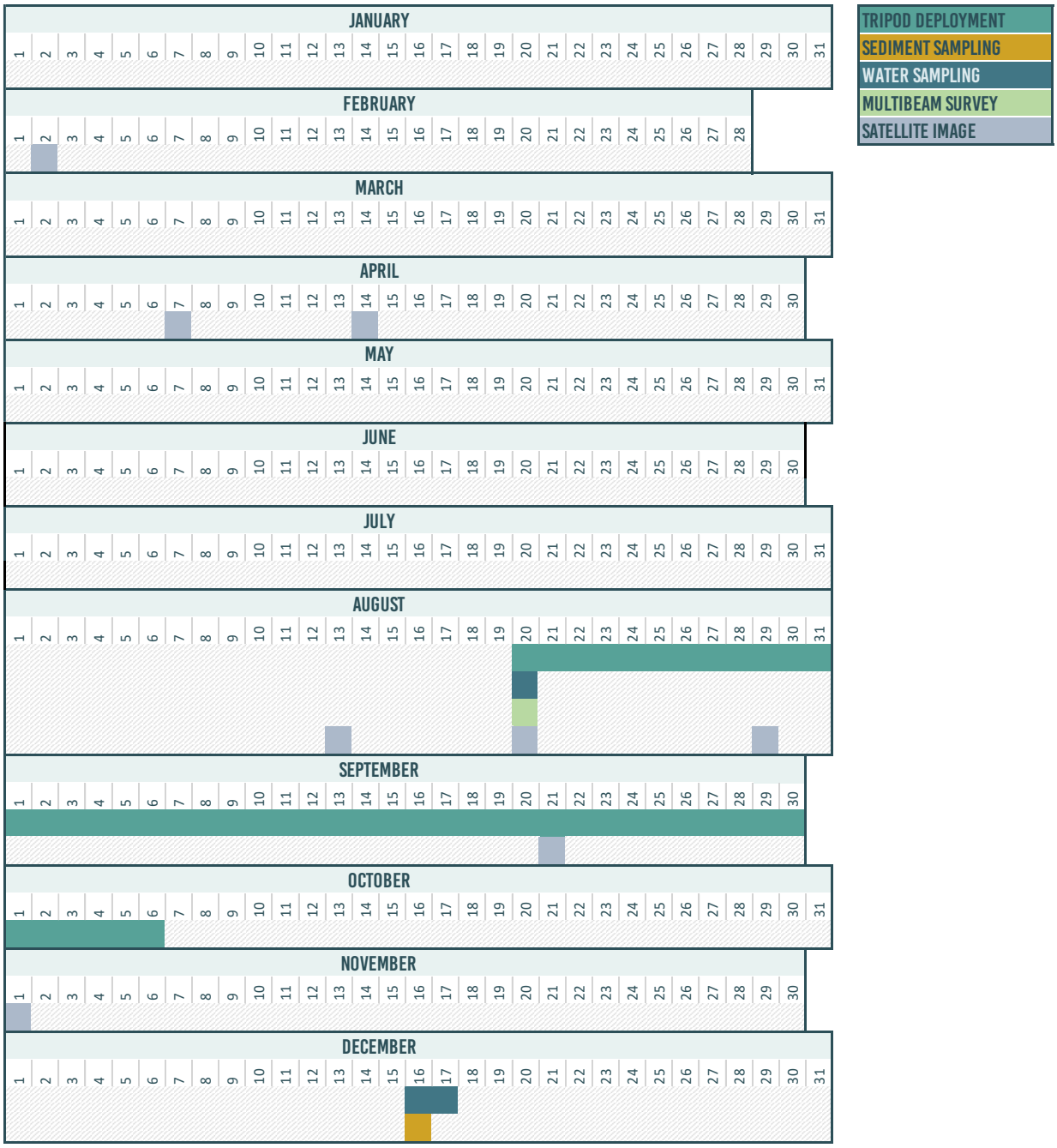

Table 2.1. Calendar of the different deployments and data recordings in 2022.

Table 2.2. Overview of the different instruments used for the CODEVCO monitoring and their derived parameters, grouped by deployment method.

	DEPLOYMENT	INSTRUMENT	DERIVED PARAMETERS	
SEABED	Transect/hull-mounted	**Multibeam echosounder**	Bathymetry (m LAT)	TASK 1.A
			Seabed backscattering strength (dB)	TASK 1.C
	Sampling	**Box corer**	Grain size distribution (%)	TASK 1.C
			Organic matter content (LOI550) (%)	TASK 1.B
			Calcium carbonate content (LOI1000) (%)	TASK 1.B
HYDROGRAPHICAL CONDITIONS	Tripod	**SBE 19plus V2 SeaCAT**	Conductivity (S/m)	
			Pressure (dbar)	
			Temperature (°C)	
			Salinity (PSU)	
		Sediment traps	Layering of SPM	TASK 2.A
			Particle size distribution (%)	TASK 2.C
		LISST-200X	Particle size distribution (%)	TASK 2.C
			Total volume concentration (µl/l)	TASK 2.B
			Mean particle diameter (µm)	TASK 2.C
			Temperature (°C)	
		OBS	Turbidity (NTU)	TASK 2.B
		Fluorometer	Chlorophyll a (mg/m³)	TASK 2.C
			Temperature (°C)	
		ADCP	Current velocity (m/s)	TASK 2.A
			Current direction (deg)	TASK 2.A
			Acoustic volume backscatter (Sv)	TASK 2.B
	Rosette	**SBE09**	Conductivity (S/m)	
			Pressure (dbar)	
			Temperature (°C)	
			Salinity (PSU)	
		OBS	Turbidity (NTU)	TASK 2.B
		LISST-100x	Particle size distribution (%)	TASK 2.C
			Total volume concentration (µl/l)	TASK 2.B
			Mean particle diameter (µm)	TASK 2.C
		LISST-Holo2	Particle size distribution (%)	TASK 2.C
			Total volume concentration (µl/l)	TASK 2.B
			Holograms of particles	TASK 2.C
			Mean particle diameter (µm)	TASK 2.C
		Water samples	SPM (mg/l)	TASK 2.B
			POC (mg/l)	TASK 2.C
			PON (mg/l)	TASK 2.C
			TEP (mg/m³)	TASK 2.C
			Chlorophyll a/b (mg/m³)	TASK 2.C
			Phaeopigment a/b (mg/m³)	TASK 2.C
	Hull-mounted	**ADCP**	Current velocity (m/s)	TASK 2.A
			Current direction (deg)	TASK 2.A
			Acoustic volume backscatter (Sv)	TASK 2.B
	Landsat-8 satellite images		SPM concentration (mg/l)	TASK 2.B
			Chla concentration (mg/m³)	TASK 2.B

2.3. METHODOLOGY FOR MONITORING IMPACTS ON THE SEABED INTEGRITY

2.3.1. Multibeam survey

2.3.1.1. Bathymetric and backscatter survey

In order to monitor that the Westdiep aquaculture activities do not have a significant impact on the seabed morphology (**task 1.A**), roughness and substrate type (**task 1.C**), a multibeam study will be carried out every year. In 2022, this survey took place during campaign ST2022/19 on board the RV Belgica on Saturday 20 August from 3.45 am to 7.30 am (local time) using the hull-mounted multibeam echosounder (Kongsberg EM2040-04 Dual RX, Single Swath Shallow Water Multibeam Echosounder) operating at 300 kHz. Following the IHO S44 standards, the EM2040-04D vertical confidence interval is estimated to be about +-26 cm at a depth of 10 m. Six lines, spaced every 20 m, were navigated at a speed of 8 knots. Deviation from these lines could not be avoided in Zone C due to the presence of buoys deployed to test the production of oysters and the transect lines could therefore not be fully followed. Compensation for pitch, roll, heave and yaw was performed automatically during the acquisition. Due to the shallow depth of the water in that area, the bottom coverage of the multibeam was only 30 to 40 m wide. Due to time and environmental constraints, only these six lines could be surveyed in 2022. The bathymetry data were processed using the software Qimera from QPS and the RTK-derived depth (Real-Time Kinematic) was recalculated to Lowest Astronomical Tide (LAT). Artefacts were corrected manually and the multibeam data were then exported as a GeoTIFF with a horizontal resolution of 1 x 1 m (Figure 2.4). Backscatter data were processed using the software FMGT from QPS. A backscatter mosaic and statistics were calculated at a resolution of 0.2 x 0.2m and 4 x 4m respectively (Figure 2.5). An automatic classification of the seabed type was also performed in FMGT (Figure 2.6) and generated nine different classes for the surveyed transects ranging from muddy sand to gravel.

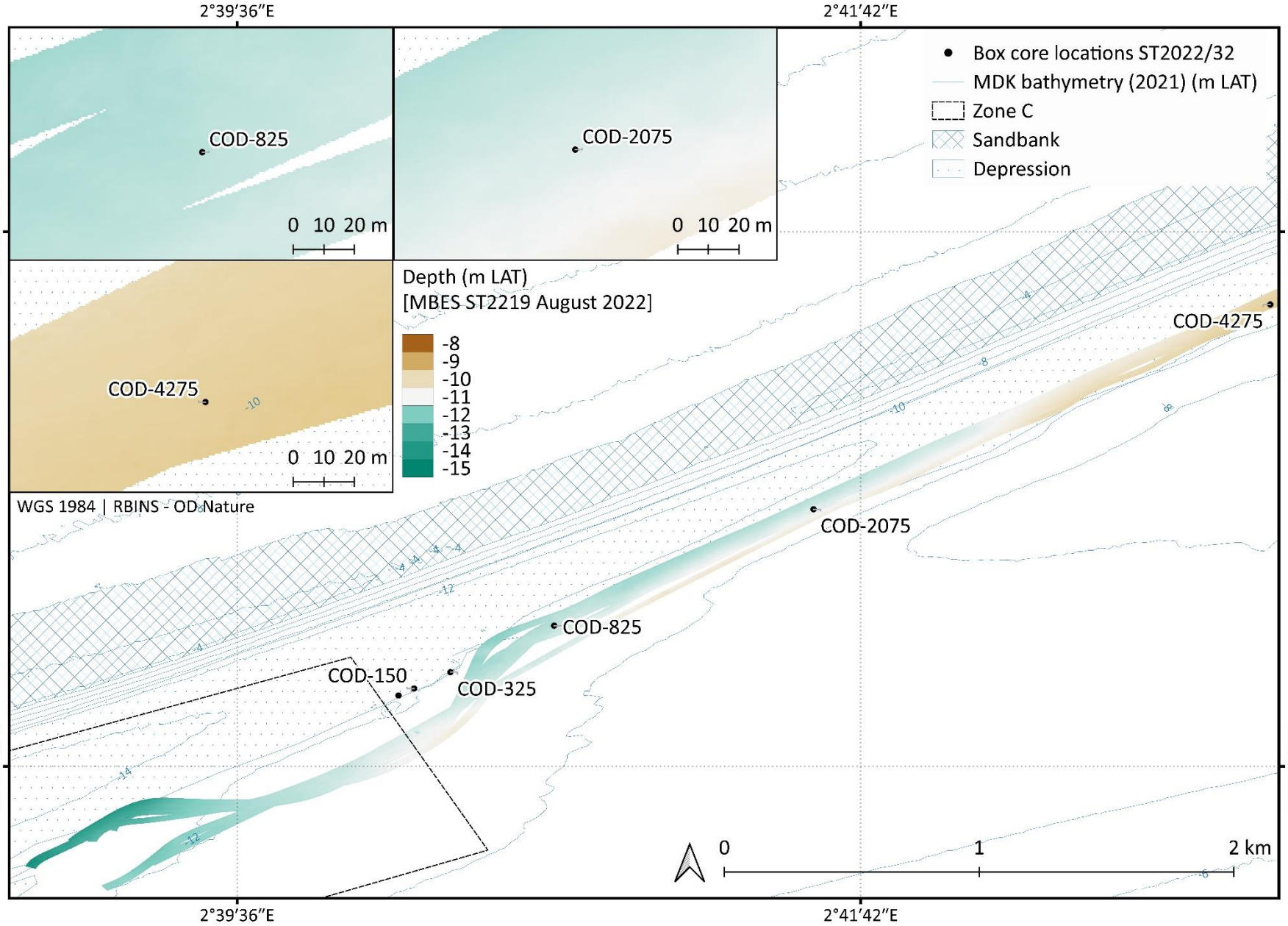

Figure 2.4. Bathymetric map (m LAT) with a 1 m resolution derived from the multibeam echosounder survey performed during campaign ST2022/19.

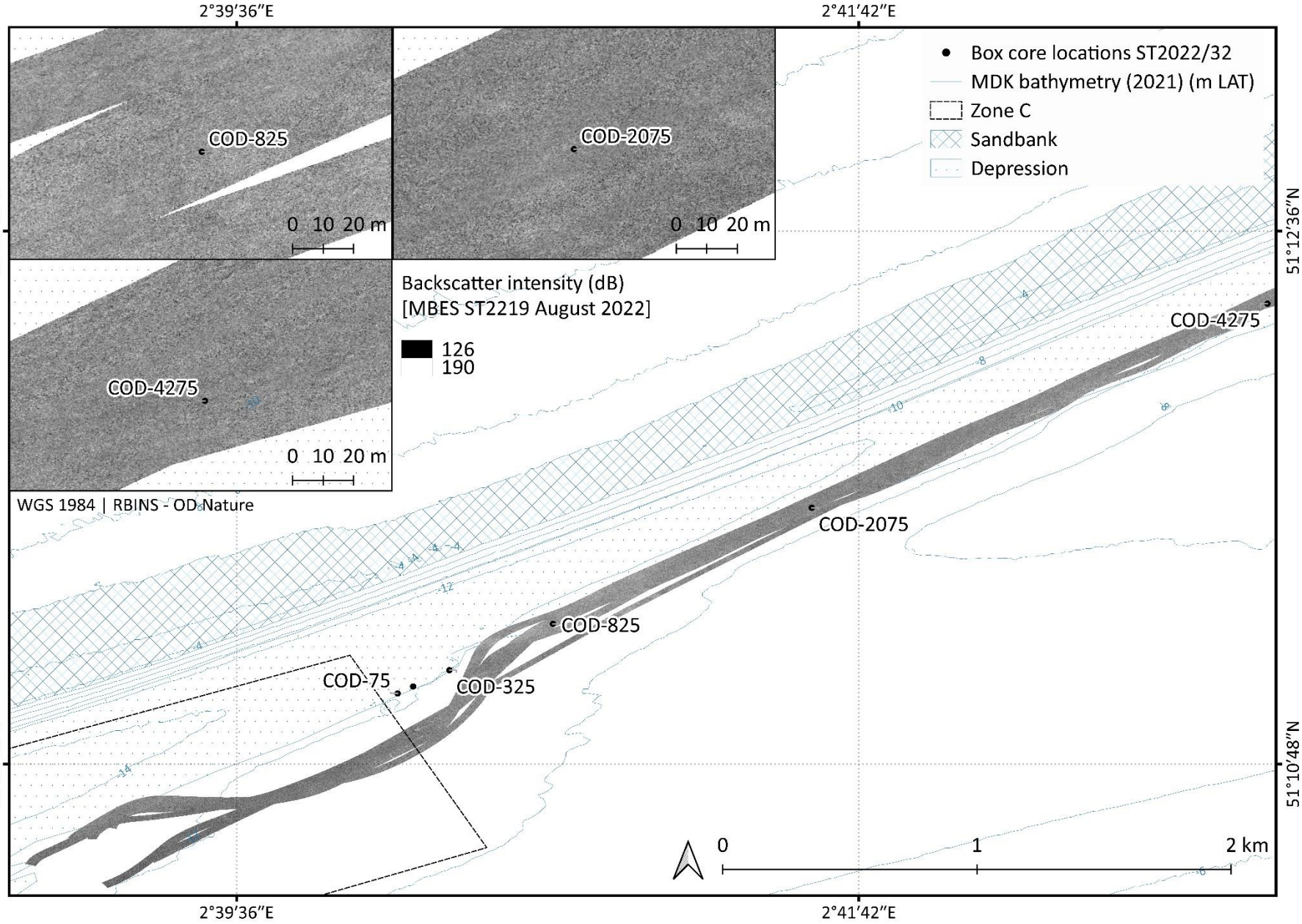

Figure 2.5. Map of the backscatter intensity (dB) with a resolution of 0.2 m derived from the multibeam echosounder survey performed during campaign ST2022/19.

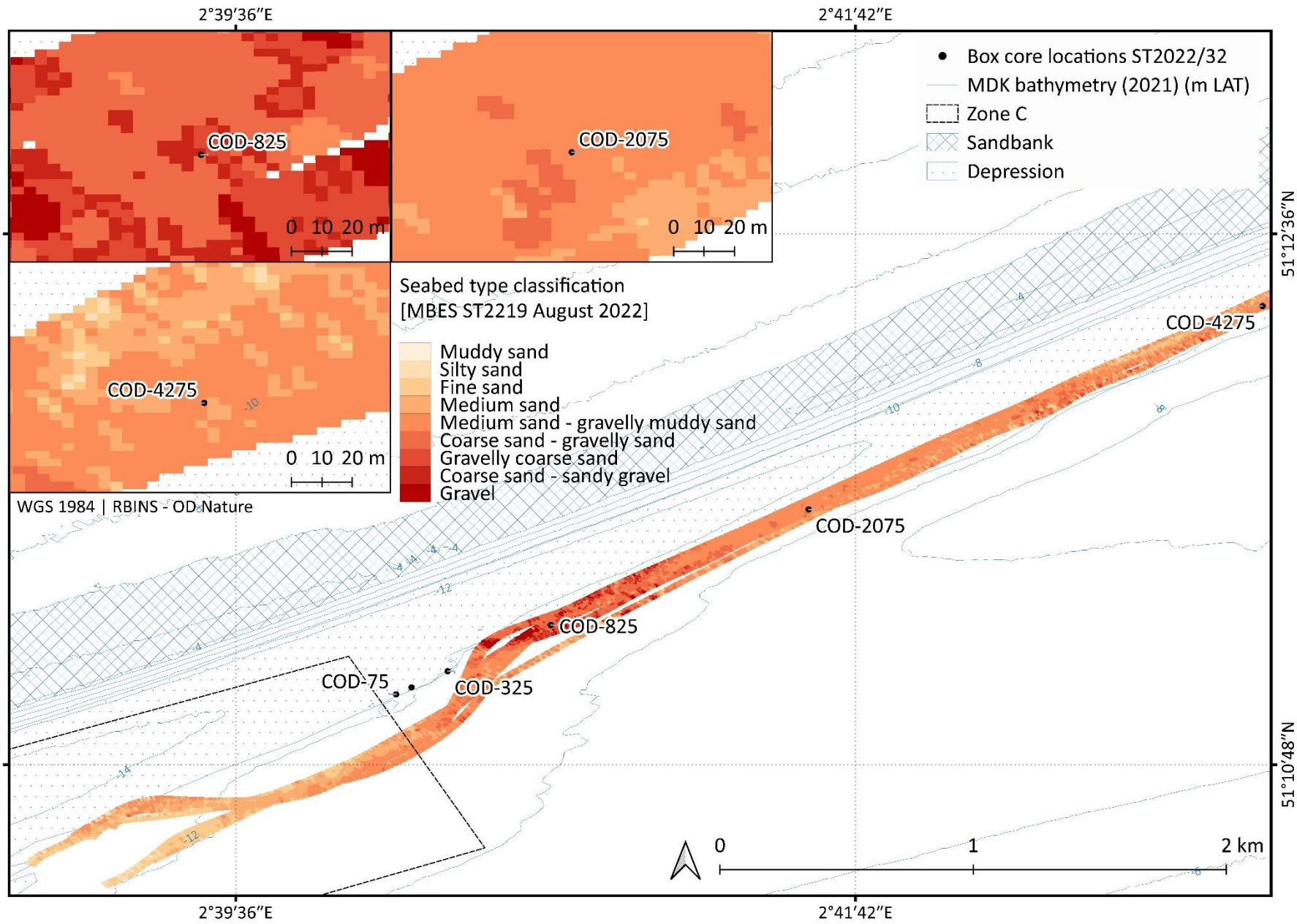

Figure 2.6. Map of the seabed type classification at a resolution of 4 m derived from the multibeam echosounder survey performed during campaign ST2022/19.

2.3.1.2. Bathymetric processing and comparison with data from the Flemish Hydrography

The multibeam data collected in August 2022 were compared with data acquired in 2017 (171219_ZUYWE_MB_300) and 2018 (180406_ZUYWE_MB) in the same area by Flemish Hydrography (Figure 2.7). These data were collected with a horizontal resolution of 1 x 1 m. They are freely available on the website of the Flemish Hydrography[2]. The comparison between the bathymetry in 2017-2018 and 2022 was made by calculating depth difference (m) (Figure 2.7) using the raster calculator in QGIS v.3.16.16 and the profiles were compared along 13 transects (one E-W transect and 12 N-S transects) (Figure 2.8 and Table 2.3).

[2] https://bathy.agentschapmdk.be/

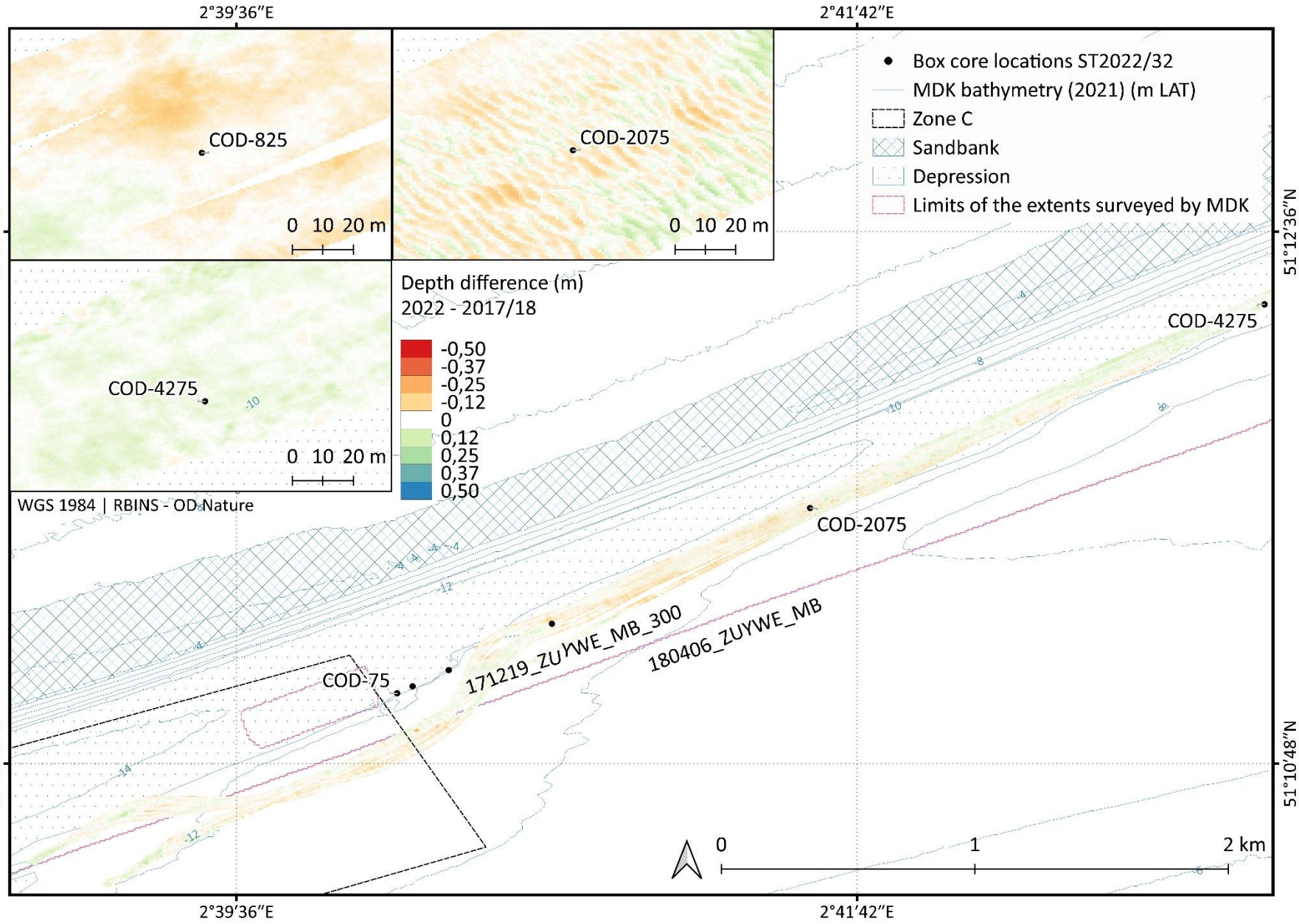

Figure 2.7. Depth difference (m) between the multibeam survey conducted by RBINS in 2022 and the ones conducted by MDK in 2017 and 2018.

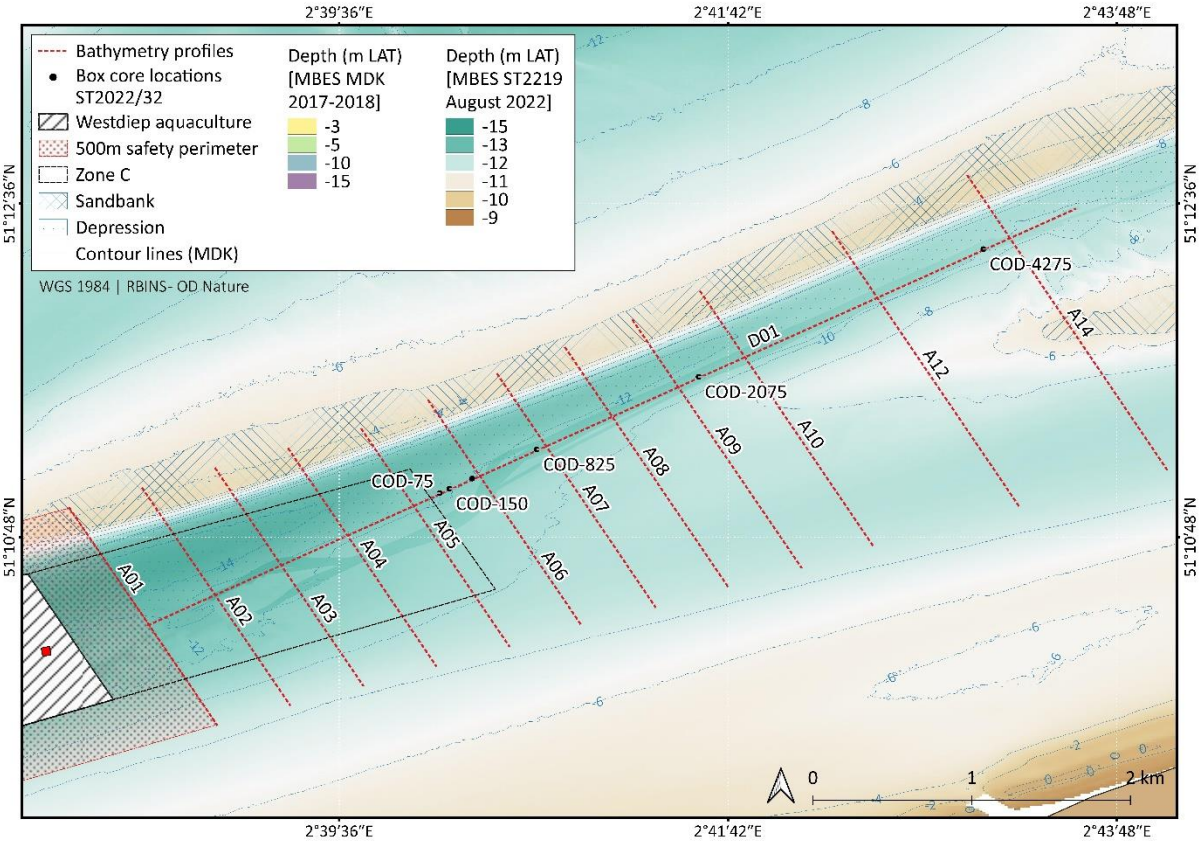

Figure 2.8. Location of the transect lines for the bathymetry monitoring.

Table 2.3. Coordinates of the bathymetric profiles monitored in the framework of Codevco.

POINT ID	TRANSECT ID	LATITUDE	LONGITUDE
D01-East	D01	51°N 12.57	002°E 43.57
D01-West		51°N 10.33	002°E 38.57
A01-North	A01	51°N 10.96	002°E 38.14
A01-South		51°N 09.77	002°E 38.94
A02-North	A02	51°N 11.06	002°E 38.54
A02-South		51°N 09.89	002°E 39.33
A03-North	A03	51°N 11.17	002°E 38.93
A03-South		51°N 10.00	002°E 39.73
A04-North	A04	51°N 11.28	002°E 39.33
A04-South		51°N 10.11	002°E 40.12
A05-North	A05	51°N 11.38	002°E 39.72
A05-South		51°N 10.21	002°E 40.52
A06-North	A06	51°N 11.54	002°E 40.08
A06-South		51°N 10.32	002°E 40.91
A07-North	A07	51°N 11.68	002°E 40.45
A07-South		51°N 10.42	002°E 41.31
A08-North	A08	51°N 11.82	002°E 40.82
A08-South		51°N 10.53	002°E 41.70
A09-North	A09	51°N 11.97	002°E 41.19
A09-South		51°N 10.64	002°E 42.10
A10-North	A10	51°N 12.12	002°E 41.55
A10-South		51°N 10.74	002°E 42.49
A12-North	A12	51°N 12.45	002°E 42.26
A12-South		51°N 10.95	002°E 43.28
A14-North	A14	51°N 12.75	002°E 42.99
A14-South		51°N 11.17	002°E 44.07

2.3.2. Sediment sampling

2.3.2.1. Sampling locations

Sediment samples were taken using a box core at six stations (Table 2.4, Figure 2.9, Figure 2.10, Figure 2.11 and Figure 2.12) during the ST2022/32 campaign onboard the RV Belgica on 16 December 2022 from 5 am to 7.15 am (UTC time). Three replicates were taken from every box core using a plastic cylinder with a diameter of 3.6 cm and then stored in plastic containers in a -20°C freezer. Out of those three replicates, one was sliced every centimeter while the others stored in intact state. Coordinates below were not yet corrected for the position of the box core within the ship.

Table 2.4. Coordinates of the stations sampled during campaign ST2022/32.

NAME	LATITUDE	LONGITUDE	DEPTH (M LAT)	DATE & TIME (UTC)
COD-75	51°11.04	002°40.14	12.27	16/12/23 06:58
COD-150	51°11.06	002°40.20	12.32	16/12/23 06:40
COD-325	51°11.12	002°40.32	12.01	16/12/23 07:16
COD-825	51°11.27	002°40.67	11.53	16/12/23 06:10
COD-2075	51°11.67	002°41.54	11.15	16/12/23 05:45
COD-4275	51°12.35	002°43.08	10.12	16/12/23 05:01

Figure 2.9. Pictures of the box core (left image) and of the subsampling (right image).

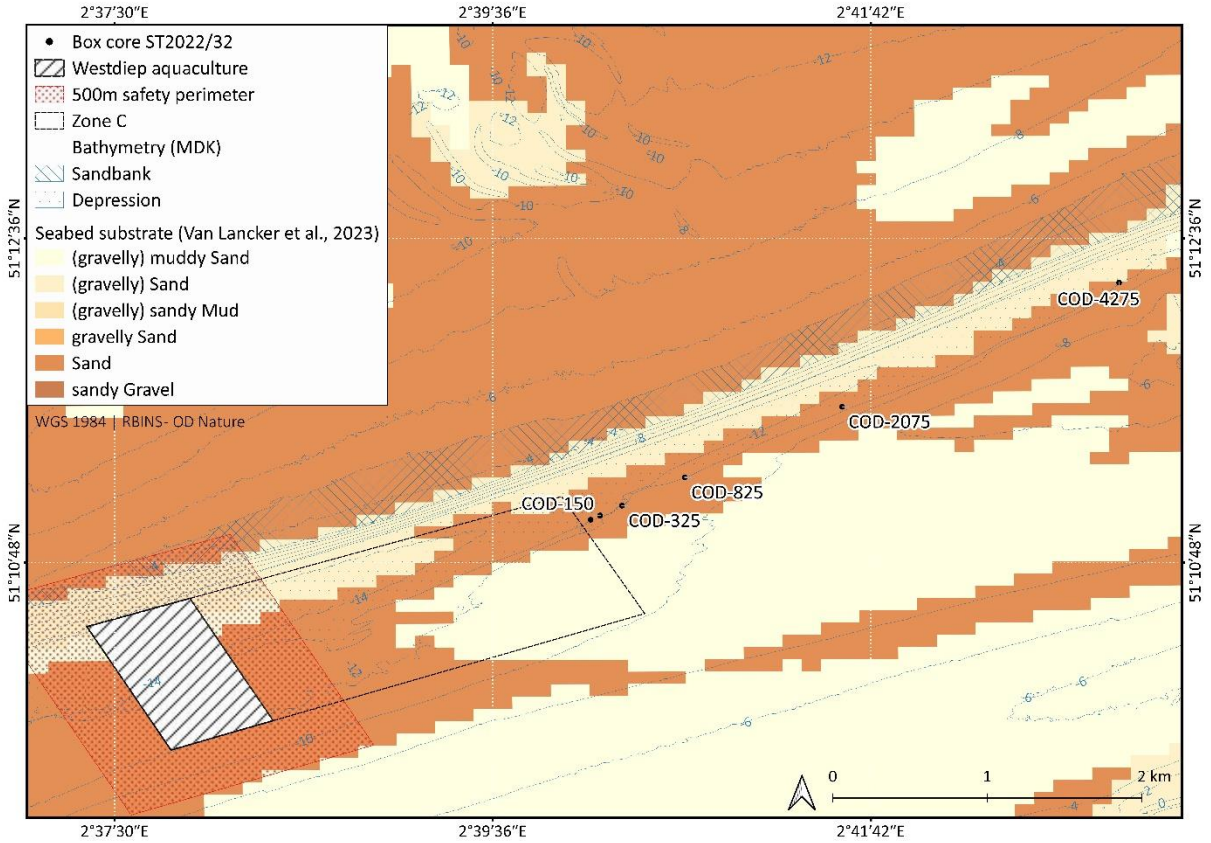

Figure 2.10. Locations where box core samples were taken during campaign ST2022/32 in reference to the surficial seabed substrate type based on the map produced by Van Lancker et al. (2023). This map was produced using automated classification of the seabed in six classes (merged Folk classification) based on multibeam surveys.

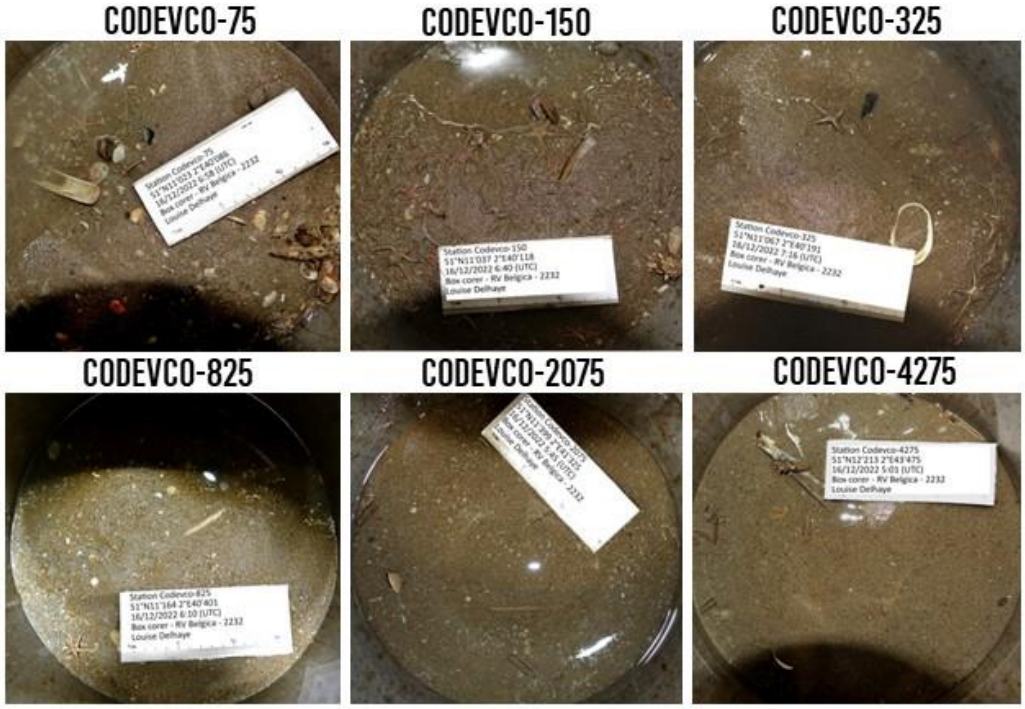

Figure 2.11. Top views of the box core samples taken during campaign ST2022/32.

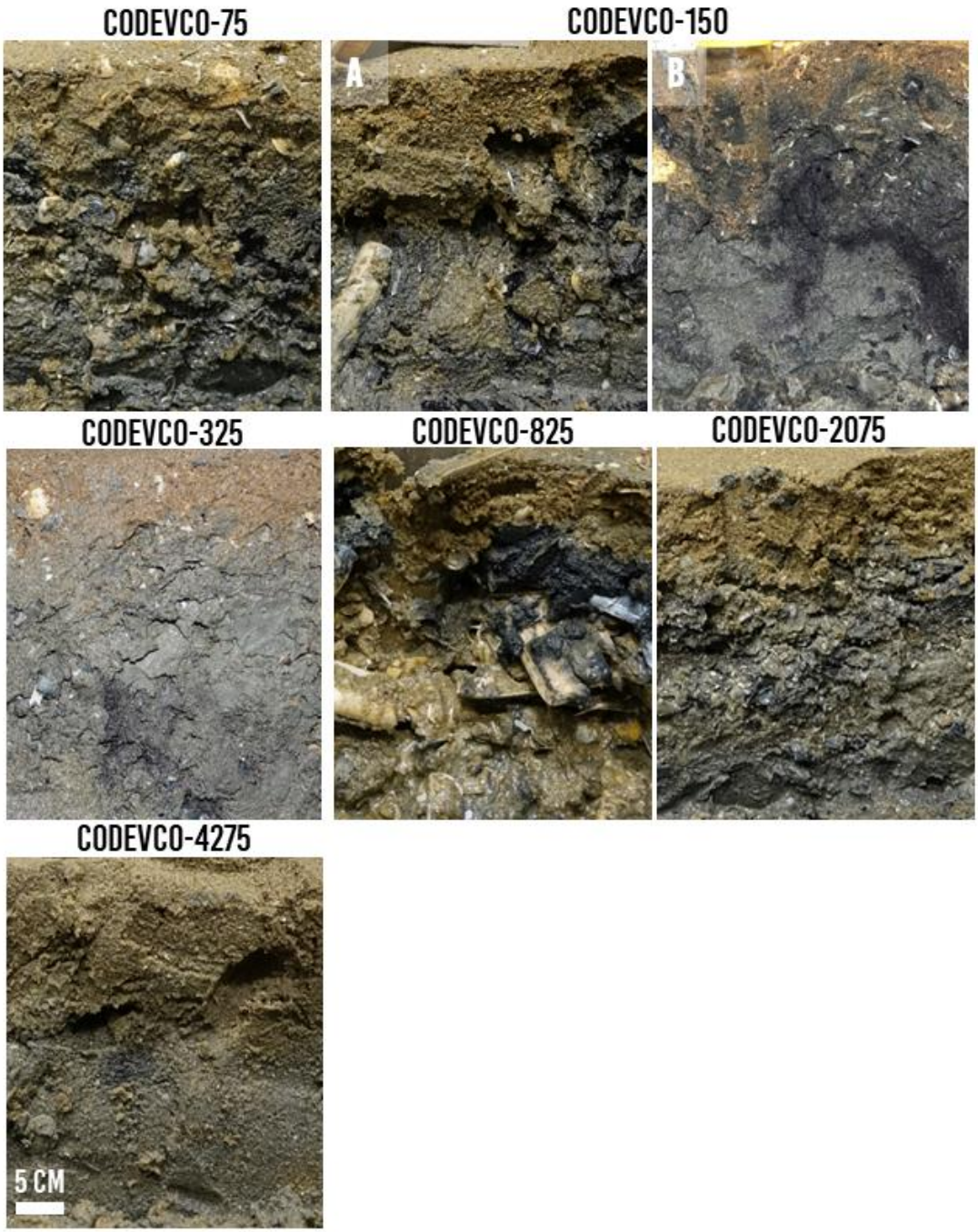

Figure 2.12. Cross sections of the box core samples taken during campaign ST2022/32.

2.3.2.2. Determination of organic matter and calcium carbonate content

The content of organic matter and calcium carbonate was measured using the Loss-on-Ignition (LOI) method in the sedimentological laboratory of Ghent University (Renard Centre of Marine Geology). The sediments were first dried at 60°C before about 4g of each sample was placed in pre-weighted ceramic crucibles and heated in an oven at 105°C for 24 hours. After weighing the remaining samples, they were then placed for 4h in a muffle furnace at 550°C and then weighted again in order to obtain the organic matter content. The latter is estimated as the difference between the weights of the samples before and after being burned at 550°C as the organic matter is completely depleted at that temperature. Carbonate minerals, however, are only destroyed at higher temperatures. Therefore, a

final step was to place the samples in the muffle furnace at 1000°C for 5h and the remaining weight enabled us to calculate the calcium carbonate content. Three replicates of one sample (layer 10-11 cm at COD-325) were taken in order to estimate the precision of the method (Figure 2.13).

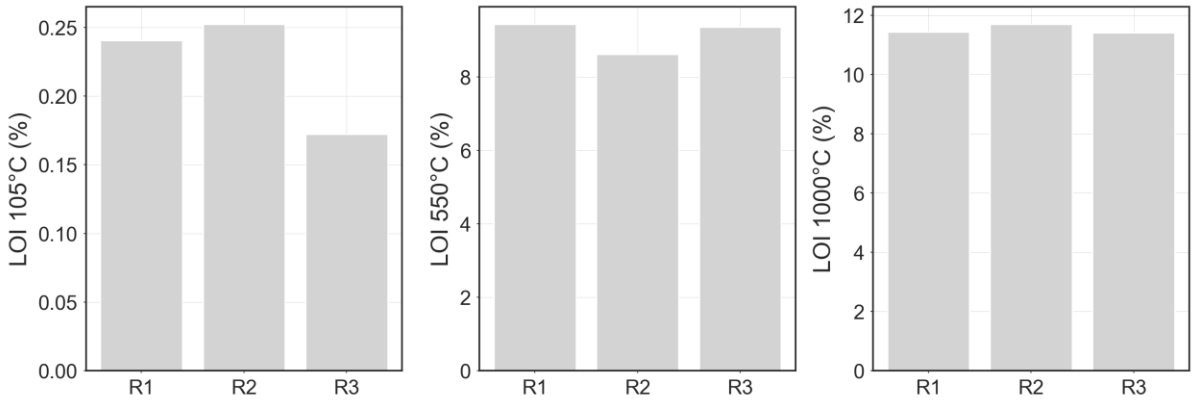

Figure 2.13. Precision of the LOI analysis at 105, 550 and 1000°C based on three replicates of one sample.

2.3.2.3. Determination of grain size distribution

Determination of the grain size distribution of the samples was performed using a Malvern Mastersizer 3000 available at Ghent University (Renard Centre of Marine Geology). Prior to the Malvern measurements, around 1 g of each sample was first sieved to separate the fraction superior to 1 mm from the rest of the sample. Both fractions were then dried in the oven at 60°C and weighted in order to obtain the ratio between the large and small fractions. The latter was then boiled with milliQ water and 2 µL of H_2O_2 in order to remove the organic matter and left to settle overnight before discarding the milliQ and refilling again. After a new settling of the particles, the milliQ content was removed until only 10 ml remained in the vial. In order to ensure the complete separation of the grains, 1 µL of Calgon was added to the sample and the preparation was boiled again. After this preparation, the samples were introduced into the Malvern in order to measure grain size distribution. Three measurements were made for each sample to estimate the precision of the instrument, and three replicates of one sample (layer 9-10 cm at COD-2075) were measured in order to estimate the representativeness of the subsampling and the two subsamples taken within one box core (full sub-core and sliced sub-core) were compared to test for the spatial variability. They all show a good concordance, confirming the validity of the analyses (Figure 2.14). The data from the Malvern were corrected in Excel to include the volume of grains larger than 1 mm that were sieved out of the sample prior to the processing. The volume of each class of particle was then normalized to take into account the total volume of the sample rather than only the volume passed through the Malvern.

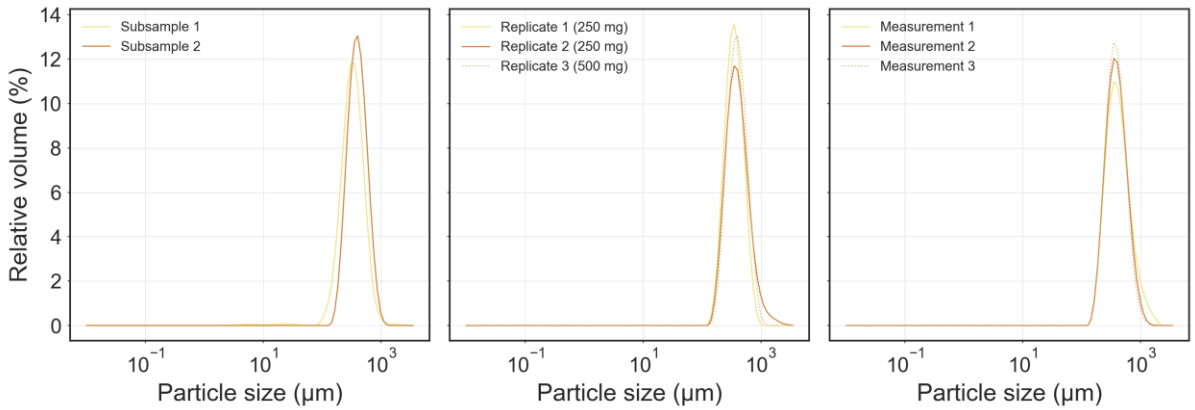

Figure 2.14. Spatial variability inside one box core (first graph), representativity of subsamples (second graph) and precision of the Malvern measurements (third graph).

2.3.2.4. Statistical analysis

For statistical analyses, graphs were produced using Python v3.9 and R Studio v2022.12.0. Spearman correlations between the different variables (depth, organic matter and calcium carbonate content, clay fractions, silt, fine sand, medium sand and coarse sand) were calculated in R Studio using the ggpairs function.

2.4. METHODOLOGY FOR MONITORING IMPACTS ON THE HYDROGRAPHICAL CONDITIONS

2.4.1. Water column monitoring during campaign ST2022/19

During the ST2022/19 campaign on board the RV Belgica, various activities were carried out as part of the sedimentological monitoring between August 19th and August 21st 2022. CTD profiles were carried out for 1 hours (one tidal cycle) and surface and bottom water samples were collected every hour with Niskin bottles in order to perform laboratory analysis. These activities were conducted East of the seafarm (Table 2.5, Figure 2.15). Multibeam transects were also carried out (see section 2.3.1), the hull-mounted ADCP recorded data during the whole water sampling time and one tripod (T001) was deployed (see section 2.4.2).

Table 2.5. Coordinates of the water sampling performed during campaign ST2022/19.

NAME	UTM ZONE 31N		WGS84		DEPTH (M LAT)
	EASTING	NORTHING	DDX	DDY	
COD-TC-E	475144.861	5669275.529	2°38.667	51°10.462	-14.54

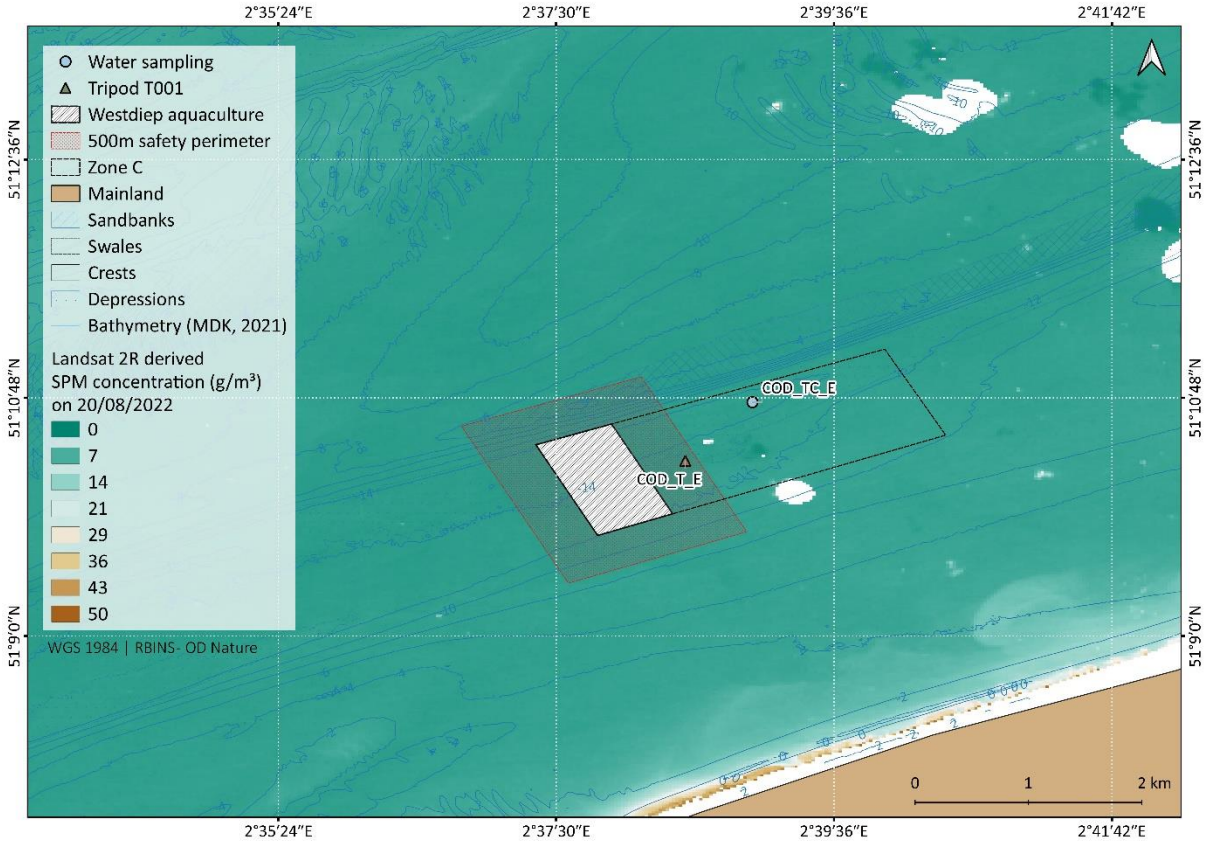

Figure 2.15. Location of the tripod T001 and of the water sampling performed during campaign ST2022/19 and SPM concentration estimated from a Landsat 8 image obtained on the same day.

2.4.1.1. Water sampling and laboratory analysis

Surface and bottom water samples were taken 13 times over a full tidal cycle, every hour between 10.30 am and 10.30 pm on 20 August (Table 2.6, Figure 2.16). Bottom and surface samples were filtrated for SPM concentration, pigments (chlorophyll a and b, phaeopigments a and b), POC, PON and TEP (Table 2.7). The turbidity was also measured directly on board using a turbidity meter from Hach. Finally, the pH and temperature of the seawater was measured at the surface of the water.

Filtration processes can be found by contacting Ecochem[3]. In the framework of other monitoring programs, these analyses were carried out using the same protocol at other locations of the Belgian part of the North Sea for the past 15 years and were therefore used as a reference for comparison. These data can be downloaded via the Belgian Marine Data Center (BMDC).

Table 2.6. Name of the stations, date and time of the surface and bottom water samples taken with the Niskin bottles during campaign ST2022/19.

STATION ID	DATE	TIME (UTC)	SURFACE	BOTTOM
ST1	20/08/2022	10:30	x	x
ST2	20/08/2022	11:30	x	x
ST3	20/08/2022	12:30	x	x
ST4	20/08/2022	13:30	x	x
ST5	20/08/2022	14:30	x	x
ST6	20/08/2022	15:30	x	x
ST7	20/08/2022	16:30	x	x
ST8	20/08/2022	17:30	x	x
ST9	20/08/2022	18:30	x	x
ST10	20/08/2022	19:30	x	x
ST11	20/08/2022	20:30	x	x
ST12	20/08/2022	21:30	x	x
ST13	20/08/2022	22:30	x	x

Table 2.7. Number of laboratory measurements conducted in the water samples collected during campaign ST2022/19 (number of stations x number of water samples per station (surface and/or bottom) x number of replicates).

HACH	SPM	PIGMENT	POC / PON	DOC	PAHS / OTIN	TEP	SALINITY	TNTP + NUTS	TA / DIC + PH	IN-SITU PH + TEMP	IN-SITU OXYGEN + OXYGEN SATURATION
13x2x3	13x2x3	13x2x2	13x2x1	NA	NA	13x2x3	NA	NA	NA	13x1x1	NA

2.4.1.2. Continuous measurements of the water column

Between water samples, the rosette, equipped with a CTD, a LISST-100x, a LISST-Holo2 and an OBS remained in the water to measure these different parameters. Every 20 minutes on average, a complete profile of the water column was taken. A total of 13 casts were carried out during the ST2022/19 campaign (Table 2.8). Data from the CTD, LISST-100x and LISST-Holo2 were processed in their respective software (SBEDataProcessing-Win32, LISST-SOPv5 and Holo-Batch), and outliers above the 0.95 quantile and below the 0.05 quantile were filtered out in Python using the stats module from scipy. Because of the high range of the OBS compared to the low turbidity of the water, these data could not be used for further analysis.

[3] ecochem@naturalsciences.be

Table 2.8. Name of the stations, time and duration and instruments used for the measurements of the water column with the rosette during campaign ST2022/19.

CAST	STATION ID	TIME (LOCAL)	CTD SBE09	LISST-HOLO2	LISST-100X
A	ST0 – ST1	12:31 – 12:35	x	NA	x
B	ST1 – ST2	12:42 – 13:35	x	x	x
C	ST2 – ST3	13:40 – 14:34	x	x	x
D	ST3 – ST4	14:40 – 15:34	x	x	x
E	ST4 – ST5	15:42 – 16:35	x	x	x
F	ST5 – ST6	16:41 – 17:36	x	x	x
G	ST6 – ST7	17:44 – 18:35	x	x	x
H	ST7 – ST8	18:44 – 19:35	x	x	x
I	ST8 – ST9	19:41 – 20:34	x	x	x
J	ST9 – ST10	20:41 – 21:34	x	x	x
K	ST10 – ST11	21:46 – 22:34	x	x	x
L	ST11 – ST12	22:39 – 23:34	x	NA	x
M	ST12 – ST13	23:46 – 00:33	x	NA	x

2.4.1.3. Meteorological conditions during water sampling and measurements

Wave heights during the measurements remained between 45 and 65 cm most of the time (Figure 2.16), with a peak at 85 cm shortly before high tide (casts G, H, I), with a generally stable wave period (3 to 3.2 s) until the last cast when the period suddenly rose to 3.4 s. As for the wind, it rose up to 9m/s until 6 pm before dropping to 6 m/s for the last part of the measurements. At 6 pm, its direction also changed from WNW (280°) to SW (220°) (Figure 2.17).

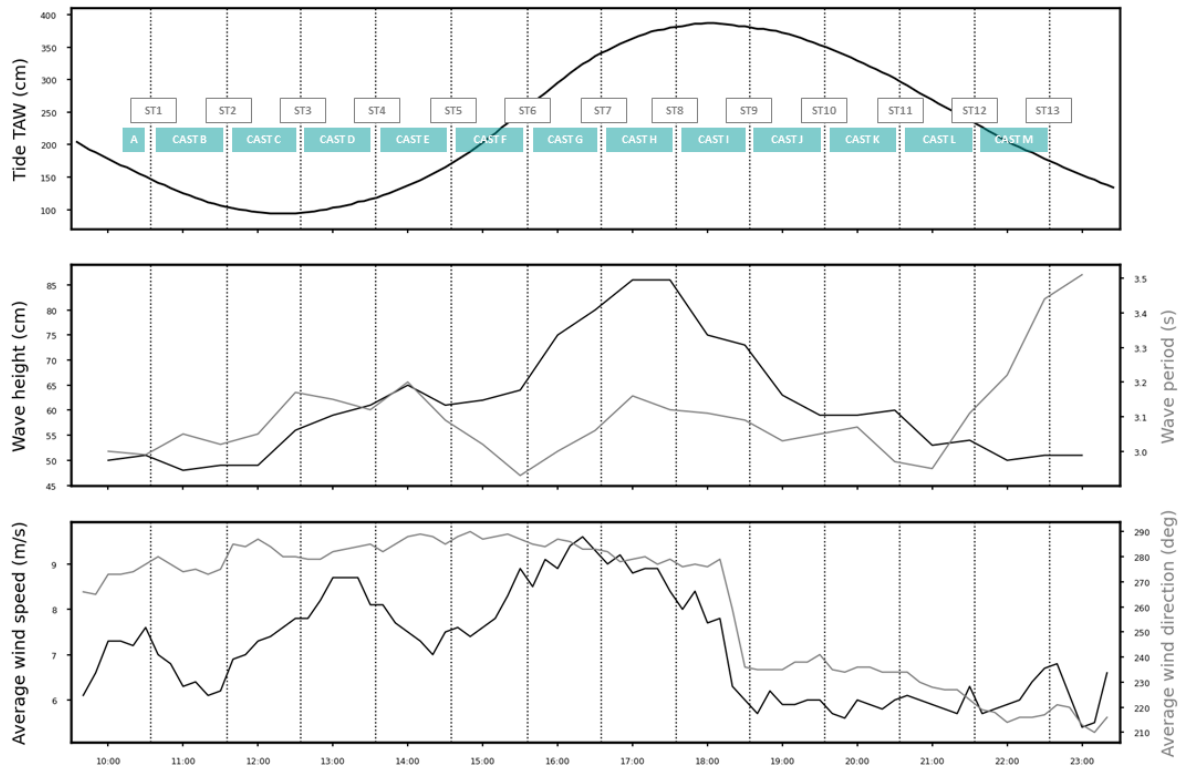

Figure 2.16. Wave height and period, wind speed and direction during the water column sampling and measurements performed during campaign ST2022/19.

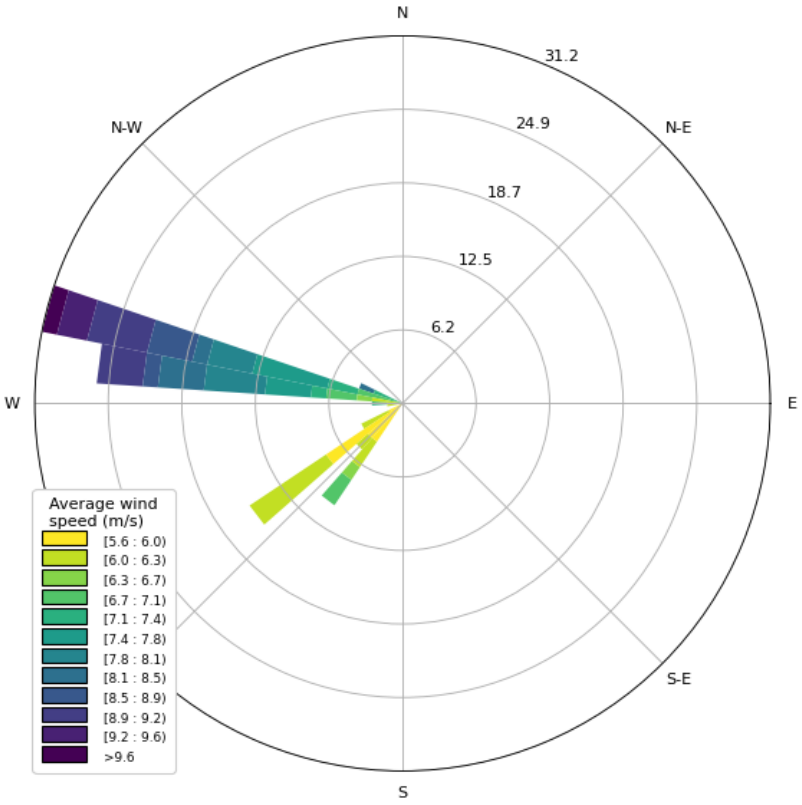

Figure 2.17. Wind speed and direction during the water column sampling and measurement performed during campaign ST2022/19.

2.4.1.4. ADCP survey

The hull-mounted ADCP (Teledyne RD Instruments Workhorse Mariner at 600 kHz) recorded data for the entire duration of the water sampling. Data were processed in R using the open-source package 'oce'. The workflow consisted in [1] despiking the data, [2] removing the data too close from the sensor or from the bottom (only 90% of the water column was kept) and [3] calculating the mean backscatter coefficient of all four beams using the formulae developed by Teledyne RD Instruments (Deines, 1999; Mullison, 2017) and applying the background noise corrections specific to each beam. The draught of the ship was assigned by default to 4.5 m and the band width used was set to 1, following the settings of the ADCP, meaning the C value was calculated to be equal to -149.14 dB. Data were then compared to the hydrodynamics models developed by the Belgian Marine Forecasting Center (MFC), part of the Royal Belgian Institute of Natural Sciences, and downloaded online[4].

[4] https://erddap.naturalsciences.be/erddap/griddap/BCZ_HydroState_V1.html

2.4.2. Tripod T001

The deployment of a benthic platform (tripod) close to the marine farm will enable us to study the dynamics of the currents (**task 2.A**) and sediments (**task 2.B**) as well as their composition (**task 2.C**) close to the seabed over a longer time scale. To that end, the first tripod was deployed during campaign ST2022/19 on board the RV Belgica at Codevco-T-East (Table 2.9, Figure 2.15, Figure 2.18, Figure 2.19), east of the aquaculture, for a period of six weeks from the 20th of August 2022 to the 6th of October 2022. It was equipped with a LISST-200x at 2 mab, an ADCP (RDI Workhorse Sentinel) upward-looking at 2 mab, an ADP (Nortek Signature 1000) downward-looking at 2 mab, a CTD (Seabird 19plus V2 SeaCAT) at 1 mab, two turbidity meters (Seapoint x5) at 1 and 2 mab, a fluorometer (WiMo) at 1 mab and four sediment traps (two with 5 mm holes and two with 10 mm holes) (Figure 2.19).

Table 2.9. Coordinates of the tripod T001 deployed during campaign ST2022/19.

NAME	UTM ZONE 31N		WGS 84		DEPTH (M LAT)
	EASTING	NORTHING	DDX	DDY	
COD-T-EAST	474921.10	5669020.83	2°38.476	51°10.324	13.59

Figure 2.18. Pictures of the tripod before deployment (left image) and after recovery (right image).

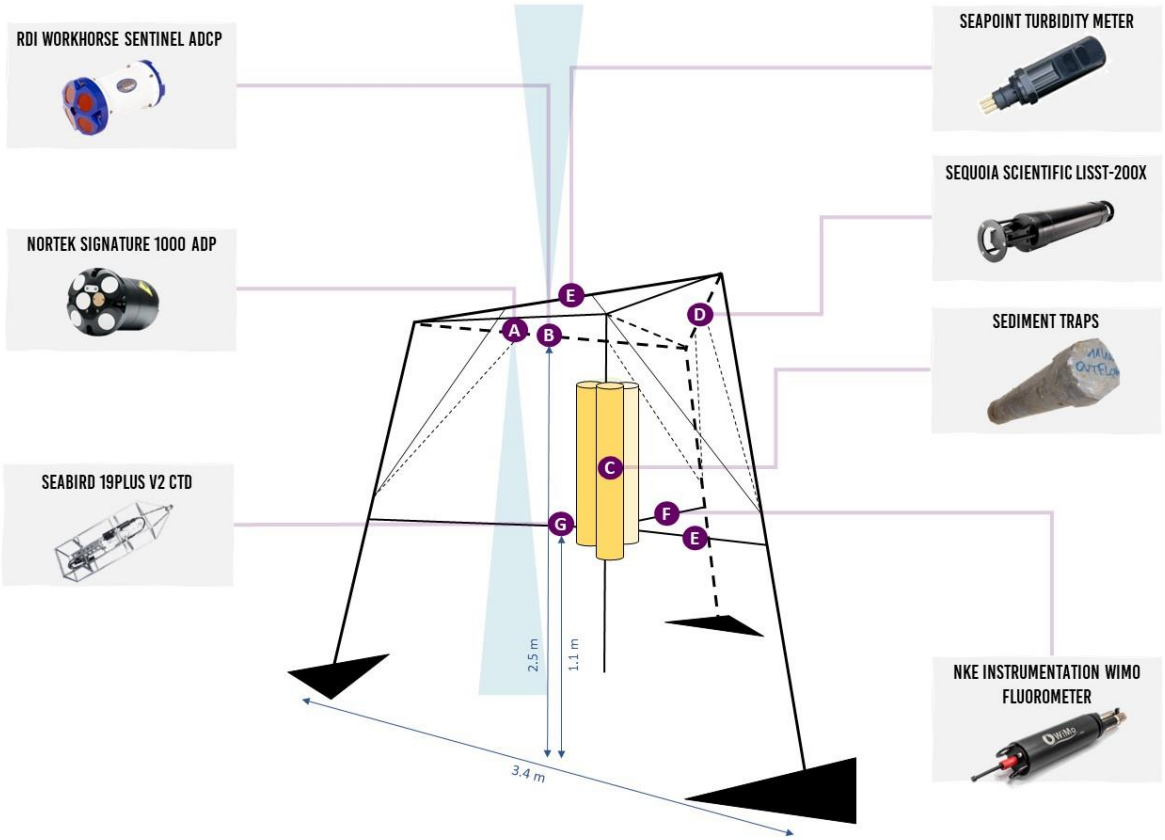

Figure 2.19. Schematic of the configuration of the T001 tripod equipped with all instruments.

2.4.2.1. Overview of the deployment

An overview of all the parameters measured by the sensors on the tripod T001 is shown in Figure 2.20 below. The values for wind direction, wind speed, wave height and wave period were taken from the Meetnet Vlaams Banken site[5] at Nieuwpoort.

[5] https://meetnetvlaamsebanken.be/

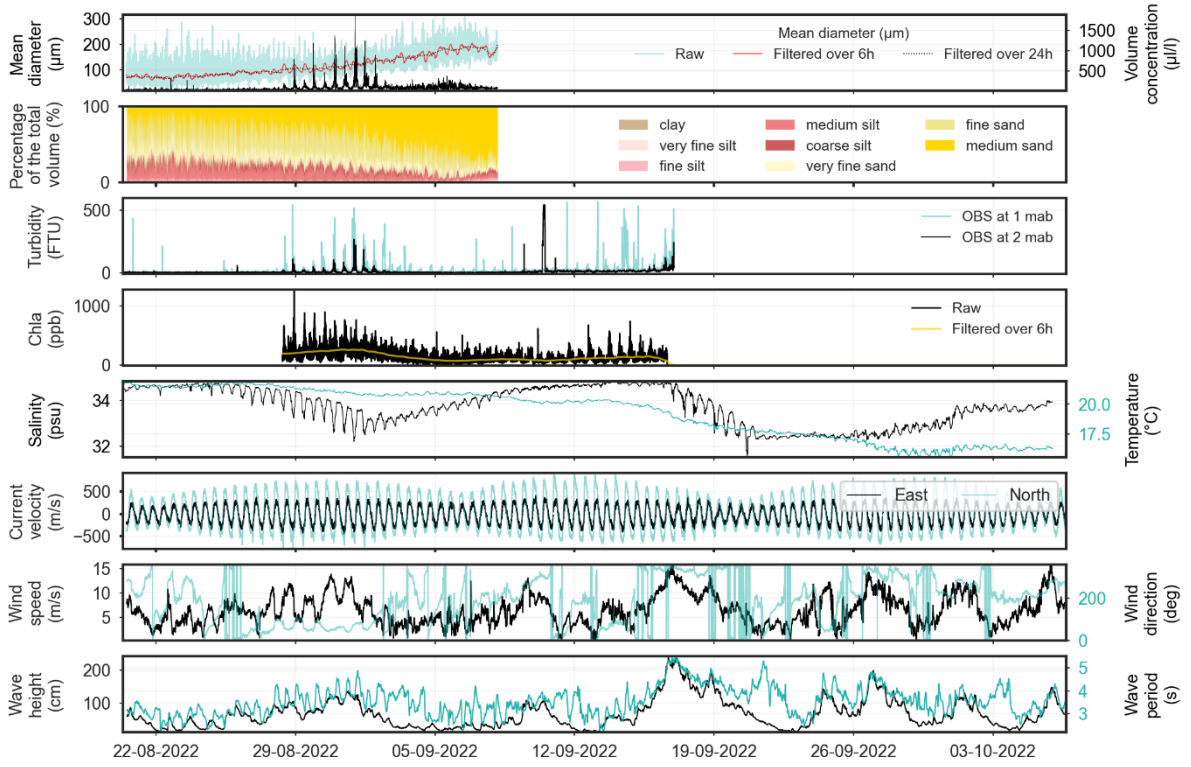

Figure 2.20. Overview of all the parameters measured during the deployment of tripod T001 from August to October 2022.

2.4.2.2. LISST-200x

A first visual observation of the raw LISST-200x parameters showed a gradual decrease in data quality, similar to those observed in biofouling cases. When the computed optical transmission over path dropped to values below 0.1, the data were considered to be suspicious and were therefore rejected. Data between 0.1 and 0.3 should be analyzed with caution, as well as values above 0.98. After a first filtering of the data, only data between the 20th of August 2022 09:36:50 and the 8th of September 2022 08:15:50 were kept. Measuring background scattering is essential to ensure good performance of the LISST-200x, particularly in clear water where transmission is greater than 90%. The closer the background curve is to the factory background, the better. Too much deviation between the two, especially in the middle of the distribution, indicates that the windows and/or the water were not clean when the background was taken. With the original background, taken before the deployment, the deviation from the factory one was not acceptable and a new background was therefore taken in MilliQ water after a thorough cleaning of the windows. Effect of this background quality was checked and the mean diameter was slightly overestimated with a bad background.

2.4.2.3. Fluorometer WiMo

Due to a programming error, the fluorometer did not start recording data until one week after the deployment of the tripod (i.e. on the 28th of August). It was set to record fluorescence of chlorophyll a in bursts of 12 pulses every ten minutes. Low-pass filters were then applied on these raw data in Python.

2.4.2.4. ADCP RDI 1200 kHz

ADCP data from the RDI mounted upward-looking on the tripod at 2 mab were processed in two different ways. The backscatter data (Figure 3.13) were processed in R Studio v.2022.12.0 using the

script initially developed for the hull-mounted ADCPs explained in section 2.4.1.4 and adapted for the tripod-mounted ADCPs. The velocity data were pre-processed in WinADCP and then imported in Python to generate graphs.

2.4.2.5. ADP Nortek Signature 1000

Due to a technical issue, there was no ADP measurement during the deployment of this tripod. The external battery was improperly attached to the ADP and it could only work for two hours before being damaged. The two hours of data are not usable as the quality cannot be assured due to the malfunction of the instrument.

2.4.2.6. SBE 19 plus v2 & Seapoint turbidity meters

Data from the CTD (mounted on the tripod at 1 mab) and the connected turbidity meters were taken every 2.5 minutes. The two Seapoint turbidity meters placed at 1 and 2 mab were converted from voltage to FTU using the conversions derived from the calibrations carried in the lab by MSO on 26th of October 2020 (Figure 2.21). As there was a suspicion of biofouling on the turbidity meters, data after the 17th of September were discarded.

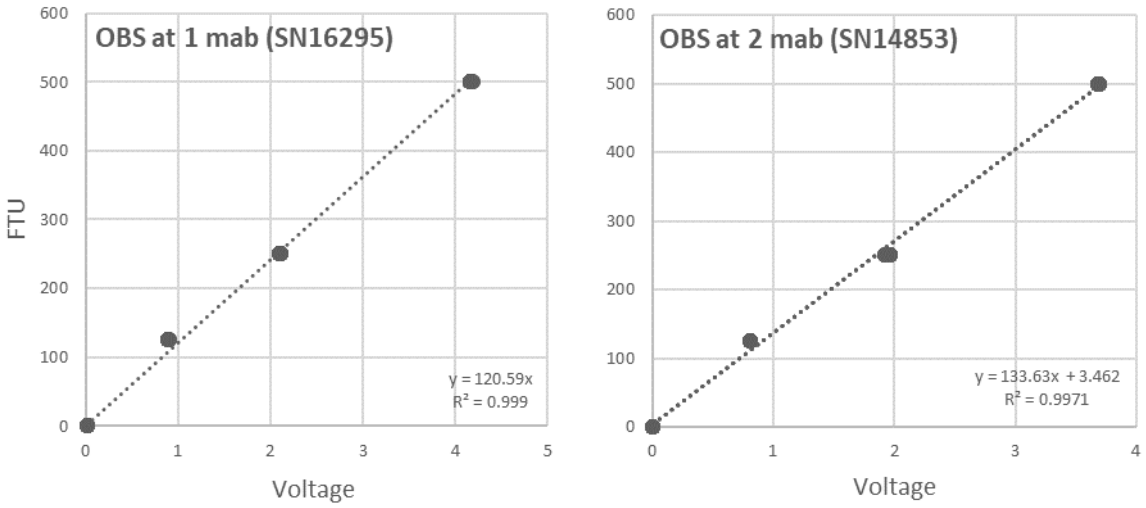

Figure 2.21. Calibrations of the two Seapoint turbidity meters deployed on tripod T001.

2.4.2.7. Sediment traps

Four sediment traps with a height of 50 cm and a diameter of 7.5 cm were placed on the tripod, between 1 mab and 2 mab, with holes situated on top of the traps. Two of them had holes of 5 mm and two other had holes of 10 mm. One of each was used for calibration of the WiMo fluorometer placed on the Westdiep buoy inside the aquaculture farm and managed by Colruyt. The two remaining traps were cut in two in order to be scanned in the Geotek lab in UGent. However, due to technical issues with these instruments at the time of analysis, one half of each trap was sliced every centimeter (Figure 2.22), freeze-dried and then prepared for Malvern analysis as explained in section 2.3.2.3. The other half of each trap was stored as archives.

Figure 2.22. Pictures of the two sediment traps collected on tripod T001. The dotted white lines indicate the one-centimeter slices analyzed in the Malvern.

2.4.3. Water column monitoring during campaign ST2022/32

During the ST2022/32 campaign on board the RV Belgica, in addition to the seabed sampling (see section 2.3.2), water sampling was carried out in the framework of the Codevco monitoring program between December 16th and 17th 2022. CTD profiles were carried out for 12 hours (one tidal cycle) and surface and bottom water samples were collected every 1.5 hour with Niskin bottles in order to perform laboratory analysis. These activities were conducted West of the seafarm (Table 2.10, Figure 2.23). Finally, data were recorded from the hull-mounted ADCP during the full water sampling.

Table 2.10. Coordinates of the water sampling performed during campaign ST2022/32.

NAME	UTM ZONE 31N		WGS84		DEPTH (M LAT)
	EASTING	NORTHING	DDX	DDY	
COD-TC-WEST	472695.321	5667661.515	2° 36.572	51°09.585	-14.49

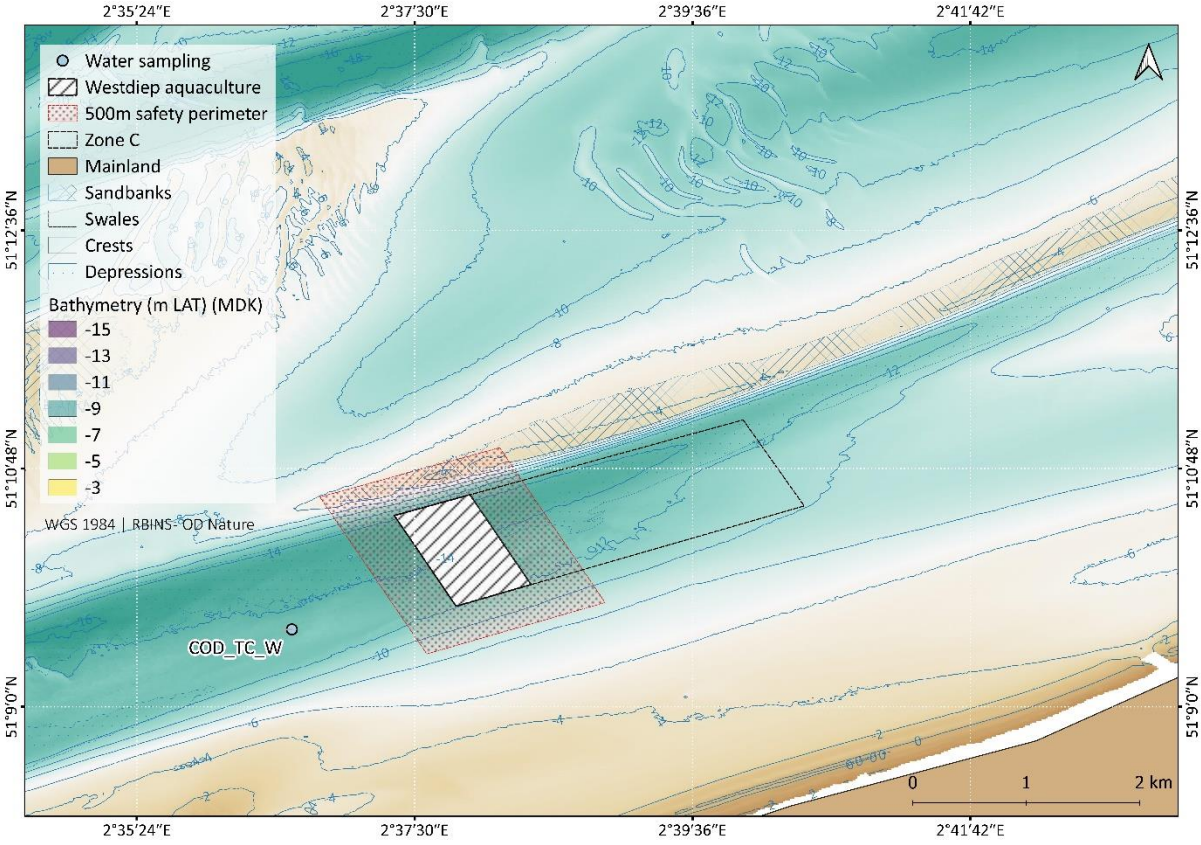

Figure 2.23. Location of the water sampling performed during campaign ST2022/32.

2.4.3.1. Water sampling and laboratory analysis

Surface and bottom water samples were taken nine times over a full tidal cycle, every 1.5 hour between 2:00 pm and 2:00 am on 16-17 December (Table 2.11, Figure 2.25). Bottom and surface samples were filtrated for SPM concentration, pigments (chlorophyll a and b, phaeopigments a and b), POC and PON (Table 2.12). The turbidity was also measured directly on board using a turbidity meter from Hach. Finally, the pH and temperature of the seawater was measured at the surface of

the water. Filtration processes can be found by contacting ECOCHEM[6]. At the time of writing this report, some results are not yet available. These are: POC, PON, Phaeo A and B for ST8 and 9 (bottom and surface); and ChlB for ST8 and ST9 (bottom).

Table 2.11. Name of the stations, date and time of the surface and bottom water samples taken with the Niskin bottles during campaign ST2022/19.

STATION ID	DATE	TIME (UTC)	SURFACE	BOTTOM
ST1	16/12/2022	14:13	x	x
ST2	16/12/2022	15:30	x	x
ST3	16/12/2022	17:00	x	x
ST4	16/12/2022	18:30	x	x
ST5	16/12/2022	20:00	x	x
ST6	16/12/2022	21:30	x	x
ST7	16/12/2022	23:00	x	x
ST8	17/12/2022	00:30	x	x
ST9	17/12/2022	02:00	x	x

Table 2.12. Number of laboratory measurements conducted in the water samples collected during campaign ST2022/32 (number of stations x number of water samples per station (surface and/or bottom) x number of replicates).

HACH	SPM	PIGMENT	POC / PON	DOC	PAHS / OTIN	TEP	SALINITY	TNTP + NUTS	TA / DIC + PH	IN-SITU PH + TEMP	IN-SITU OXYGEN + OXYGEN SATURATION
9x2x3	9x2x3	9x2x2	9x2x1	NA	NA	NA	NA	NA	NA	9x1x1	NA

2.4.3.2. Measurements of the water column

Between water samples, the rosette, equipped with a CTD, a LISST-100x, a LISST-Holo2 and an OBS, remained in the water to measure these different parameters. Every 20 minutes on average, a complete profile of the water column was taken. A total of nine casts were carried out during the ST2022/32 campaign (Table 2.13). Data from the CTD, LISST-100x and LISST-Holo2 were processed in their respective software (SBEDataProcessing-Win32, LISST-SOPv5 and Holo-Batch), and outliers above the 0.95 quantile and below the 0.05 quantile were filtered out in Python using the stats module from scipy. For the CTD data, the first profile of each cast was discarded as the sensors need time to adjust once in the water.

[6] ecochem@naturalsciences.be

Table 2.13. Name of the stations, time and duration and instruments used for the measurements of the water column with the rosette during campaign ST2022/32.

CAST	STATION ID	TIME (LOCAL)	CTD SBE09	LISST-HOLO2	LISST-100X
A	ST0 – ST1	14:13 – 14:17	x	x	x
B	ST1 – ST2	14:29 – 15:38	x	x	x
C	ST2 – ST3	15:55 – 17:07	x	x	x
D	ST3 – ST4	17:18 – 18:37	x	x	x
E	ST4 – ST5	18:53 – 20:08	x	x	x
F	ST5 – ST6	20:18 – 21:36	x	x	x
G	ST6 – ST7	21:47 – 23:06	x	x	x
H	ST7 – ST8	23:13 – 00:37	x	15 minutes	x
I	ST8 – ST9	00:51 – 02:07	x	NA	x

The conversion of the raw OBS values (voltage 2) to the estimated SPM concentration was obtained by calculating a direct linear regression between the OBS values indicated at the time the bottles were closed and the average of the SPM samples filtered from the water in these bottles (see equation below and Figure 2.24). With an R^2 of 0.94, the correlation between the two values is acceptable.

Estimated SPM = 60.648 * voltage2

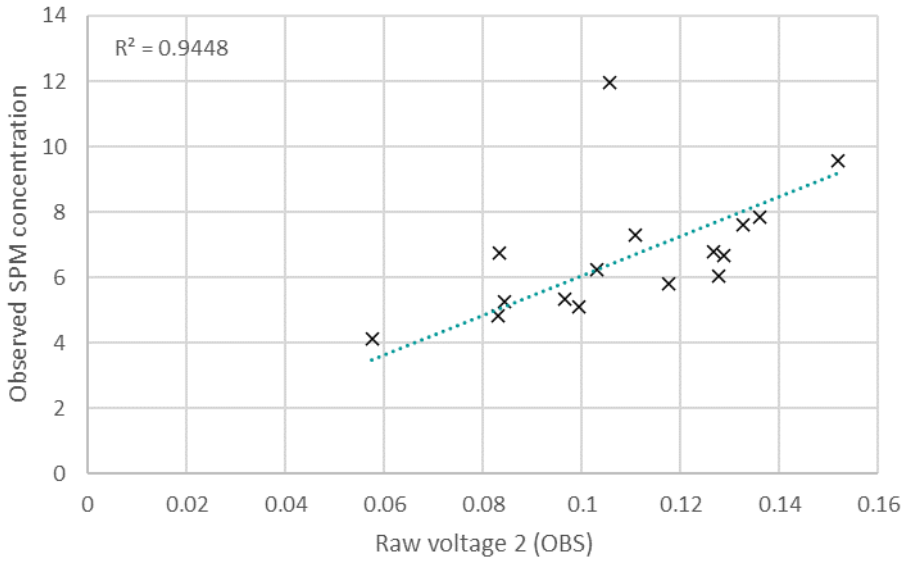

Figure 2.24. Linear regression between raw voltage values (OBS) and filtered SPM concentrations.

2.4.3.3. Meteorological conditions during water sampling and measurements

During the cycle of water measurements, the wave height decreased rather steadily from 63 cm up to 35 cm, while the period peaked at 19:00 (UTC) at 5.2 s and then decreased to 3.8 s (Figure 2.25). The wind speed increased from 2.5 m/s at 2pm to 7 m/s at around 2am. Regarding the wind direction, it first came from the south for about an hour before shifting to the south-west (Figure 2.26).

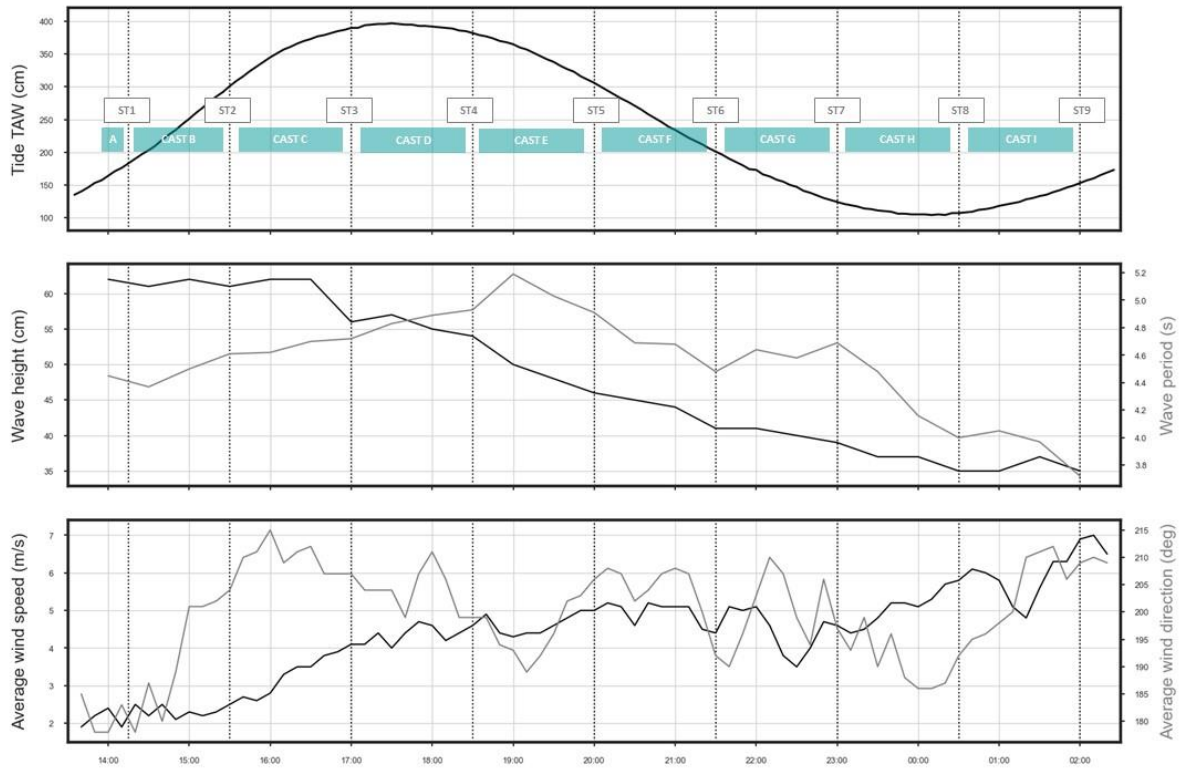

Figure 2.25. Wave height and period, wind speed and direction during the water column sampling and measurements performed during campaign ST2022/32.

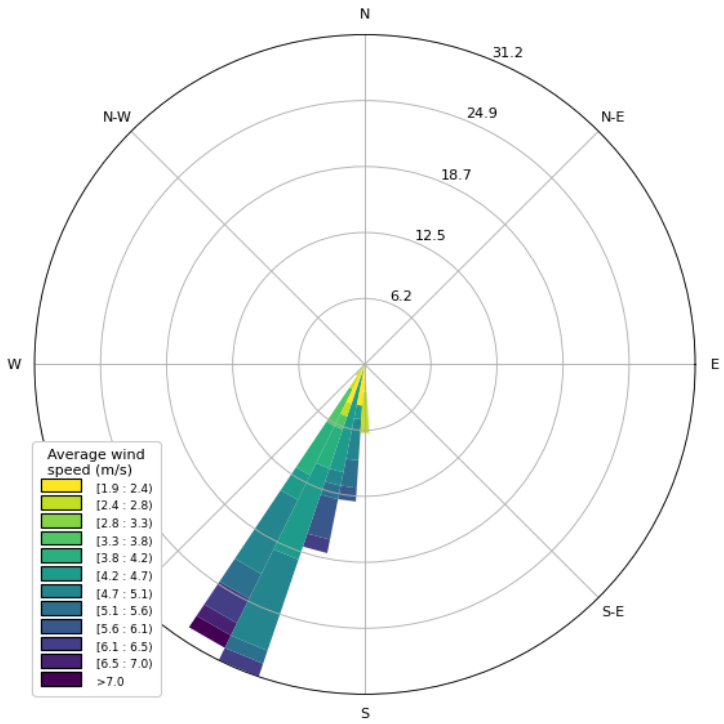

Figure 2.26. Wind speed and direction during the water column sampling and measurement performed during campaign ST2022/32.

2.4.3.4. ADCP survey

ADCP data were collected using the same procedure as detailed in section 2.4.1.4. The band width used was this time set to 0, following the settings of the ADCP, so the C value was calculated to be equal to -139.09 dB.

2.4.4. Tripod T002

The second tripod of the project could not be deployed, as initially planned during the ST2022/32 campaign, due to a defect in the functioning of the pop-up buoy.

2.4.5. Remote sensing

Because the in-situ data are sporadic both in space and time, this entails a risk of incorrectly interpreting their results, for example because fluctuations in the monitored parameters can be due to natural inter-annual and spatial variability or to the influence of a factor external to the aquaculture farm. To limit this underlying risk, it is essential to place these data in a wider context both spatially, in particular by understanding the variations in the patterns of turbidity and the changes in the extent of the turbidity maximum zone (TMZ), and temporally, by extending our analyses over a wider temporal range within the year than our field surveys allow. Moreover, satellite data also enable us to carry out an analysis of the area prior to the installation of the farm, when in-situ data are scarce or unavailable. The use of remote sensing imagery will therefore strengthen our results and provide us a better understanding of the impacts of the seafarm on the dynamics of suspended sediments (**task 2.B**).

A total of 260 satellite images from Landsat 7 (25), Landsat 8 (46), Landsat 9 (44), Sentinel 2A (72) and Sentinel 2B (73) were retrieved for 2022. These images were pre-processed for atmospheric correction (L2R). Out of these 260 images, only 64 were considered usable after verification of the cloud cover (Figure 2.27). When needed, sun glint correction and cloud masking were applied.
Suspended particulate matter and chlorophyll-a concentrations were derived from the selected images using ACOLITE (Python). The first parameter was calculated using the Nechad et al. (2009, 2010) (spm_nechad) algorithm while the second was calculated using the ocean chlorophyll blue/green ratio algorithm (chl_oc3) calibrated by Franz et al. (2015) (Vanhellemont & Ruddick, 2016).

The values of SPM concentrations and chlorophyll a were then extracted at four locations and compared with in-situ sampling or sensor data. In addition to that, images devoid of any trace of cloud were averaged using the raster calculator in QGIS 3.16.16 for each season. There were respectively 14, 7, 14 and 1 images for the winter (21/12-20/03), spring (21/03-20/06), summer (21/06-20/09) and autumn (21/09-20/12) seasons. The extent of the Yser river discharge plume was mapped based on visual observation on 11 satellite images (09/01; 02/02; 17/02; 27/02; 09/03; 26/03; 09/06; 08/08; 20/08; 29/11 and 16/12) (full lines on Figure 2.27).

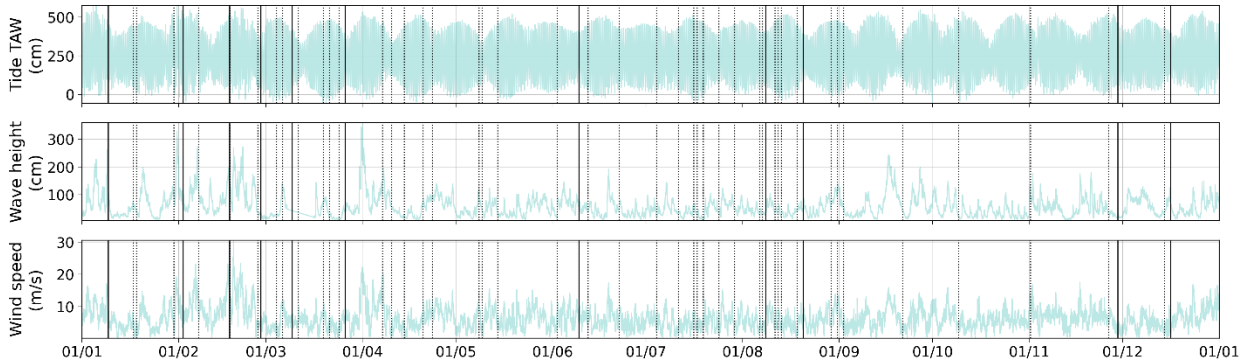

Figure 2.27. Comparison of the timing of the usable satellite images with the tides, wave and wind conditions. Full lines represent images where the plume of the Yser river was clearly visible.

L9/OLI 2022-01-09 10:40:17
ρ_s RGB

L8/OLI 2022-01-17 10:40:14
ρ_s RGB

S2B/MSI 2022-01-18 11:04:24
ρ_s RGB

S2A/MSI 2022-01-30 10:55:43
ρ_s RGB

L8/OLI 2022-02-02 10:40:10
ρ_s RGB

S2B/MSI 2022-02-07 11:02:44
ρ_s RGB

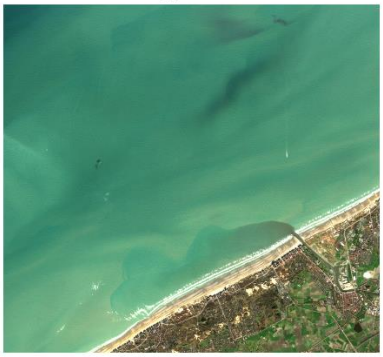

L9/OLI 2022-02-17 10:46:23
ρ_s RGB

L9/OLI 2022-02-26 10:40:06
ρ_s RGB

S2B/MSI 2022-02-27 11:00:43
ρ_s RGB

S2A/MSI 2022-03-04 11:04:50
ρ_s RGB

S2B/MSI 2022-03-06 10:54:55
ρ_s RGB

S2B/MSI 2022-03-09 10:59:38
ρ_s RGB

S2A/MSI 2022-03-11 10:54:48
ρ_s RGB

S2B/MSI 2022-03-19 10:57:31
ρ_s RGB

L9/OLI 2022-03-21 10:46:12
ρ_s RGB

S2A/MSI 2022-03-24 11:04:50
ρ_s RGB

S2B/MSI 2022-03-26 10:46:37
ρ_s RGB

L8/OLI 2022-04-07 10:39:49
ρ_s RGB

S2A/MSI 2022-04-10 10:53:42
ρ_s RGB

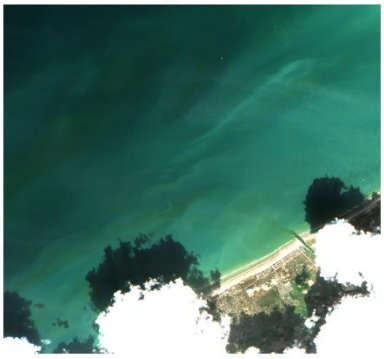

L8/OLI 2022-04-14 10:46:03
ρ_s RGB

S2A/MSI 2022-04-20 10:46:25
ρ_s RGB

S2A/MSI 2022-04-23 11:04:49
ρ_s RGB

L9/OLI 2022-05-08 10:45:53
ρ_s RGB

S2A/MSI 2022-06-02 10:56:27
ρ_s RGB

S2A/MSI 2022-06-09 10:46:29
ρ_s RGB

S2A/MSI 2022-06-12 10:59:33
ρ_s RGB

S2A/MSI 2022-06-22 10:59:36
ρ_s RGB

L9/OLI 2022-07-04 10:39:53
ρ_s RGB

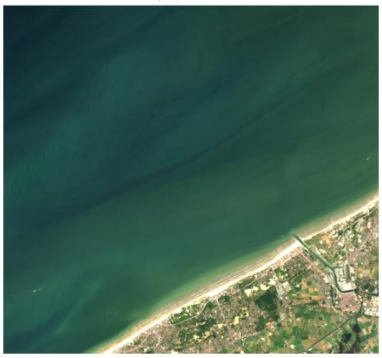

L9/OLI 2022-07-11 10:46:02
ρ_s RGB

S2B/MSI 2022-07-17 10:58:41
ρ_s RGB

L8/OLI 2022-07-19 10:46:29
ρ_s RGB

S2B/MSI 2022-07-24 10:46:25
ρ_s RGB

S2A/MSI 2022-07-29 10:54:44
ρ_s RGB

S2B/MSI 2022-08-06 10:58:40
ρ_s RGB

S2A/MSI 2022-08-08 10:46:32
ρ_s RGB

S2A/MSI 2022-08-11 10:56:31
ρ_s RGB

L9/OLI 2022-08-12 10:46:23
ρ_s RGB

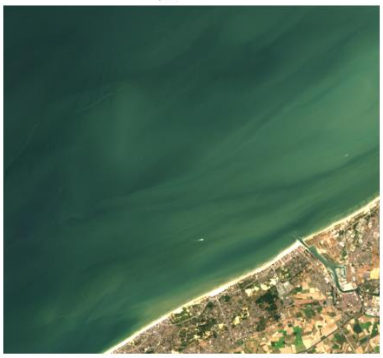

L8/OLI 2022-08-13 10:40:33
ρ_s RGB

S2A/MSI 2022-08-18 10:46:33
ρ_s RGB

L8/OLI 2022-08-20 10:46:45
ρ_s RGB

L8/OLI 2022-08-29 10:40:34
ρ_s RGB

S2A/MSI 2022-08-31 10:58:49
ρ_s RGB

S2B/MSI 2022-09-02 10:46:21
ρ_s RGB

L8/OLI 2022-09-21 10:46:51
ρ_s RGB

L8/OLI 2022-11-01 10:40:40
ρ_s RGB

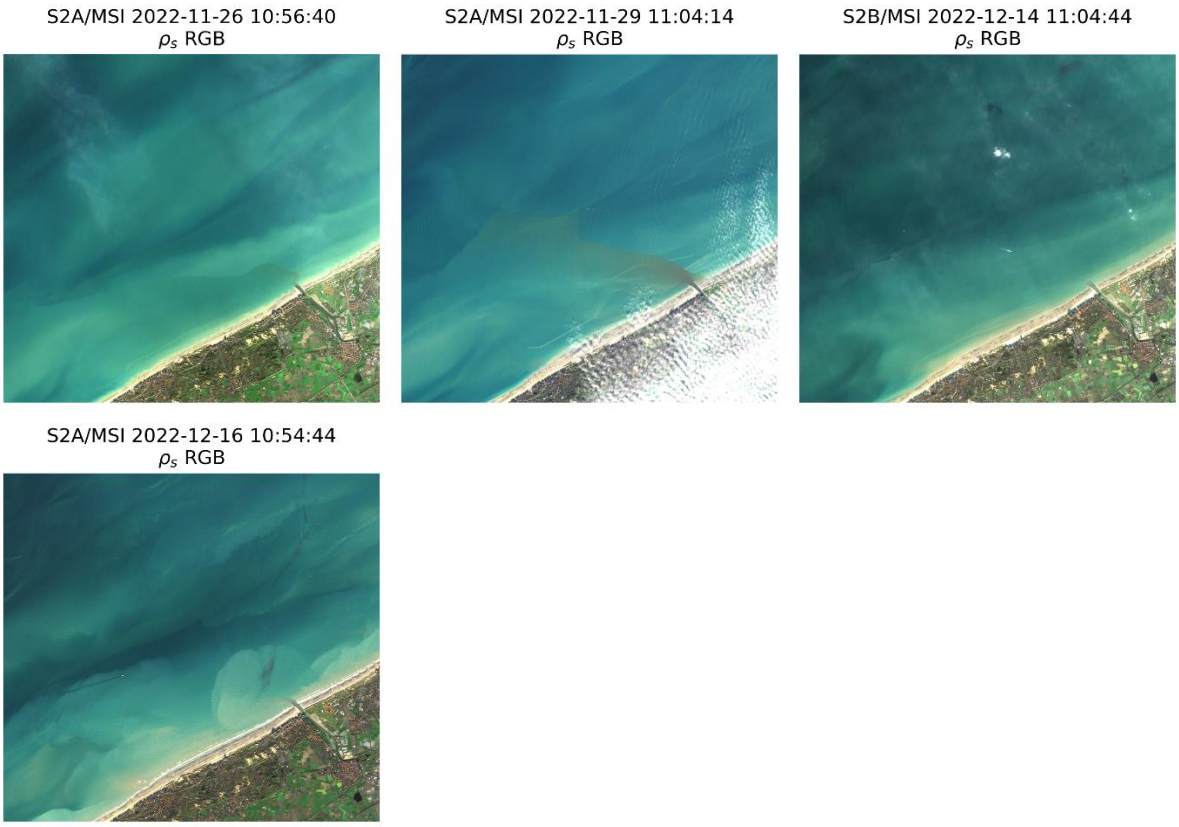

Figure 2.28. Satellite images from Landsat 7, 8, 9 and Sentinel 2 A and B usable in 2022.

3. RESULTS & DISCUSSION

3.1. IMPACTS ON THE SEABED INTEGRITY

3.1.1. Task 1.A: Assessing morphological changes

Calculating the difference between the multibeam survey conducted by RBINS in 2022 and the ones conducted by MDK in 2017 and 2018 reveals only small bathymetric differences in four years (Figure 2.7, Figure 3.1, Figure 3.2 and Figure 3.3). On the D01 transect, some accumulation seems to have occurred at around 500 m from the eastern safety limit of the aquaculture farm while a slight erosion can be observed between COD-825 and COD-2075 before accumulation is again observed between COD-2075 and COD-4275 (Figure 2.7 and Figure 3.1, left graph) but these changes are not exceeding 20 cm (Figure 3.1, right graph). In general, on this transect, accumulation occurs on the slopes, particularly at their foot, while erosion happens on the "plateaus". Over the entire surveyed area, the maximum loss and gain are of respectively 20 and 30 cm. Given a confidence limit of +/- 26 cm (see section 2.3.1.1), the differences are likely not significant. This seems to confirm the stability described in the literature for this area (Van Cauwenberghe, 1971; Mathys, 2010). Bathymetric differences in the other transects (A01-A14) are also not exceeding 20 cm and do not reveal any significant changes at this stage due to the limited extent of the multibeam survey in 2022 but are given in Figure 3.2 and Figure 3.3 for information.

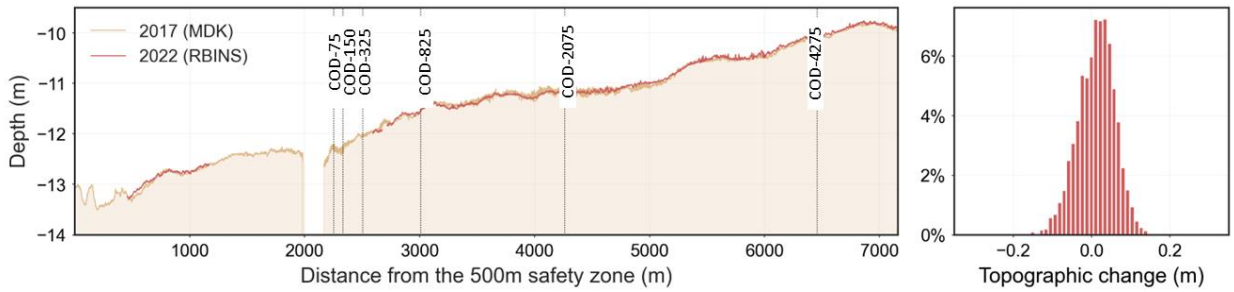

Figure 3.1. Evolution of the bathymetric transect D01 between 2017 and 2022.

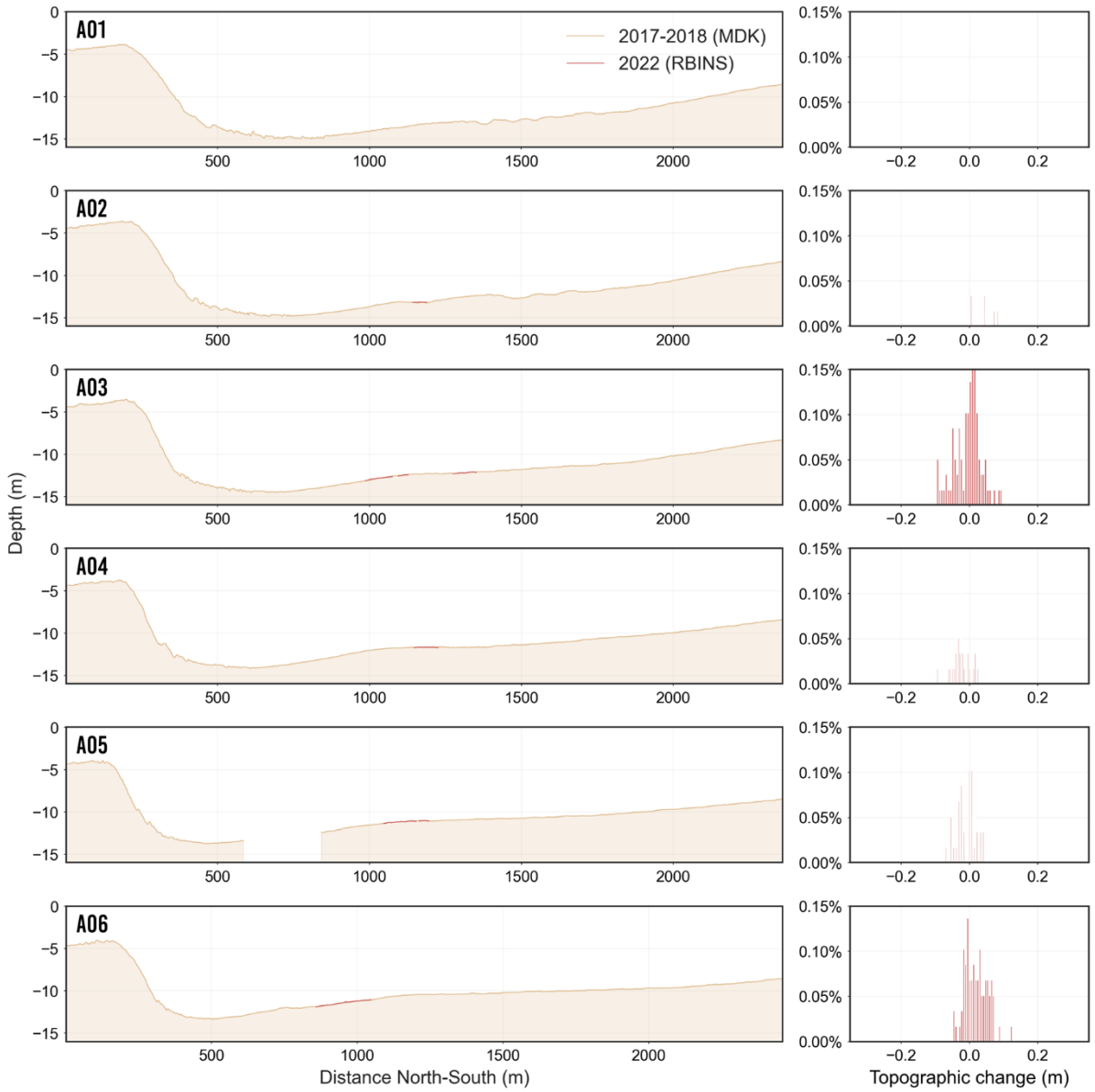

Figure 3.2. Evolution of the bathymetric transects A01 to A06 between 2017-2018 and 2022.

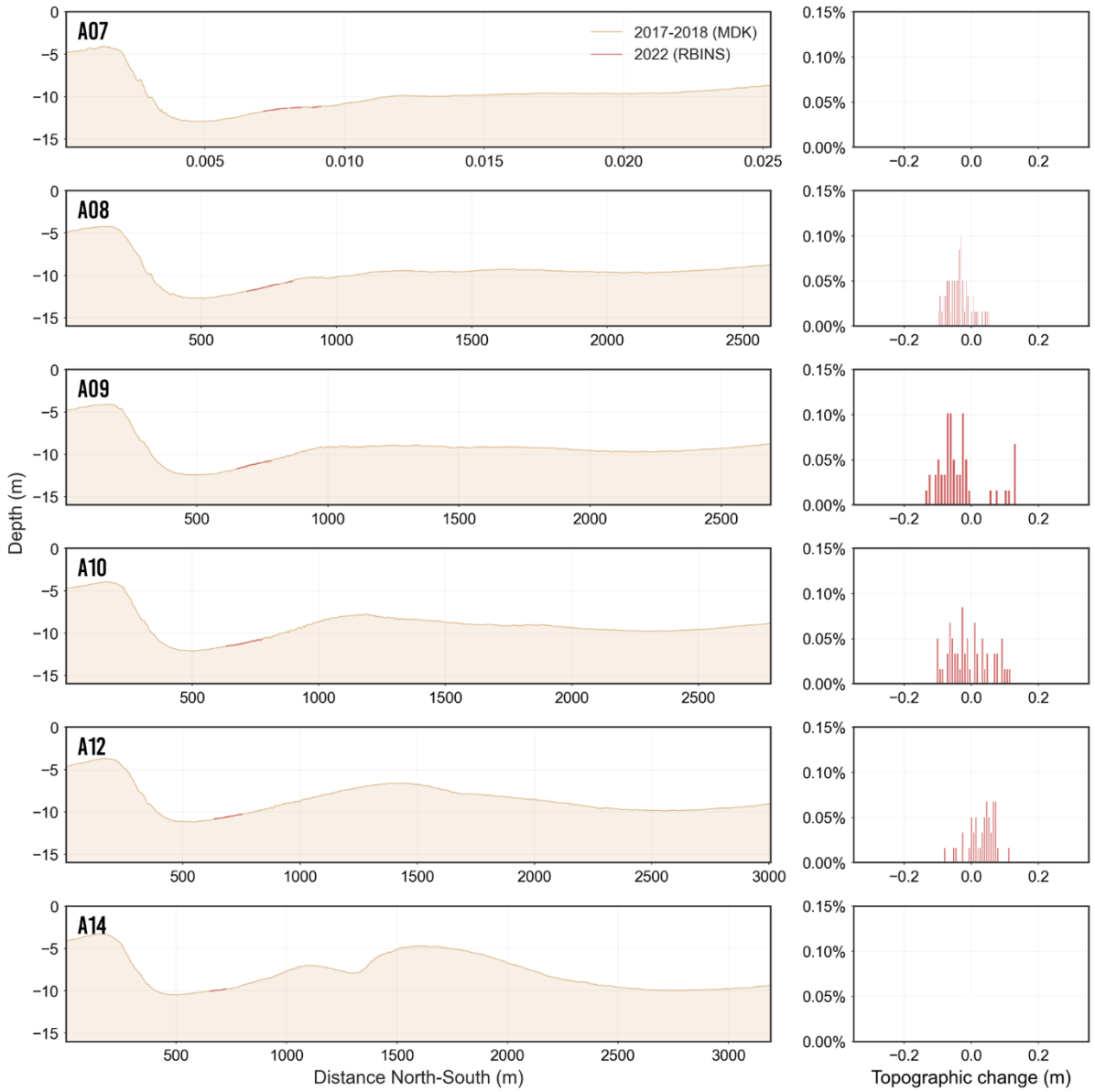

Figure 3.3. Evolution of the bathymetric transects A07 to A14 between 2017-2018 and 2022.

3.1.2. Task 1.B: Assessing changes in seabed composition

An enrichment in organic matter or calcium carbonate associated to the recently developed aquaculture farm would certainly result in an increase in their concentration in surficial sediments compared to values in the deeper layers. Here, with the exception of COD-150 and COD-4275 for which it was positively correlated (r = 0.51, p = ***), the organic matter content was not found to be significantly correlated with depth for most locations (Figure 3.4, Figure 3.5). There is a slight increase in the first layer for COD-825, COD-2075 and COD-4075 but given their distance to the aquaculture farm, this increase is likely due to natural variability (Figure 2.14). Although at the general level, no significant correlation was found between calcium carbonate content and depth, at the individual level however, both were positively correlated for every station with the exception of COD-325 which was negatively correlated (r = -0.30, p = **). Organic matter and calcium carbonate contents were significantly positively correlated at both general (r = 0.56, p = ***) and individual levels, with the exception of COD-825. These two parameters were both significantly positively correlated with the

clay, silt and coarse sand fractions and negatively correlated with the fine and medium sand fractions (Figure 3.5).

The organic matter content was similar across all sampling locations, being between 3.21 % (COD-4275) and 5.20 % (COD-325), while the calcium carbonate content was between 7.08 % and 7.85 % for all stations except for COD-825 (9.40 %) and COD-4275 (4.82 %).

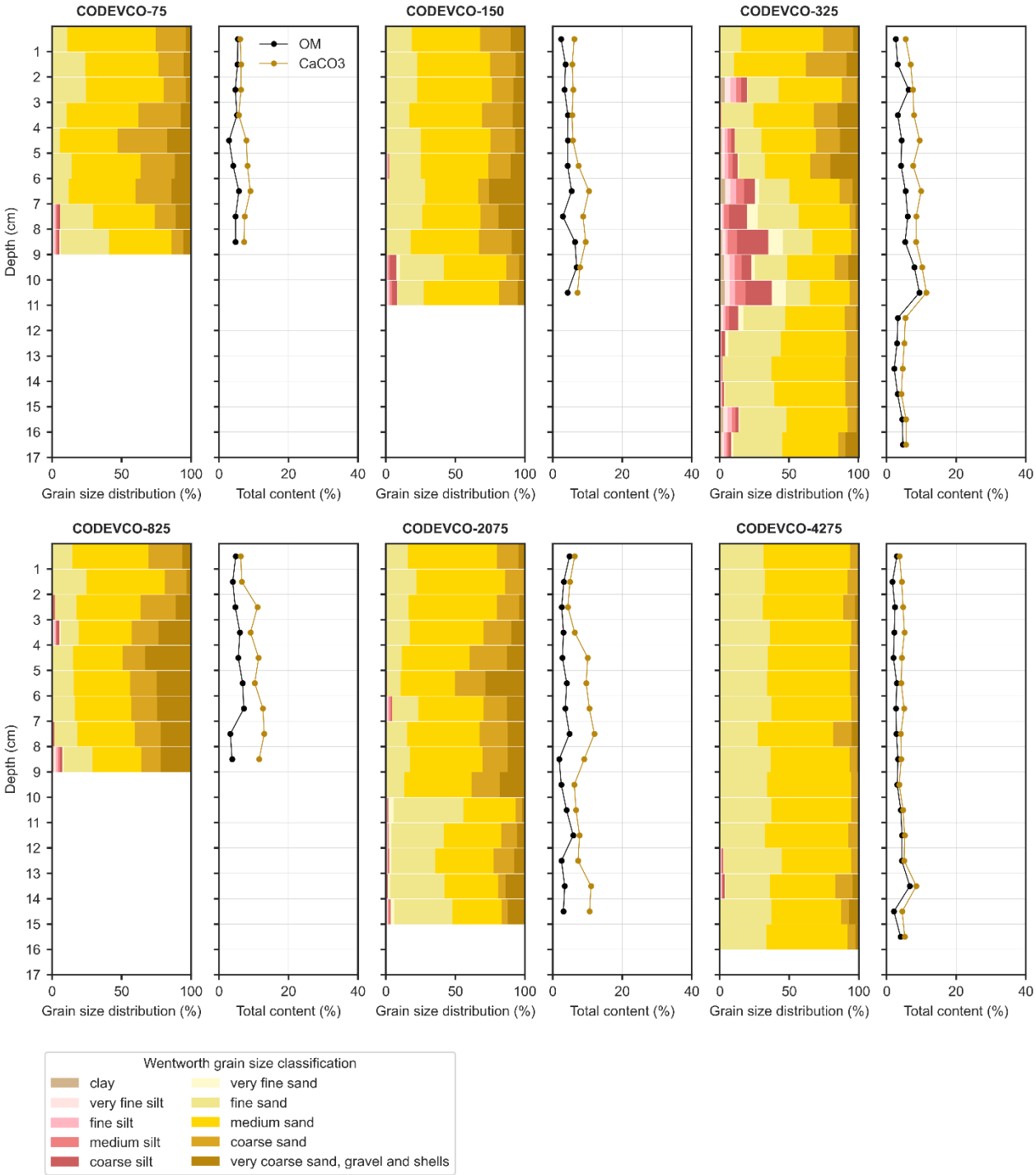

Figure 3.4. Evolution in depth of the grain size distribution, organic matter and calcium carbonate contents of the box core samples taken during campaign ST2022/32.

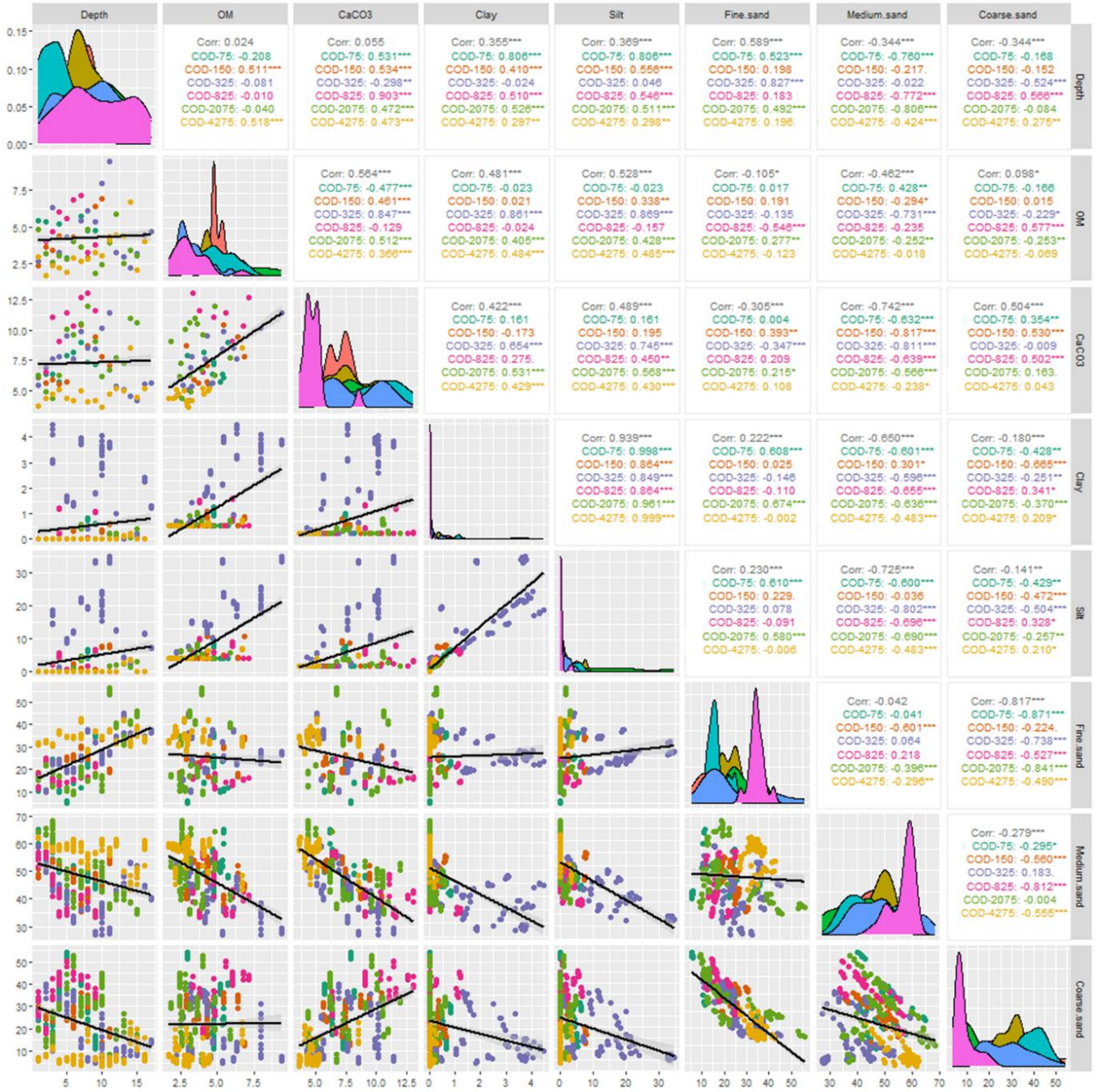

Figure 3.5. Pairwise Spearman rank correlations between depth, organic matter content, calcium carbonate content, fractions of clay, silt, fine sand, medium sand and coarse sand, overall and for every box core sample taken during campaign ST2022/32. This shows how variables are correlated with each other at every station and over the entire dataset.

3.1.3. Task 1.C: Assessing changes in seabed roughness and type

A decrease in the grain size of sediments below or in the vicinity of aquaculture farms was observed at other sites and would have a significant impact on the benthic ecosystem. In our study, the clay content was very low at all locations (between 0.02% on average at COD-4275 and 1.77% at COD-325) (Table 3.1). Similarly, the silt content was between 0.29% and 2.02% on average for all stations except COD-325 which has 13.65% silt on average with a maximum between 8 and 11 cm depth (up to 34.74%) (Figure 3.4). All locations contain in majority medium sand (250 to 500 µm following the Wentworth grain size distribution). Medium sand accounts for 40.73 % (COD-325) and 56.60 % (COD-

4275) on average of the sediment samples. The coarse fraction of the samples (coarse sand and above) varied between 26.79 % and 36.60 % for all stations except for two: COD-325 (16.00 %) and COD-4275 (8.61 %), which displayed the lowest value. Being constituted at 91% by fine to medium sands, the latter station is the most homogeneous one, both visually (Figure 2.11) and based on the lab measurements (Figure 3.4). Comparatively, station COD-825, which is also located in an area classified as "sand" according to the EMODnet Geology map (Figure 2.10) and "coarse sand (gravelly sand to sandy gravel)" according to the multibeam backscatter survey (Figure 2.6), contains a higher fraction of coarse sand and above (36.60 %) and is even the station with the highest average coarse fraction. Both COD-2075 and COD-4275, were classified as "gravelly muddy sand" following the multibeam survey while they were classified (as for all the stations sampled in this report) as "sand" on the EMODnet Geology map. The differences might be explained by the difference in scale (the EMODnet seabed substrate map was produced on a 1/250 000 scale).

Table 3.1. Minimum, mean and maximum values of the different particle size classes and organic matter and calcium carbonate content for the six locations sampled and sliced each centimeter during campaign ST2022/32.

STATISTICS		COD-75	COD-150	COD-325	COD-825	COD-2075	COD-4275
Clay content (%)	*Min*	0.00	0.00	0.00	0.00	0.00	0.00
	Mean	**0.21**	**0.15**	**1.77**	**0.27**	**0.12**	**0.02**
	Max	0.83	0.62	4.48	1.22	0.60	0.25
Silt content (%)	*Min*	0.00	0.00	0.00	0.00	0.00	0.00
	Mean	**1.70**	**1.94**	**13.65**	**2.02**	**1.04**	**0.29**
	Max	6.39	7.94	34.74	6.55	4.68	3.44
(Very) fine sand content (%)	*Min*	5.26	16.75	10.19	11.63	9.09	26.86
	Mean	**18.61**	**23.88**	**27.97**	**16.68**	**23.15**	**34.49**
	Max	36.38	34.45	45.02	25.25	56.02	42.58
Medium sand content (%)	*Min*	40.26	35.57	27.23	33.53	34.51	43.21
	Mean	**49.58**	**46.98**	**40.73**	**44.44**	**48.91**	**56.60**
	Max	64.92	55.12	59.30	57.01	68.39	62.46
Coarse sand and above (%)	*Min*	10.96	12.53	4.89	17.89	5.22	3.36
	Mean	**29.89**	**27.05**	**16.00**	**36.60**	**26.79**	**8.61**
	Max	54.37	35.95	39.97	50.50	52.71	22.94
OM content (%)	*Min*	2.92	2.38	2.19	3.28	1.84	1.68
	Mean	**4.69**	**4.64**	**5.20**	**5.09**	**3.29**	**3.21**
	Max	5.74	6.88	9.43	7.16	5.88	6.67
CaCO3 content (%)	*Min*	5.71	5.56	4.22	6.28	4.34	3.62
	Mean	**7.08**	**7.85**	**7.71**	**9.40**	**7.84**	**4.82**
	Max	9.01	10.39	11.44	13.03	11.95	8.53

Compared with the data collected with a Van Veen grab by UGent in 2021 and 2022, the clay and silt content values (in %) are similar and show a decrease in concentration with distance from the aquaculture farm (Figure 3.6). The fine and very fine sand contents show higher values in 2022, but follow the same trend, with higher concentrations near zone C, then lower around 2000 m, before increasing again with distance. Medium sand values are lower in 2022 while coarse sand values are comparable, with the exception of the ones measured at point COD-4275, which are lower in 2022 (8.6 to 19.4%) compared to 2021 (24.4 to 29.4%).

In general, it appears that the samples collected using the box core are comparable to those obtained from a Van Veen, with the exception of the medium sand values, which are much lower using the box core. This underlines the fact that the sampling method might play a role in the differences observed in the results, as already highlighted by Kint et al. (2020).

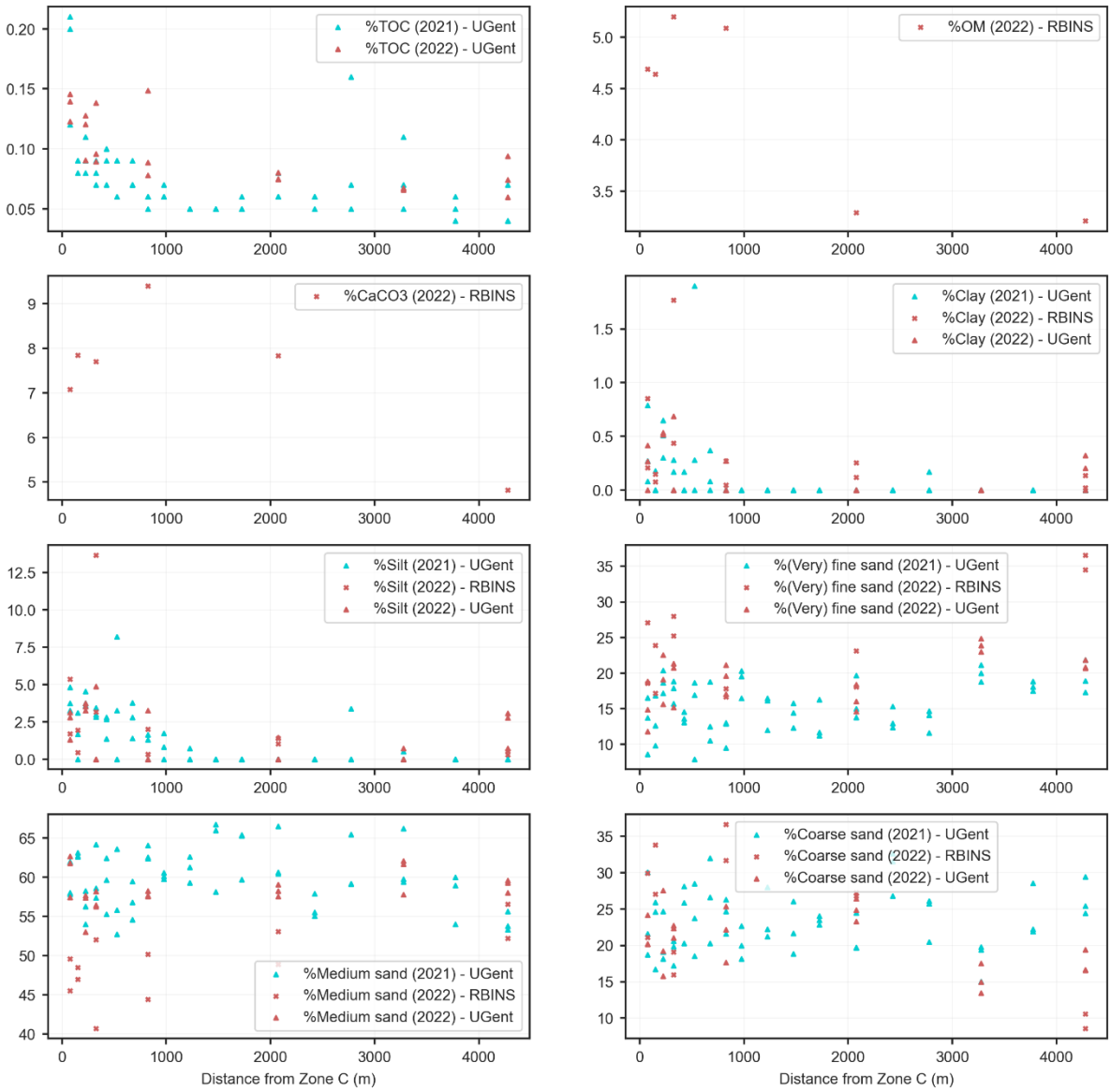

Figure 3.6. Content (in %) of TOC, OM, CaCO3, clay, silt, fine sand, medium sand and coarse sand in the sediment samples taken between 0 and 4275 m away from Zone C in 2021 and 2022.

3.2. IMPACTS ON THE HYDROGRAPHICAL CONDITIONS

3.2.1. Task 2.A: Assessing changes in hydrodynamics and sediment transport

3.2.1.1. Hydrographic conditions during campaign ST2022/19

During the sampling in August 2022, both the salinity and temperature measured by the CTD were very stable throughout the water column and with the tides, remaining at around 34.5 psu and 21.8°C. Oxygen concentration remained constant at around 6.5 mg/l throughout the water column and did not vary greatly from one cast to another, although the highest oxygen concentration values were found at high tide (6.8 mg/l) and the lowest at low tide (6.2 mg/l). For casts A to H (low tide and rising tide), there seemed to be a very slight gradient with depth, with a lower oxygen concentration at higher depth, but no gradient was visible at high or decreasing tides (casts I-M).

3.2.1.2. Hydrographic conditions during the deployment of tripod T001

From 20 August to 6 October 2022, the temperature decreased almost constantly from 22 to 16°C, while salinity varied more markedly, fluctuating between 34.7 and 32.2 psu, with a peak of 31.5 on 20 September (Figure 3.7).

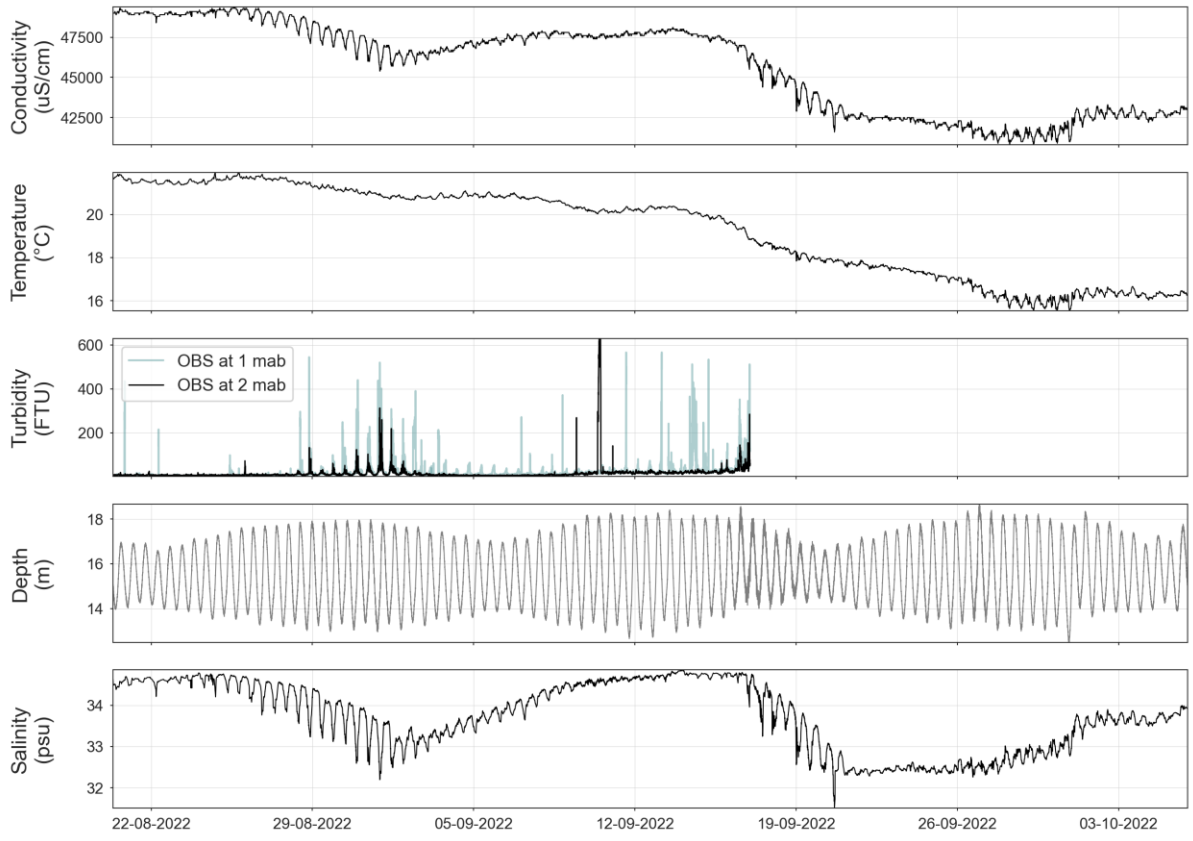

Figure 3.7. Evolution of the conductivity, pressure, temperature, turbidity and salinity during the deployment of tripod T001.

3.2.1.3. Hydrographic conditions during campaign ST2022/32

In December, most of the temperature and salinity profiles also showed a well-mixed water column with almost no variation around 7°C and 34 psu, which is a little lower than the value measured in summer (34.5 psu). Oxygen concentration remained constant at around 8.5 mg/l throughout the

water column (against 6.5 mg/l in summer). Except for temperature, which showed slightly lower values at low tide and slightly higher at high tide, no significant variation could be observed between the different casts.

3.2.1.4. Hydrodynamic conditions during campaign ST2022/19

In August, the current was maximum at high tide (0.8 m/s) and low tide (0.6 m/s) and was minimum at slack tide (0-0.2 m/s) (Figure 3.8). Five periods with a higher level of suspended material could be noted, these occurred at low tide, just after high and slack tide. During low tide, the current mainly flowed towards the WSW (250°N) while after slack tide, it shifted towards the NE (50°). These predominant current directions are also represented in the tidal ellipse (Figure 3.9) and correspond to the models in the Codevco concession (Figure 3.10). Except during slack tide, when the shift occurred, the direction of the current remained very constant. While the direction of the current seemed uniform over the entire area at high tide, it showed a more complex pattern at low and slack tides. In terms of direction, there was no significant difference throughout the water column. In terms of magnitude, the modelled current at COD-TC-E ranged from 0.2 (bottom) to 0.4 m/s (surface), which corresponds to the values measured with the hull-mounted ADCP. It ranged from 0.07 to 0.2 m/s at slack tide and 0.16 to 0.57 m/s at high tide (Figure 3.11 and Figure 3.12). The ADCP data therefore seem to confirm the model.

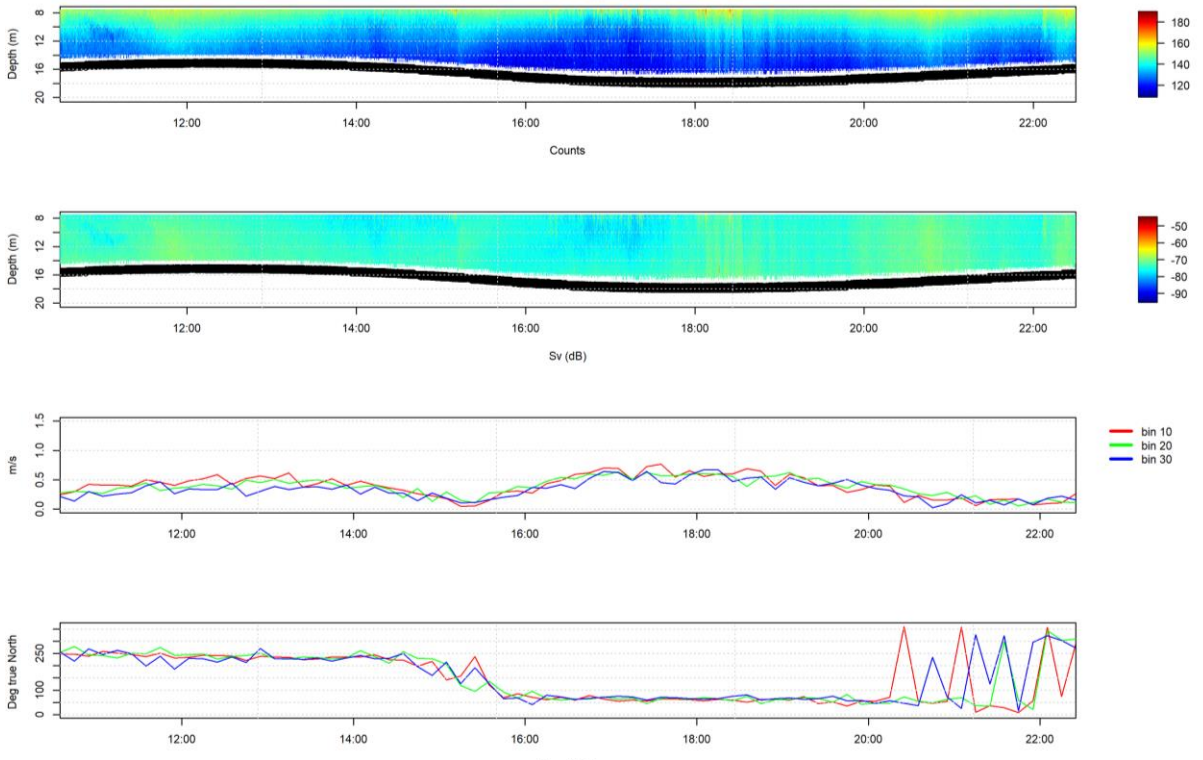

Figure 3.8. Evolution of the acoustic intensity (counts) and volume backscatter (Sv) profiles of the four beams and of the magnitude and direction of bins 10, 20 and 30 through time during the water measurements carried out during campaign ST2022/19.

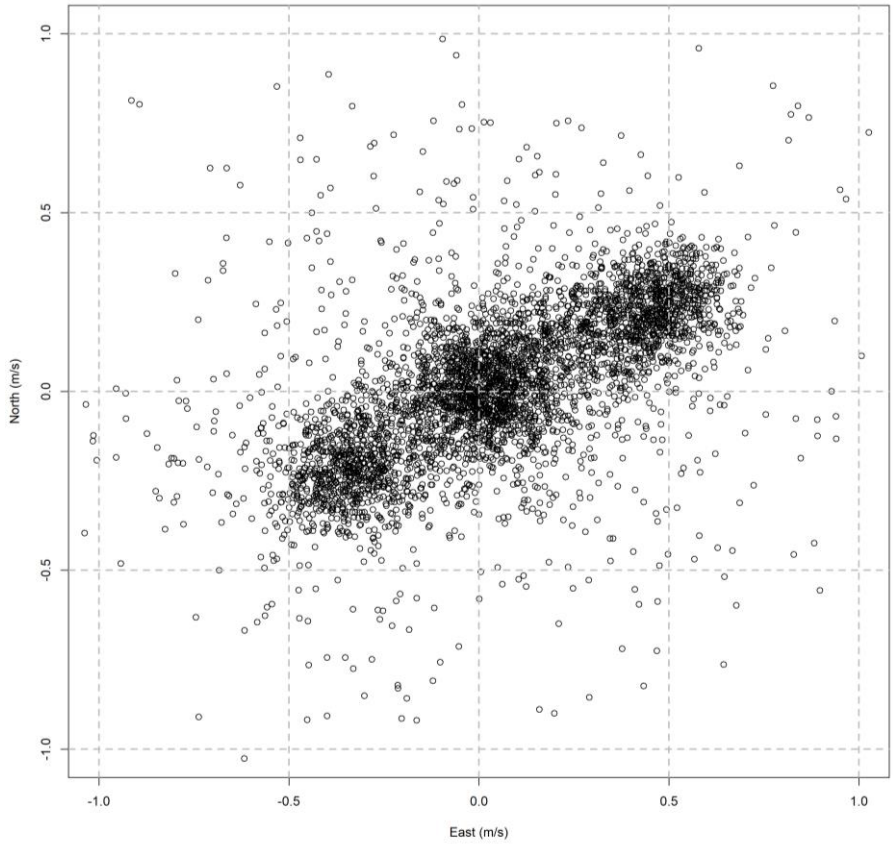

Figure 3.9. Tidal ellipse over the entire water column during the full tidal cycle performed during campaign ST2022/19.

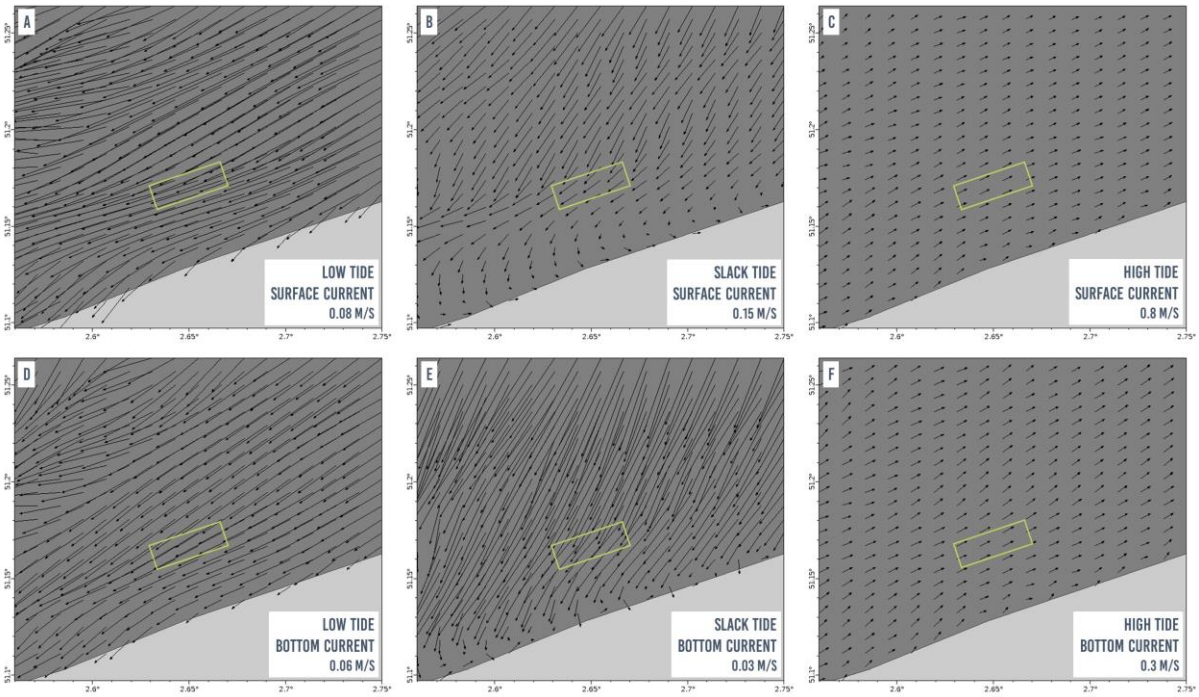

Figure 3.10. Modelled surface and bottom currents at low, slack and high tides around the Codevco aquaculture zone (in yellow) on 20/08/2022. Data are courtesy of the Marine Forecasting Center (RBINS).

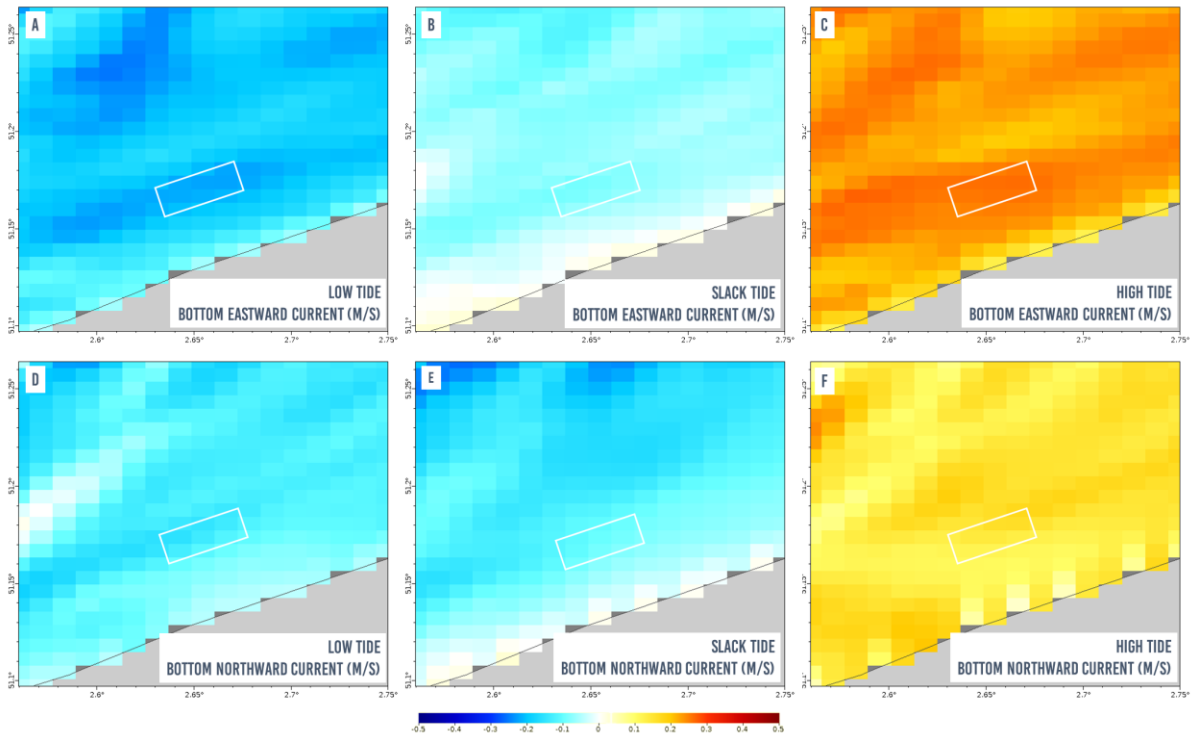

Figure 3.11. Modelled bottom current magnitude at low, slack and high tides around the Codevco aquaculture zone (in white) on 20/08/2022. Data are courtesy of the Marine Forecasting Center (RBINS).

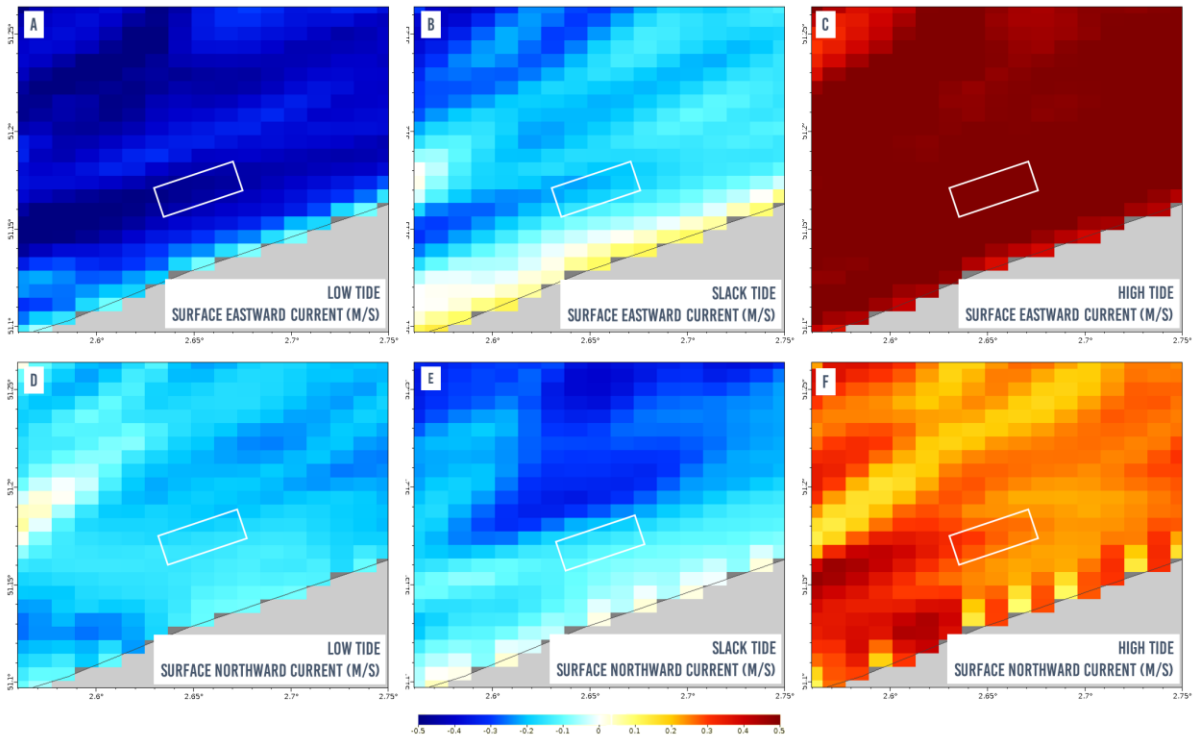

Figure 3.12. Modelled surface current magnitude at low, slack and high tides around the Codevco aquaculture zone (in white) on 20/08/2022. Data are courtesy of the Marine Forecasting Center (RBINS).

3.2.1.5. Hydrodynamic conditions during the deployment of tripod T001

The backscatter profiles (Figure 3.13) clearly show the presence of three spring tide cycles (the first from around 27 August to 4 September, the second from 7 to 17 September and the third from 21

September to 2 October), which correspond to the Moon phases (New Moon: 27 August, 25 September and Full Moon: 10 September). These periods of high backscatter are separated by a few days when it was at its minimum. The third spring tide show a comparatively higher backscatter, propagating higher into the water column. A few punctual events where the higher backscatter was more homogeneous throughout the whole water column can also be noticed (see black dotted lines on Figure 3.13 below), these seem to correspond to a combination of high wave height and/or period and strong North wind conditions (Figure 2.20). The predominant current is the Eastern one reaching between 0.5 (neap tide) and 1 m/s (spring tide) at high or low tide. During the entire deployment, velocities appear to be lower at low tide than at high tide, only exceeding 0.75 m/s occasionally. In comparison, the Northern current was weaker (around 0.25 m/s maximum) and fluctuated less during the deployment of the tripod (Figure 3.14). The tidal ellipse corresponds to that observed during the cycle of water measurements in August. It underwent no change in direction throughout the water column and the current velocities only slightly decreased with increasing depth (Figure 3.15).

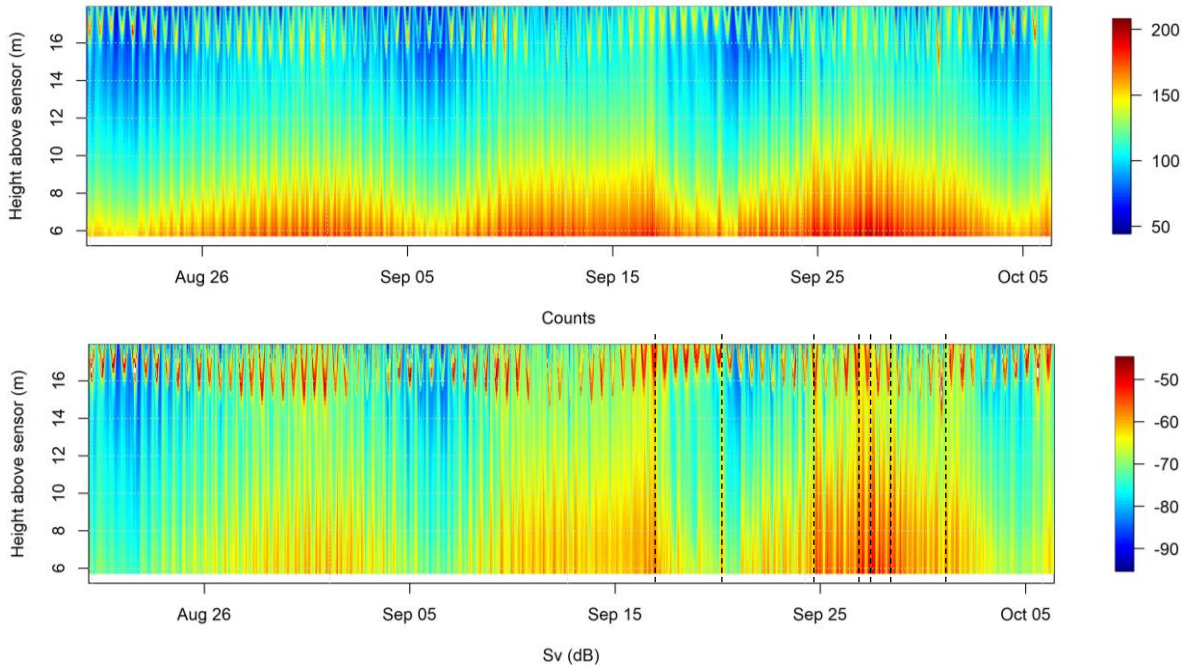

Figure 3.13. Evolution of the acoustic intensity (counts) and volume backscatter (Sv) profiles of the RDI ADCP mounted upward-looking on the tripod T001 at 2 mab. The dotted lines highlight noticeable backscattering events.

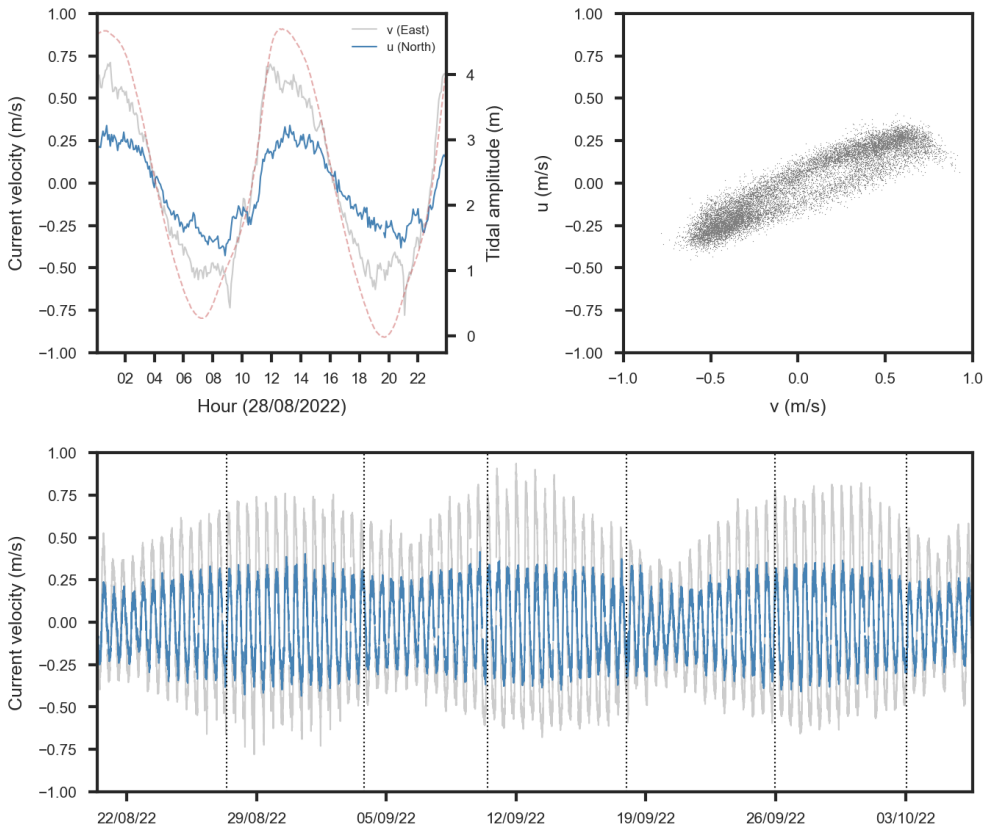

Figure 3.14. RDI ADCP-derived Eastern (v) and Northern (u) current velocities over a tidal cycle and throughout the full T001 tripod deployment, and the tidal ellipse.

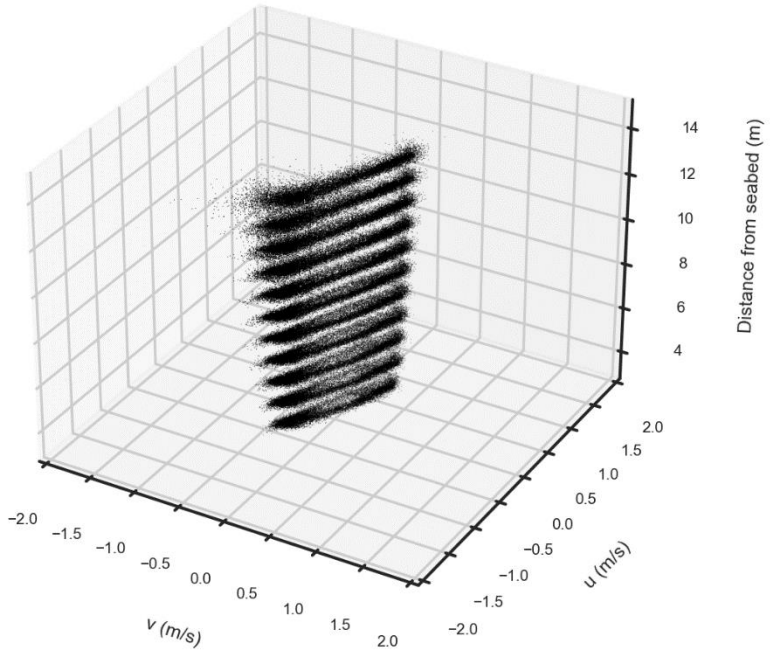

Figure 3.15. RDI ADCP-derived tidal ellipse throughout the water column during the deployment of tripod T001.

3.2.1.6. Hydrodynamic conditions during campaign ST2022/32

On Figure 3.16, it can be observed that the current was maximum at high tide (0.8 m/s) and low tide (0.6 m/s) and was minimum at slack tide (0-0.2 m/s). These results are in complete agreement with

those obtained during campaign ST2022/19 in August 2022. However, in comparison with the data collected in summer, the data of this campaign generally show a much lower backscattering with values ranging from -75 to -90 dB compared to -60 to -70 dB in August. On Figure 3.16, three periods with a higher backscattering can be noticed, these occurred at slack and low tides and the backscattering tended to show higher values close to the bottom, a trend that wasn't as obvious in August. The graph also showed the presence of some noise, supposedly due to the propellers of the ship. The direction of the current was similar to that observed during campaign ST2022/19 and during the deployment of the first tripod with current flowing towards the NE (50°) at high tide and shifting at slack tide to reach a WSW (250°) direction during low tide.

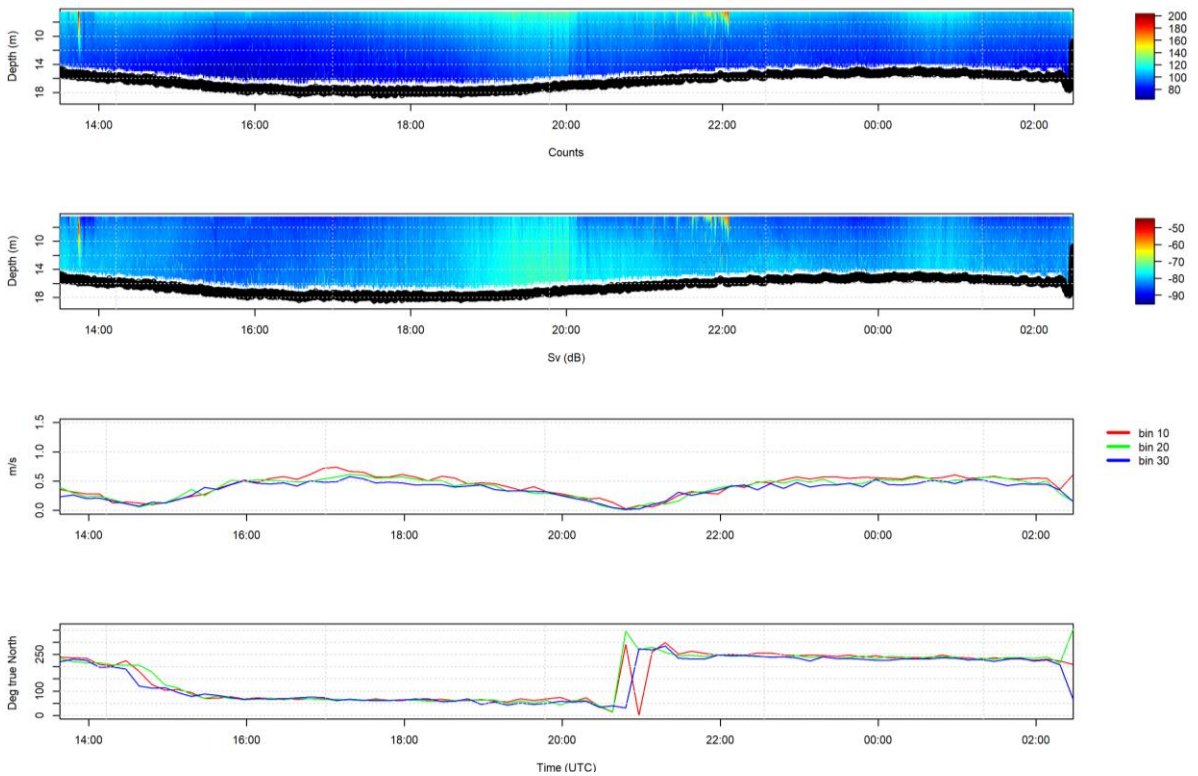

Figure 3.16. Evolution of the acoustic intensity (counts) and volume backscatter (Sv) profiles of the four beams and of the magnitude and direction of bins 10, 20 and 30 through time during the water measurements carried out during campaign ST2022/32.

3.2.2. Task 2.B: Assessing changes in turbidity and SPM concentration

3.2.2.1. Turbidity and SPM concentration during campaign ST2022/19

The SPM concentration on 20 and 21 August 2022 ranged from 2.07 mg/l to 5.9 mg/l (Table 3.2). The maximum was reached during ebb tide, more or less two hours before low tide, and was measured in the surface samples, whereas the trend for the rest of the tide was for the deep samples to be more concentrated than the surface samples (Figure 3.24). The SPM concentration was negatively correlated with the tide (r = -0.55, p = **) (Figure 3.25), confirming that high concentrations are found at lower tide, that is especially true for values measured in bottom samples. SPM was also found to be correlated with PON (r = 0.55, p = **), particularly in surface samples. The turbidity measured from the Hach turbidity meter showed values between 0.27 and 1.59 FTU (Table 3.2).

3.2.2.2. Turbidity and SPM concentration during the deployment of tripod T001

The turbidity measured at 2 mab is slightly lower than that measured at 1 mab (average of 15.62 FTU compared to 23.23 FTU at 1 mab) (Figure 3.17), even though both the minimum and maximum measured closer to the bottom are lower (0.64 – 566 FTU at 1 mab compared to 4.5 - 630 FTU at 2 mab). These values are much higher than those derived from the water samples taken during campaign ST2022/19 (0.27 – 1.59). Increases in turbidity are measured with both Seapoint sensors between the 29th of August and the 4th of September (Spring Tide 1) as well as between the 7th and 17th of September (Spring Tide 2) and are confirmed by the increased total volume concentration measured by the LISST-200x during spring tide (Figure 3.7). During about 3 hours and a half on the 10th of September, a remarkable peak of turbidity can be noticed at 2 mab (up to 630 FTU) while the turbidity at 1 mab remains at around 20 FTU.

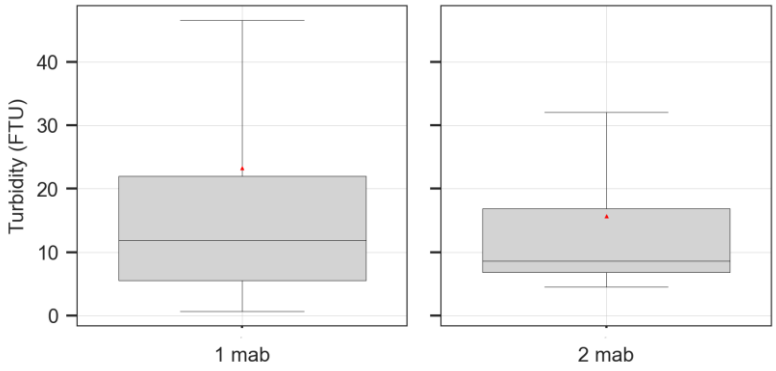

Figure 3.17. Boxplots of the turbidity measured on tripod T001 at 1 and 2 mab. The red triangles indicate the mean values.

3.2.2.3. Turbidity and SPM concentration during campaign ST2022/32

The SPM concentration on the 16-17th of December 2022 ranged from 3.47 mg/l to 12.8 mg/l, the latter being more than double the maximum value measured in August 2022 on the Eastern side of the aquaculture. However, most of the data of December are around the same range, except for two surface samples at slack (mean of 9.59 mg/l) and low tides (mean of 11.96 mg/l) which are above these values. With the exception of these two sampling, the surface and bottom samples show almost identical values, indicating that the water column is largely very well mixed, while bottom samples tended to show higher values than at the surface in summer (Figure 3.28). Like in campaign ST2022/19, the SPM concentration was negatively correlated with the tide (r = -0.54, p = *) with lower values of SPM measured around high tide. In this campaign, however, there is no significant correlation between SPM and PON or any other parameter except for the Hach measurements (r = 0.66, p = **). The OBS mounted on the rosette also generally show a well-mixed water column, with the exception of the first cast which shows lower values at the bottom (Figure 3.18).

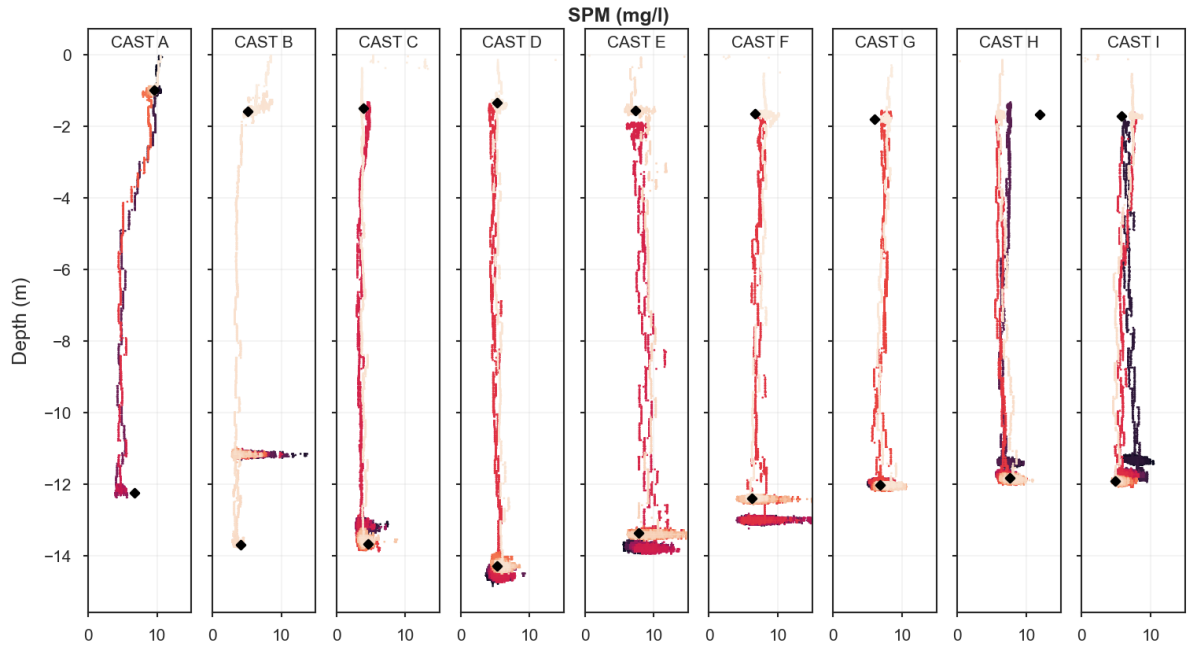

Figure 3.18. Evolution of the estimated SPM concentration (mg/l) with depth for every CTD cast carried out during campaign ST2022/32. The colors indicate different profiles and the black diamonds indicate the values of the filtrated water samples.

3.2.2.4. Analysis of the Landsat-derived SPM concentrations

The satellite-derived and in situ observed SPM concentrations (from samples and turbidity sensors placed on a buoy managed by the Colruyt Group within the farm) are rather consistent and follow the same trends (Figure 3.19), which supports the validity of the results obtained by remote sensing. According to these images, the maximum SPM concentration is reached in February and September while the minimum one is found in late March and June. Although to a lower extent, it also decreases in December and January, especially at COD-TC-W.

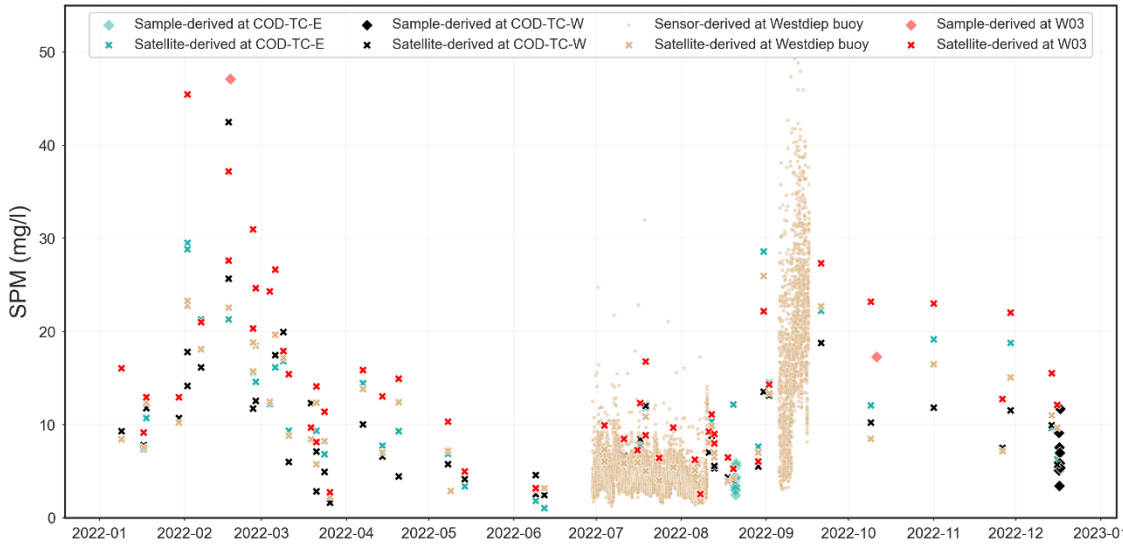

Figure 3.19. Evolution of the observed and estimated SPM concentration at COD-TC-E, COD-TC-W, Westdiep buoy and W03 in 2022.

Spatially, the concentration of SPM is highest close to the coast as well as at around 4 km north-east of the concession, along the Stroom bank (Figure 3.20). The coastal zone with the highest SPM

concentration extends further offshore in winter, until it reaches the Southern limit of the farm, then decreases in spring and summer. As there is only one image that can be used in autumn, no conclusions can really be drawn at this stage. Both Figure 3.19 and Figure 3.20 show that COD-TC-W naturally displays a lower SPM concentration throughout the year compared to COD-TC-E.

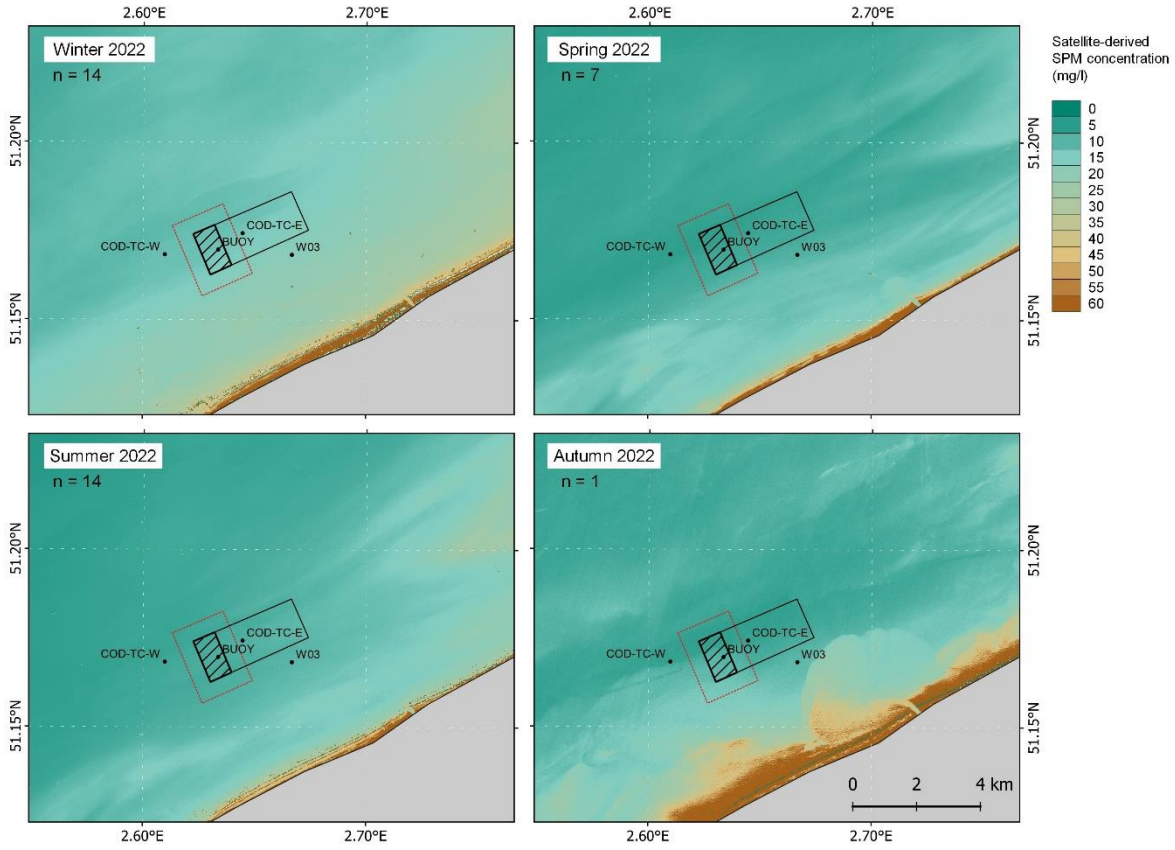

Figure 3.20. Satellite composites of seasonally-averaged SPM concentration (mg/l) in 2022.

3.2.2.5. Analysis of the Landsat-derived chlorophyll a concentrations

As for the SPM concentrations, the satellite-derived and observed (sample) concentrations of chlorophyll a follow the same trends (Figure 3.21). According to these images, the maximum concentration in chlorophyll a is reached in March and April (spring phytoplankton bloom), July and late August/early September (late summer bloom). The minimum chlorophyll a concentration is reached in June, when the SPM concentration is also at its minimum (Figure 3.19) as well as in winter. This peak in chlorophyll is also found around the first of September at 1 mab by the fluorometer mounted on the tripod T001 (see section 2.4.2.3).

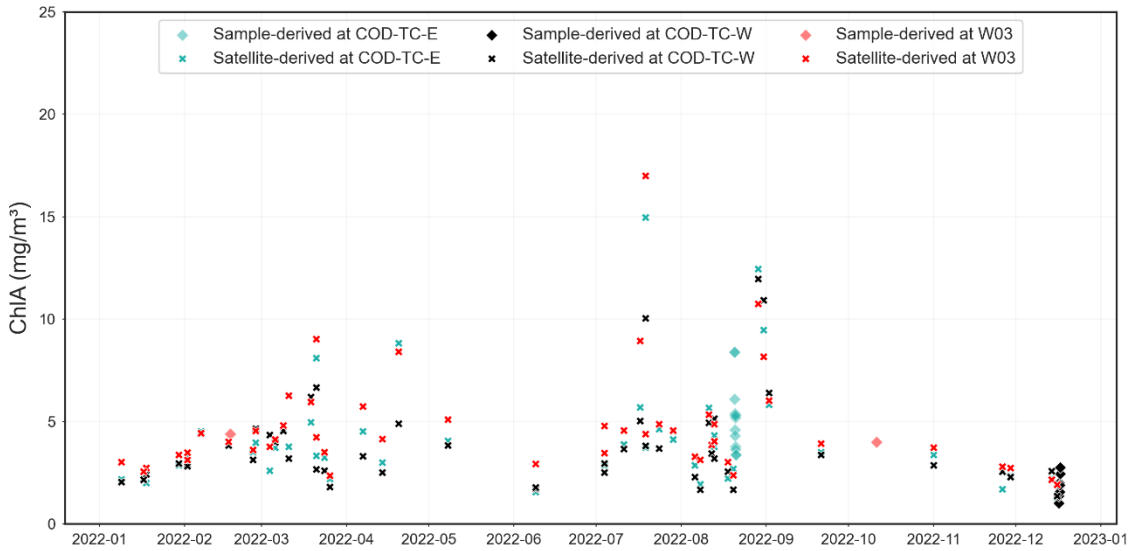

Figure 3.21. Evolution of the observed (sample and sensor) and satellite-derived chlorophyll a concentration at COD-TC-E, COD-TC-W and W03 in 2022.

In spring, the chlorophyll a concentration show a sharp increase near the coast and at around two kilometers south-west of the farm (Figure 3.22). In summer, this zone of higher concentration extends further offshore and to the north-east of the farm, while the zone to the south-west is no longer as visible. In winter, the distribution of chlorophyll a concentration appears to be more homogenous throughout the entire study area. In general, the highest concentration is found at W03 while the lowest is generally found at COD-TC-W (Figure 3.21, Figure 3.22).

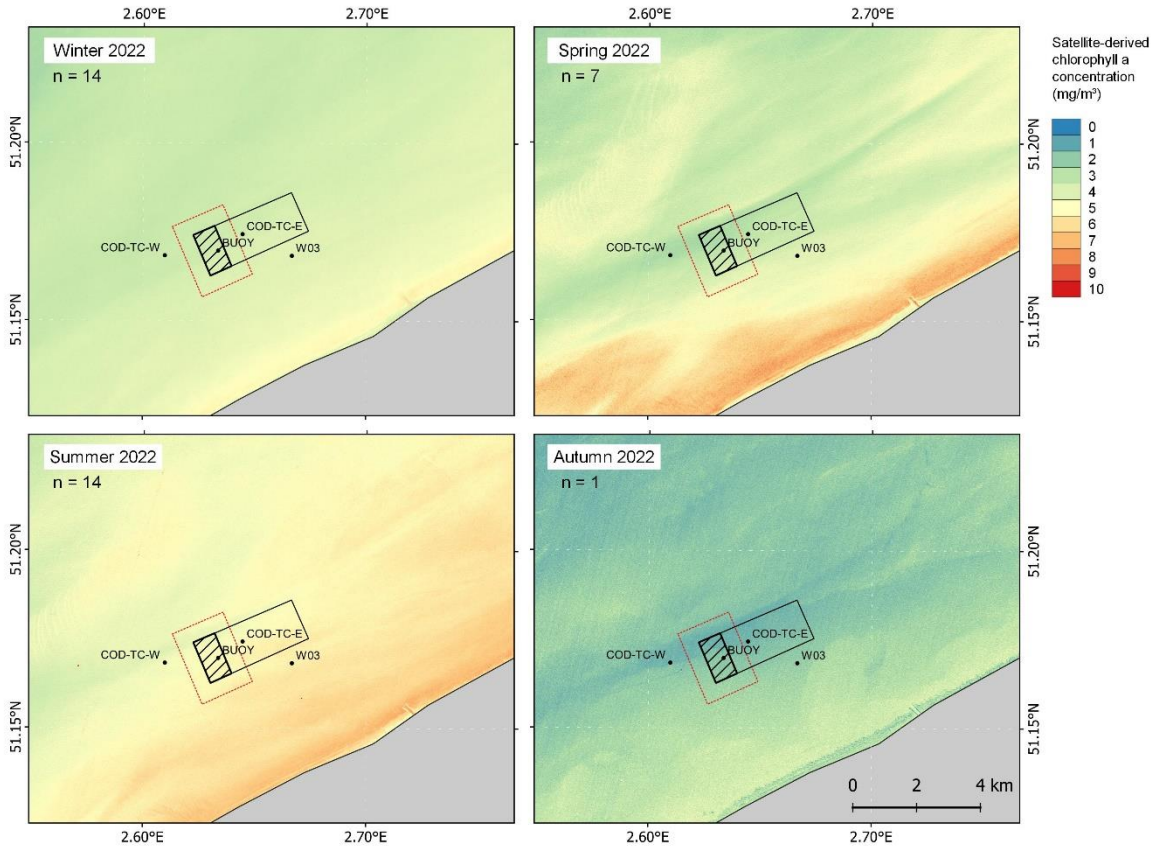

Figure 3.22. Satellite composites of seasonally-averaged chlorophyll a concentration (mg/m³) in 2022.

3.2.2.6. Impact of the Yser river on the aquaculture site

On eleven of the 64 images used in 2022, the plume of the Yser river could be seen (Figure 3.23). On the basis of these observations, it was found that, under certain conditions, the Yser can have an impact extending as far offshore as the aquaculture zone. The next step will be to correlate the occurrence of these events with hydrological and meteorological parameters and to understand how this stronger influence of the Yser alters the concentration and type of particles as well as the hydrographical conditions in the study site.

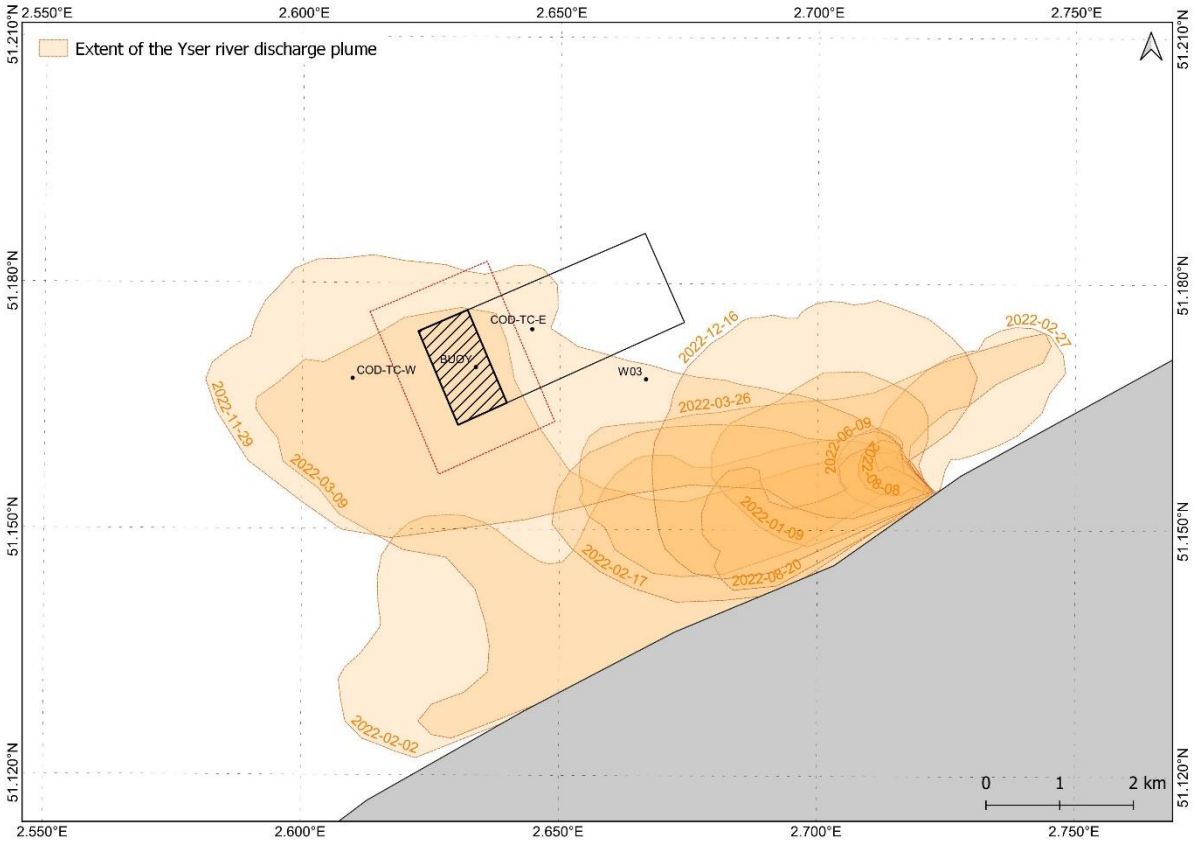

Figure 3.23. Thematic map showing the extent of the discharge plume of the Yser river based on visual observation on eleven satellite images from 2022.

3.2.3. Task 2.C: Assessing changes in particle size and composition

3.2.3.1. Content in POC, PON, TEP, chlorophyll and phaeopigments during campaign ST2022/19

POC and PON values follow the same trends and are correlated to each other (r = 0.61, p = ***), with the highest values measured during ebb or low tide, reaching 0.61 and 0.08 mg/l respectively. The lowest values (0.41 and 0.05 mg/l respectively) are measured just after low tide as well as during high tide. Concentrations of chlorophyll A and B and phaeopigments A are correlated to each other (Figure 3.25) and are higher at the surface than in the bottom samples, except at ebb tide, a few hours before low tide, which is a trend opposite to that of the SPM. Only the concentration in phaeopigments A is correlated with the tide (r = -0.43, p = *), with higher concentrations found when the tide is lower. The measured concentrations of phaeopigments B are always below the detection limit (< 0.05 mg/m³). The TEP, on the other hand, seems to follow the variations in the SPM concentrations apart from a little before high tide, when there is more TEP at the surface than at the bottom. The TEP values are between 0.79 and 1.97 µg eq Xg/ml. TEP concentrations are negatively correlated with concentrations

in Chla, Chlb and phaeopigments A in surface samples (Figure 3.25) but are positively correlated with the ChlB concentrations in bottom samples (r = 0.69, p = **).

Table 3.2. Minimum, mean and maximum values of the concentrations in SPM, Hach, TEP, Chla, Chlb, PhaeoA, POC and PON measured during campaign ST2022/19.

STATISTICS	SPM (MG/L)	HACH (FTU)	POC (MG/L)	PON (MG/L)	CHLA (MG/M^3)	CHLB (MG/M^3)	PHAEOA (MG/M^3)	TEP (µG EQ XG/ML)
Min	2.07	0.275	0.406	0.049	1.97	0.148	0.021	0.79
Mean	**4.03**	**1.15**	**0.5**	**0.06**	**4.35**	**0.31**	**0.046**	**1.36**
Max	5.9	1.59	0.612	0.078	8.4	0.48	0.085	1.97
Std dev	1.00	0.29	0.05	0.01	1.54	0.10	0.01	0.29

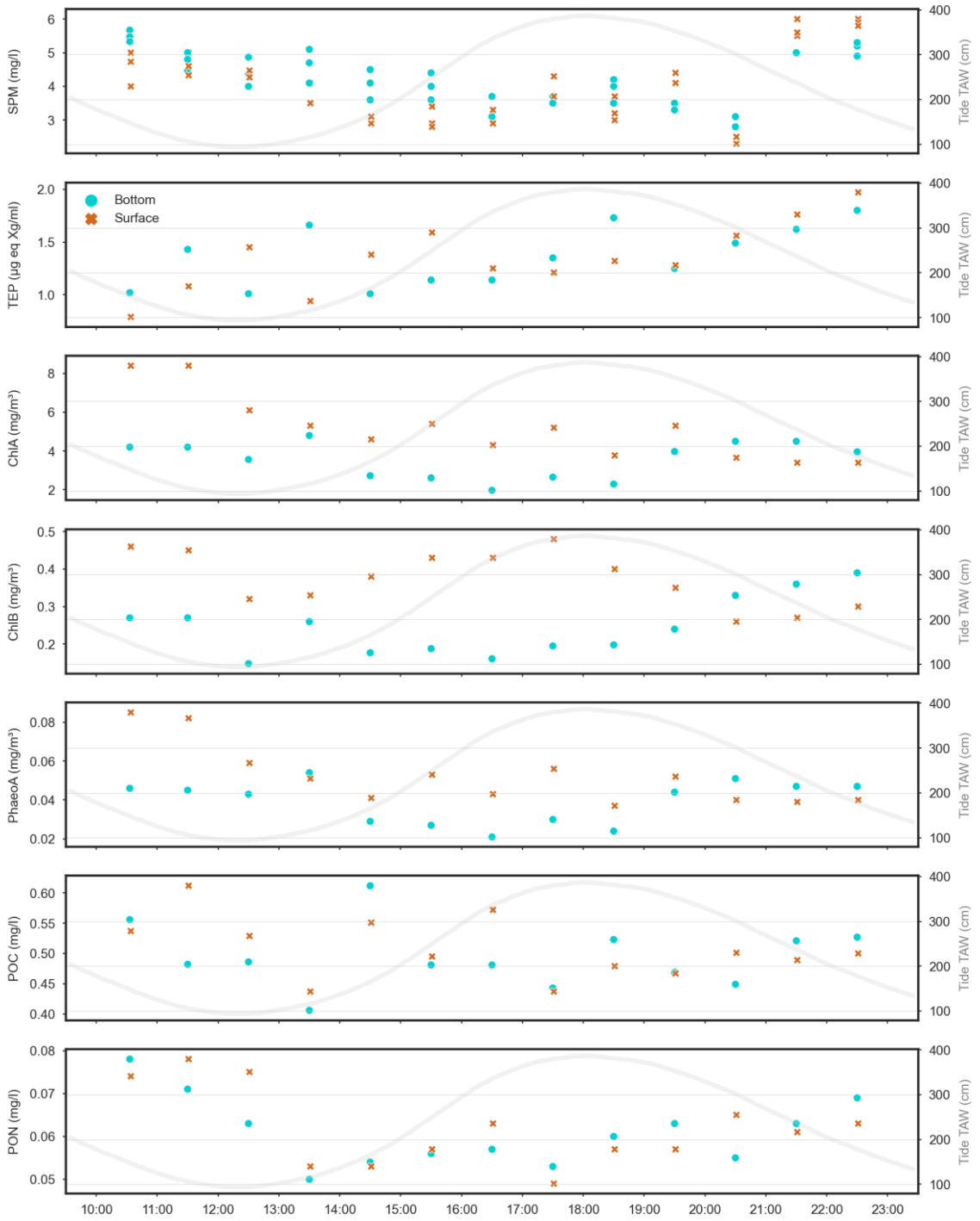

Figure 3.24. Evolution of the concentrations in SPM, TEP, Chla, Chlb, PhaeoA, POC and PON with tides and depth during campaign ST2022/19.

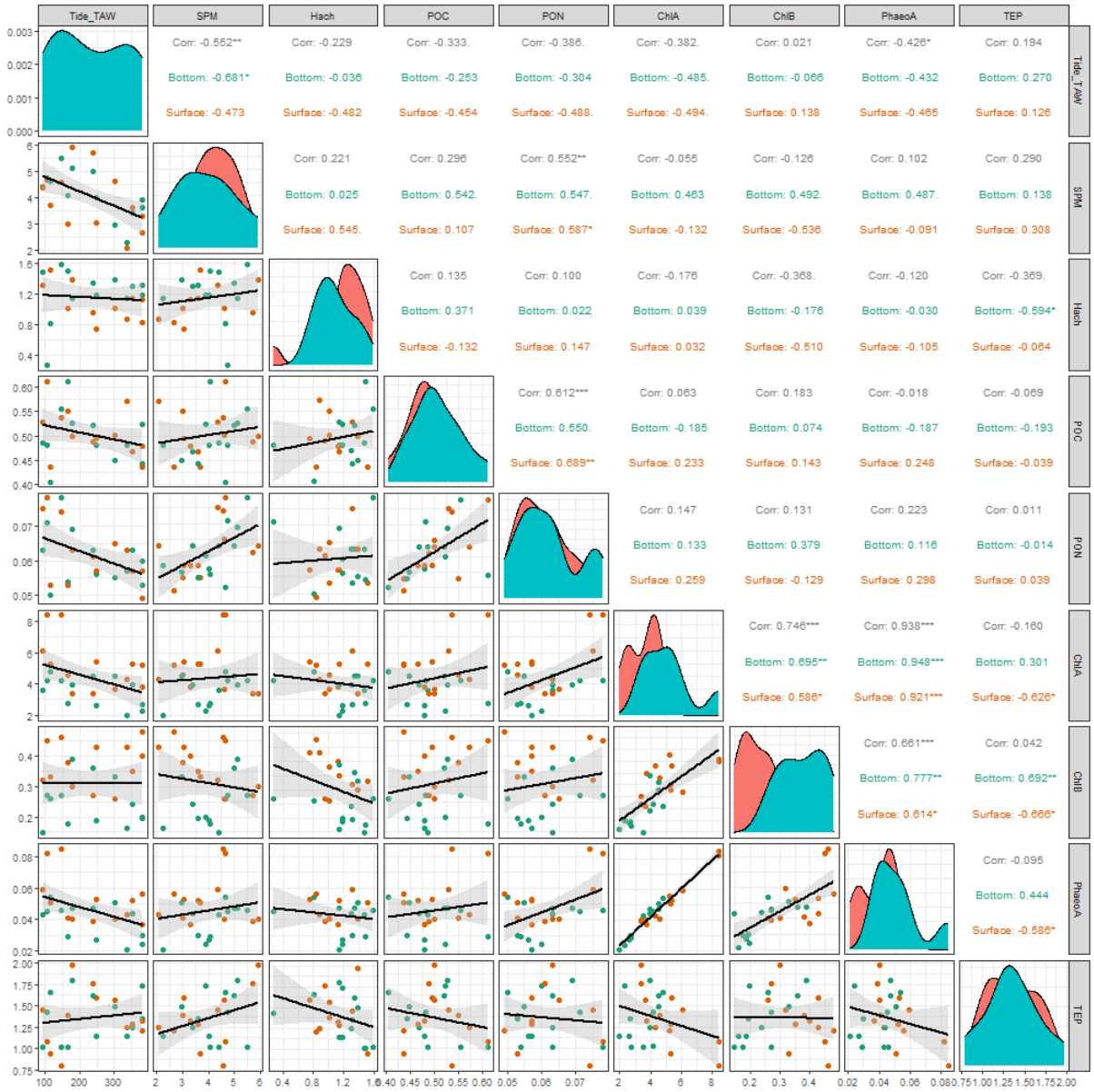

Figure 3.25. Spearman rank correlations between the tides, Hach values and concentrations in SPM, TEP, Chla, Chlb, PhaeoA, POC and PON measured during campaign ST2022/19.

3.2.3.2. Comparison with data from the Belgian part of the North Sea in August

When the ratios of POC:SPM, PON:SPM and TEP:SPM acquired during this campaign are compared to data collected during the same month since 2005 at other locations of the Belgian part of the North Sea, these values are well within the trends observed in the BPNS and show no deviation from the values observed at W05 and W08, for example. Only two points show a slightly higher POC:SPM and PON:SPM ratio than the rest. This suggests that no major changes in POC, PON, TEP or SPM caused by the aquaculture have been detected at this time (Figure 3.26).

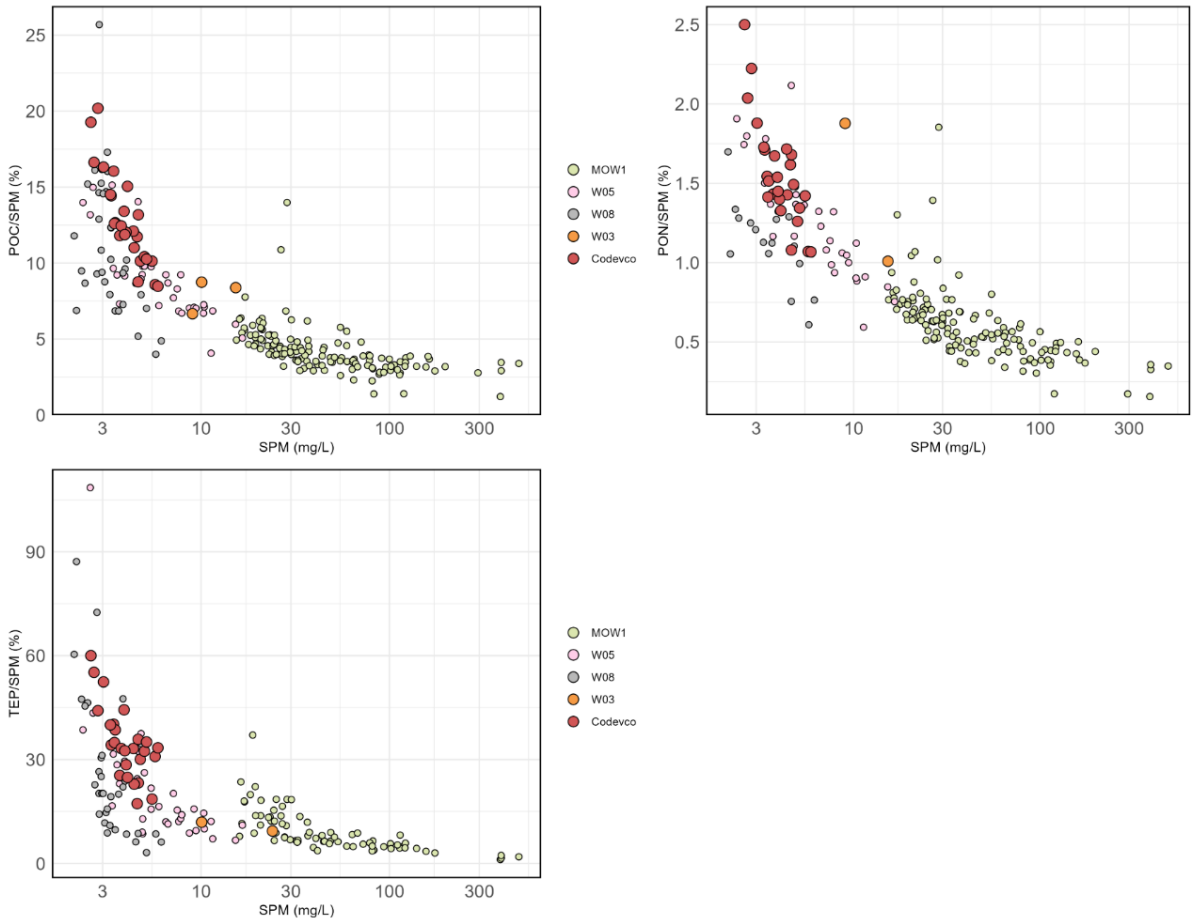

Figure 3.26. Comparison of the data collected on the Eastern side of the Codevco aquaculture during campaign ST2022/19 with ratios of POC:SPM, PON:SPM and TEP:SPM collected in August since 2005 at other locations of the North Sea (the graphs are courtesy of Saumya Silori).

3.2.3.3. Content in chlorophyll during the deployment of tripod T001

Following the cycles of the tides, the concentration in Chlorophyll a (ppb) has two peaks per day at high tide (Figure 3.27). Over the course of the deployment, the concentration of chlorophyll reaches its maximum around the first of September, which corresponds to the “spring tide” period discussed earlier. That day is also the day when the highest total volume concentration was recorded by the LISST-200x, suggesting that the increase in particle volume would be due to the late summer phytoplankton bloom.

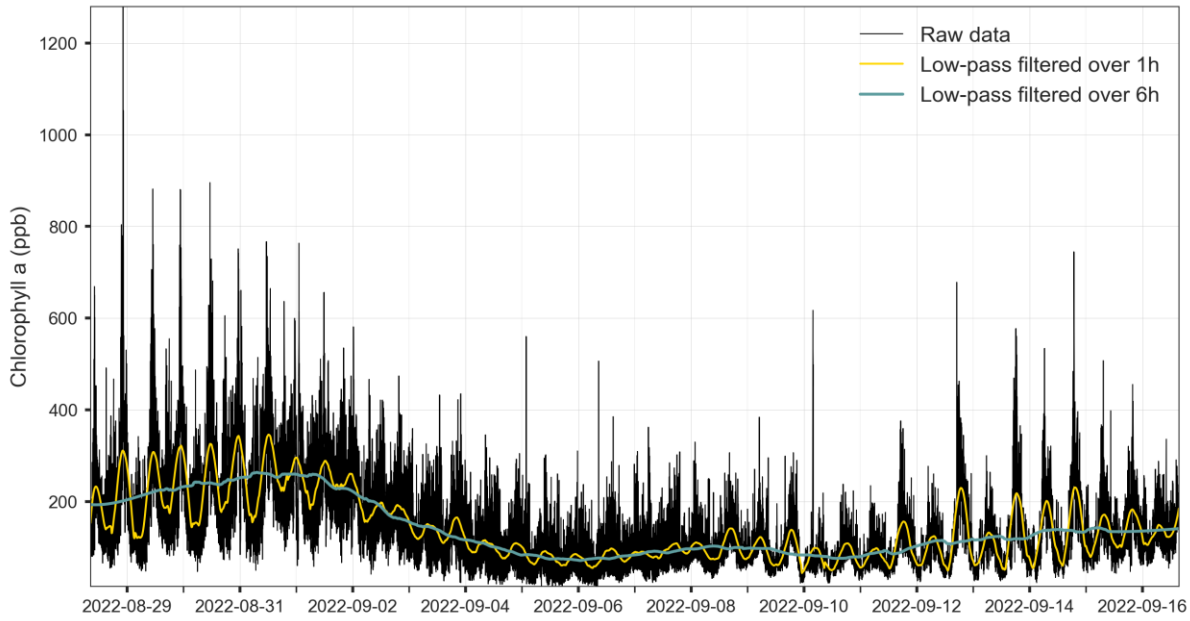

Figure 3.27. Evolution of the concentration in Chlorophyll a (ppb) measured by the WiMo multiparameter sensor placed on the tripod T001 at 1 mab.

3.2.3.4. Content in POC, PON, TEP, chlorophyll and phaeopigments during campaign ST2022/32

POC and PON values are highly correlated to each other (r = 0.86, p = ***), with the highest values measured during ebb or low tide, reaching 0.31 and 0.05 mg/l respectively, which is lower than the values measured in summer (0.61 and 0.08 mg/l). The minimum values measured in December (0.17 and 0.03 mg/l) are also well below the minimum values found during campaign ST2022/19 (0.41 and 0.05 mg/l).

Regarding the chlorophyll a and b and phaeopigments A, their values are generally higher at the bottom than at surface, which is an opposite trend compared to what was observed in summer. Chla and Chlb are positively correlated with each other (r = 0.89, p = ***) and they are both positively correlated with PhaeoA (p = ***). Except for SPM (r = -0.54, p = *), no other parameter is significantly correlated with tide. Like in summer, the measured concentrations of phaeopigments B are also always below the detection limit (< 0.05 mg/m³). TEP wasn't measured during campaign ST2022/32.

Table 3.3. Minimum, mean and maximum values of the concentrations in SPM, Hach, Chla, Chlb, PhaeoA, POC and PON measured during campaign ST2022/32.

STATISTICS	SPM (MG/L)	HACH	POC (MG/L)	PON (MG/L)	CHLA (MG/M³)	CHLB (MG/M³)	PHAEOA (MG/M³)
Min	3.96	1.89	0.17	0.03	1.01	0.03	0.02
Mean	**6.18**	**3.58**	**0.23**	**0.04**	**2.03**	**0.04**	**0.03**
Max	11.96	5.62	0.31	0.05	2.85	0.05	0.04
Std dev	1.93	1.10	0.04	0.00	0.47	0.01	0.01

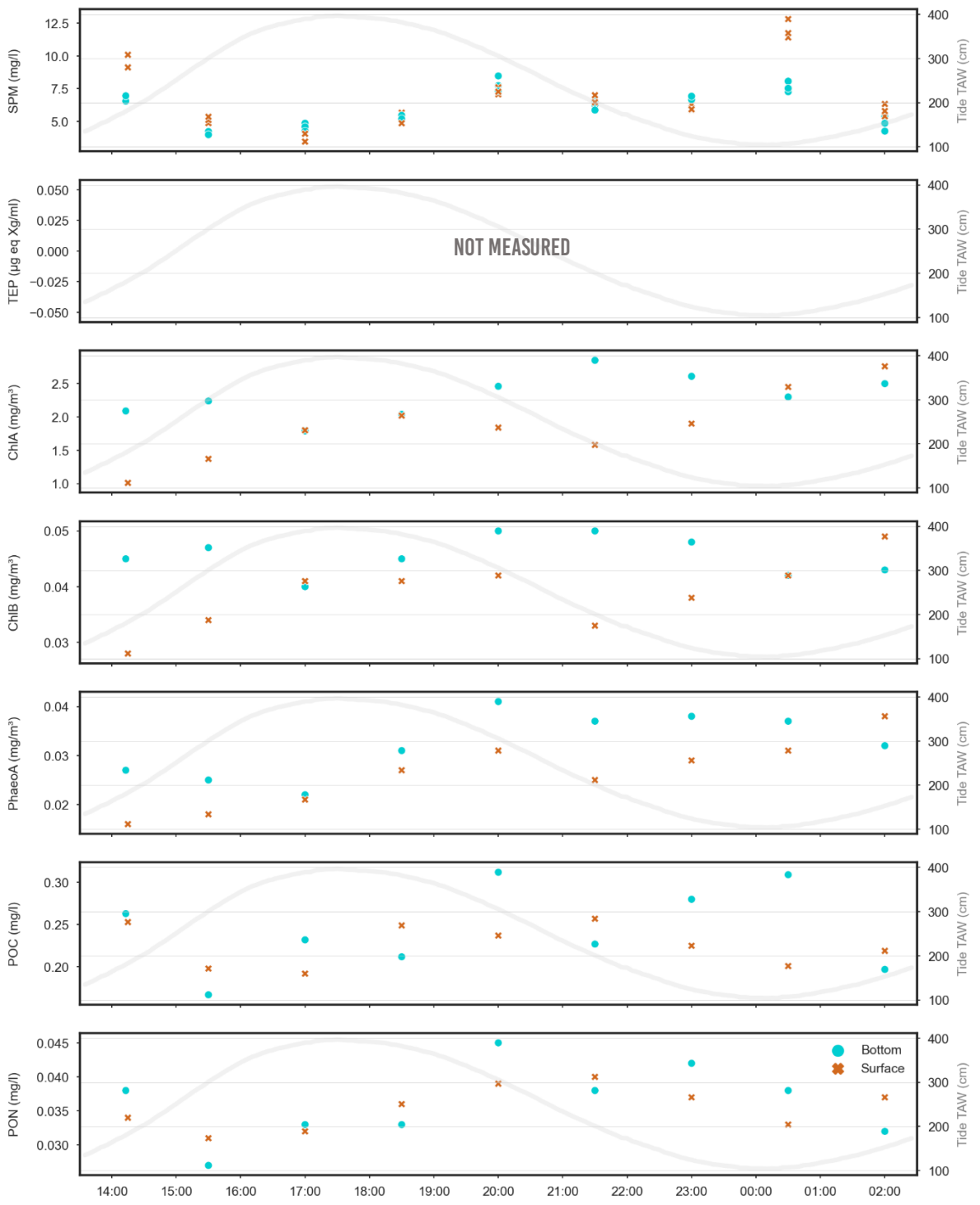

Figure 3.28. Evolution of the concentrations in SPM, Chla, Chlb, PhaeoA, POC and PON with tides and depth during campaign ST2022/32.

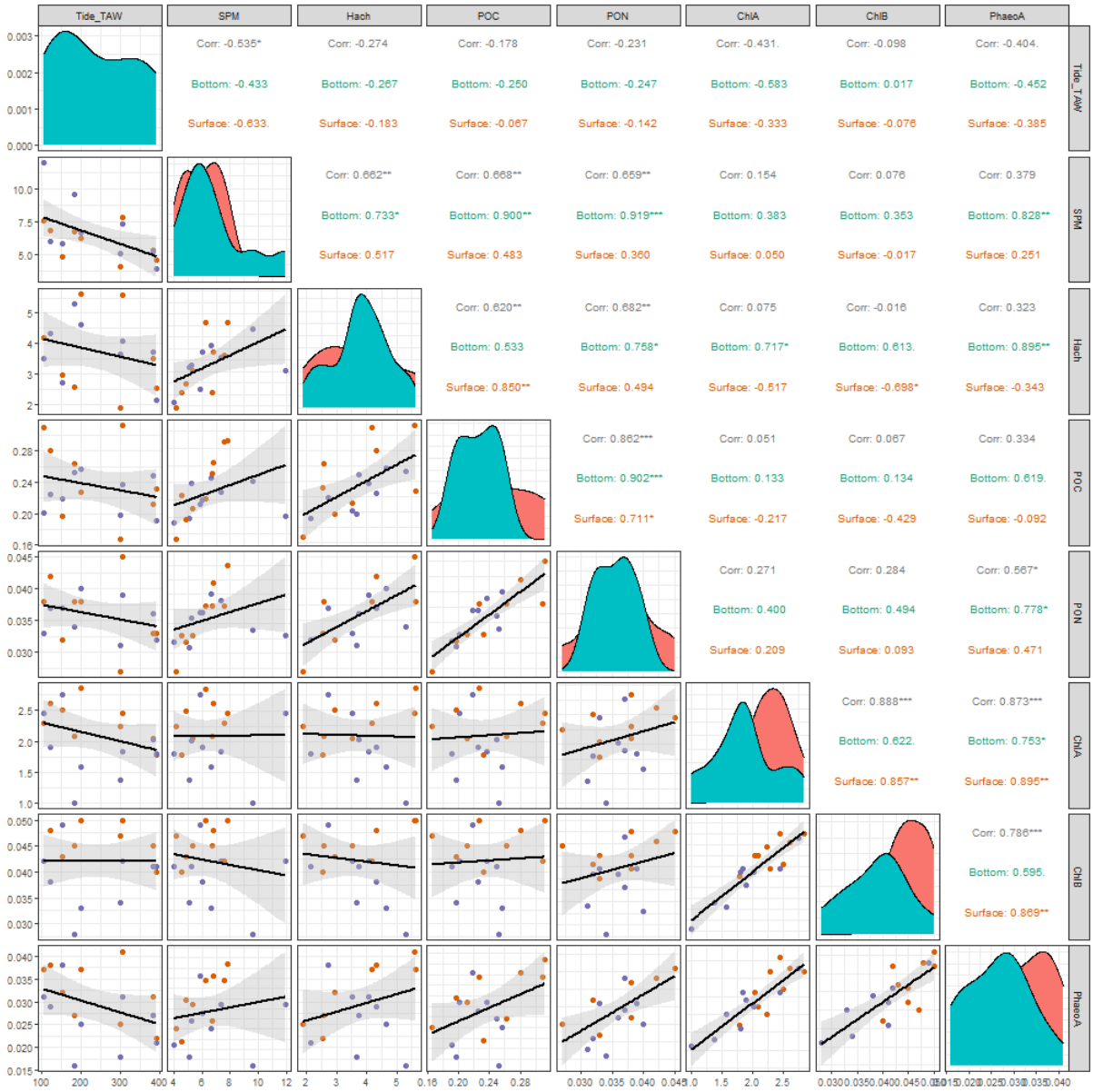

Figure 3.29. Spearman rank correlations between the tides, Hach values and concentrations in SPM, Chla, Chlb, PhaeoA, POC and PON measured during campaign ST2022/32.

3.2.3.5. Comparison with data from the Belgian part of the North Sea in December

Ratios of POC:SPM and PON:SPM acquired during this campaign are also within the trends observed at other locations of the BPNS. The absence of deviation from data collected at W05 or W08 suggests that no major changes in POC, PON or SPM caused by the aquaculture have been detected at this time (Figure 3.30).

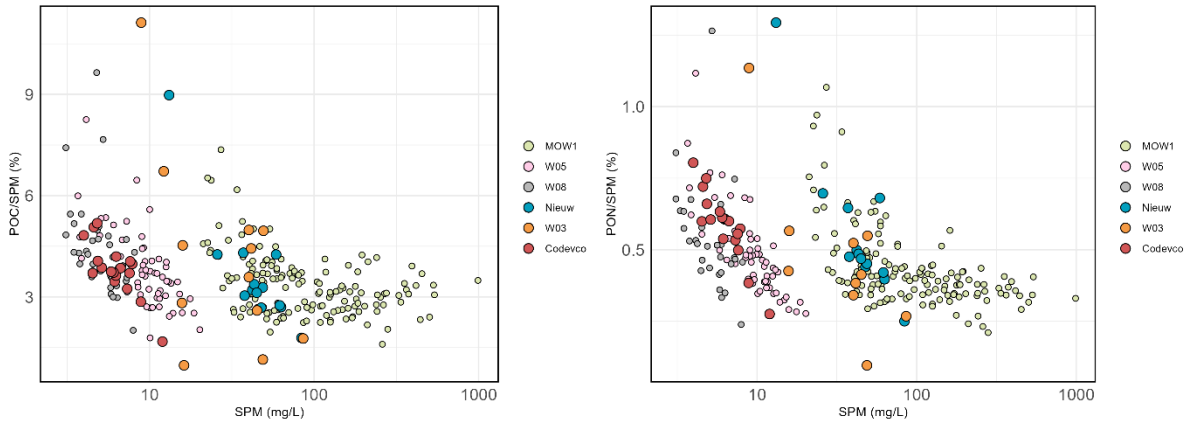

Figure 3.30. Comparison of the data collected on the Western side of the Codevco aquaculture during campaign ST2022/32 with ratios of POC:SPM and PON:SPM collected in December since 2005 at other locations of the North Sea (the graphs are courtesy of Saumya Silori). Nieuw stands for a sampling point near Nieuwpoort.

3.2.3.6. Size and volume of the particles during campaign ST2022/19

The LISST-100x measures particles between 2.5 and 500 microns (clay to medium sand) while the LISST-Holo2 measures particles between 12 and 2500 µm (fine silt to very fine pebbles), which highlights the complementarity of these two instruments. In the case of COD-TC-E in August, the LISST-100x shows a trimodal distribution with peaks at 25 (medium silt), 60 (coarse silt) and 300 µm (medium sand size) while the LISST-Holo2 shows a bimodal distribution with peaks at 90 (very fine sand) and 500 µm (medium to coarse sand size) (Figure 3.31). For particles ranging from coarse silt to very fine to fine sand sizes, the LISST-100x measures a higher relative concentration at low tide (and even higher just before). The relative concentration of medium silt and particles ranging from 200 to 350 µm is higher at slack tide. The LISST-Holo2, on the other hand, shows an opposite trend with smaller particles prevailing at high tide, and particles between 70 and 500 µm prevailing at slack tide. Particles around 700 µm are prevailing at low tide. The highest total volume of particles is found around low and high tides by the LISST-Holo2 while the LISST-100x measures a higher total volume at low and slack tides (Figure 3.32, upper graph). When compared on their overlapping measuring size range (12-500 µm), the two instruments show a generally good correlation (Figure 3.32, middle graph), suggesting that the main differences in trends with the tides would be explained by particles below or above that range. It can indeed be observed that the volume of particles larger than 500 µm is higher around low and high tides while the volume of particles smaller than 12 µm is higher at low tide (when the current comes from the West) and lower at high tide (Figure 3.32, lower graph). The highest amount of particles in the holograms is found just before and after low tide (casts B and D), as well as just after high tide (J) (Figure 3.33). The lowest number of particles is found around slack tide (E, F, G).

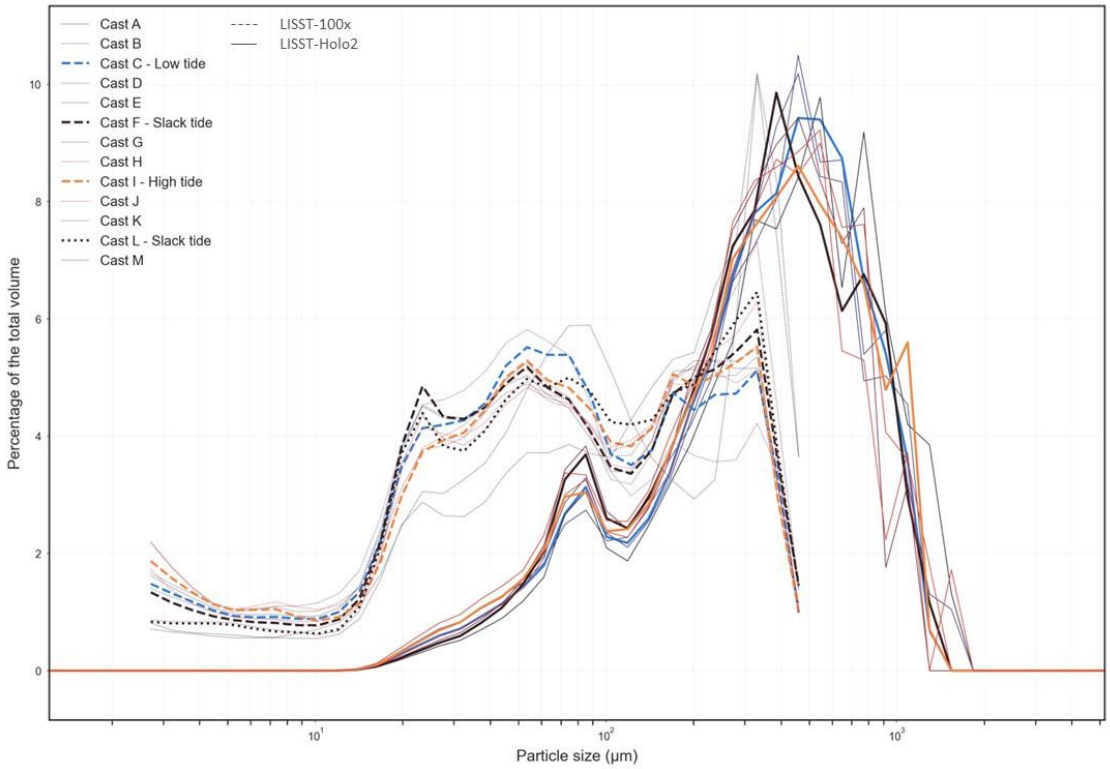

Figure 3.31. Particle size distributions for each cast during campaign ST2022/19 as measured with the LISST-Holo2 (full lines) and with the LISST-100x (dotted lines).

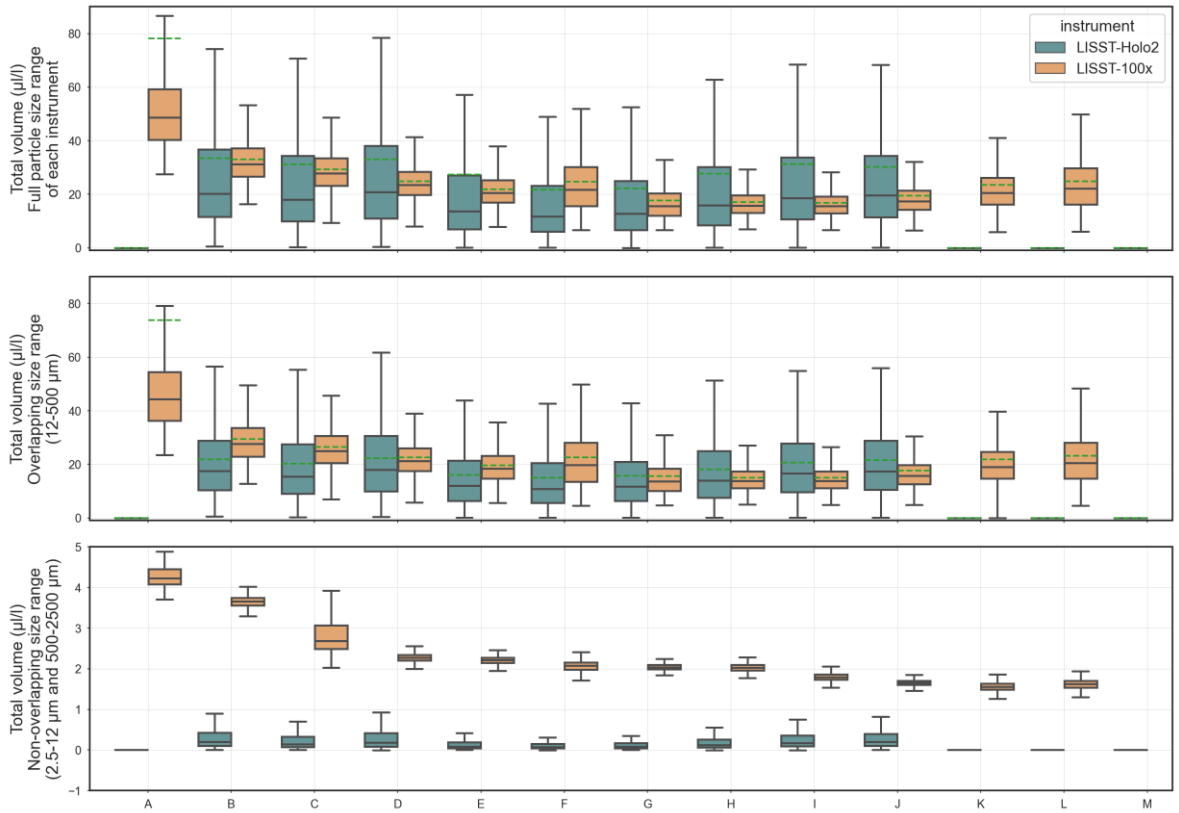

Figure 3.32. Box plots of the total volume of particles measured with the LISST-Holo2 and the LISST-100x for each cast during campaign ST2022/19. The upper graph represents the data containing the full size ranges of each instrument, the middle graph represents only the data in the overlapping size range and the lower graph represents the data outside the overlapping size range (2.5-12 µm for the LISST-100x and 500-2500 µm for the LISST-Holo2).

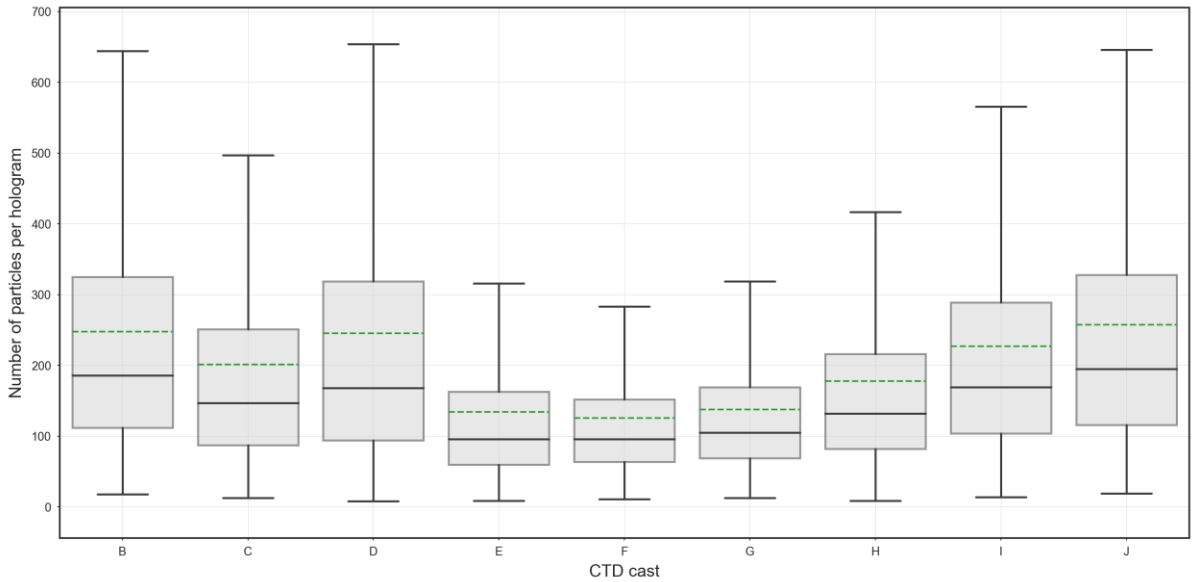

Figure 3.33. Boxplots of the number of particles found per hologram for each cast during campaign ST2022/19.

3.2.3.7. Size and volume of the particles during the deployment of tripod T001

During the deployment of tripod T001, the average diameter of the particles increased steadily from around 75 µm between 21 and 23 August to around 190 µm between the 6th and 8th of September (Figure 3.34). This duration can be divided in three phases that can almost perfectly be related to the different phases of the Moon: neap tide 1 (before New Moon), spring tide (after New Moon) and neap tide 2 (after the First Quarter). The estimated total concentration of particles was low until the 27th of August (< 50 µl/l) and the tidal signal not visible (neap tide 1). In the low-passed data, the mean diameter filtered over six or twelve hours stops showing the tidal signal around the 25th of August, this corresponds to a period when the wind came from the North (Figure 2.20). In general, the mean diameter of the particles is higher at high tide. This is particularly visible between the 27th of August and the 3rd of September (spring tide), when concentrations increased sharply (up to 1750 µl/l) and the tidal signal was very clearly visible with two peaks of high concentrations around high tide. Finally, from the 3rd until the 8th of September, concentrations remained high (between 50 and 100 µl/l) but the tidal signal weakened. The majority of the particles were then composed of medium sand size class, and the medium silt, which was relatively more important at the start of the deployment, became relatively less abundant. While the particle size distributions during the first neap tide and spring tide are bimodal and show a first peak at 17.7 to 20.9 µm and a second at respectively 92.6 to 109 µm and 297 to 354 µm, the particle size distribution during neap tide 2 has a more unimodal trend, with a very small peak at 109 to 129 µm and a strong one at 425 to 500 µm (on average 15% of the total estimated volume) (Figure 3.35).

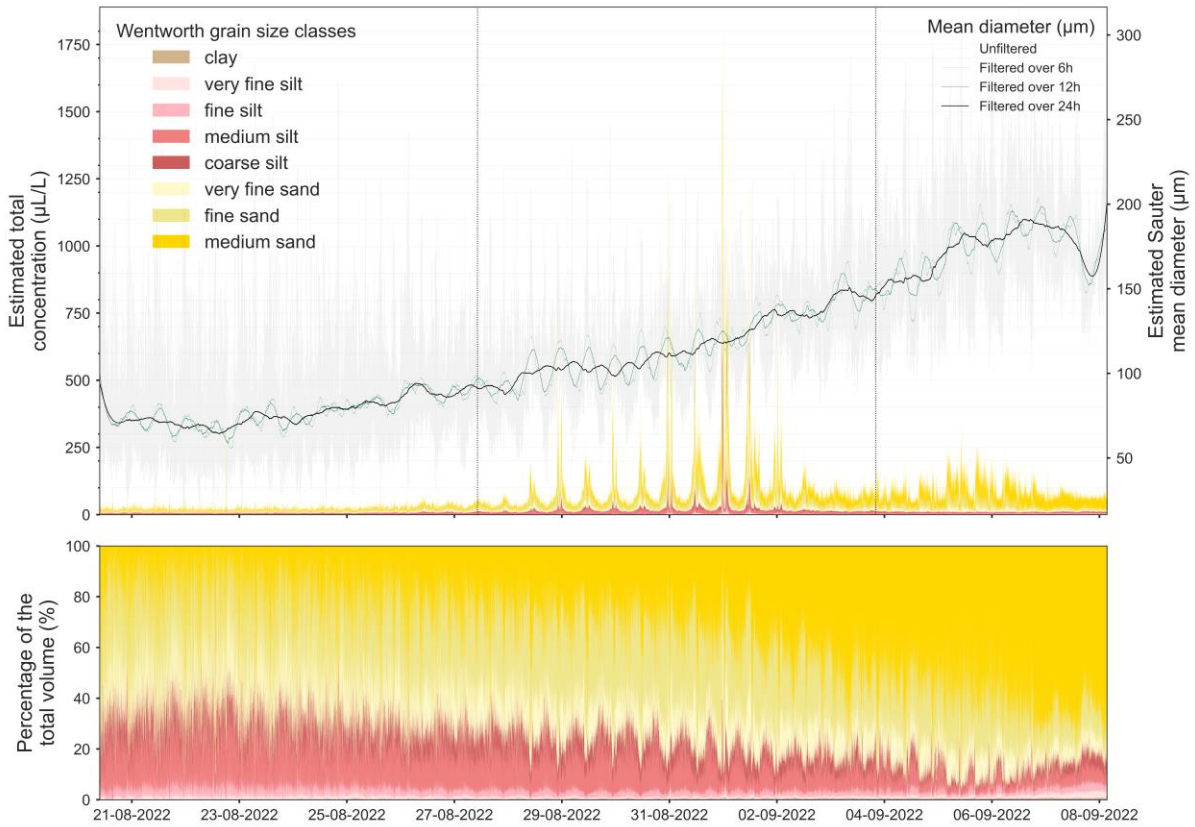

Figure 3.34. Evolution of the particle size distribution and mean diameter unfiltered (light grey), filtered over 6h (dotted red line), 12h (stroke red line) and 24h (black line). Vertical dotted lines indicate the different phases of the Moon: New Moon is on the 27th of August and the first quarter is on the 3rd of September (top graph) and evolution of the relative contribution of each particle size class to the estimated total volume concentration (bottom graph).

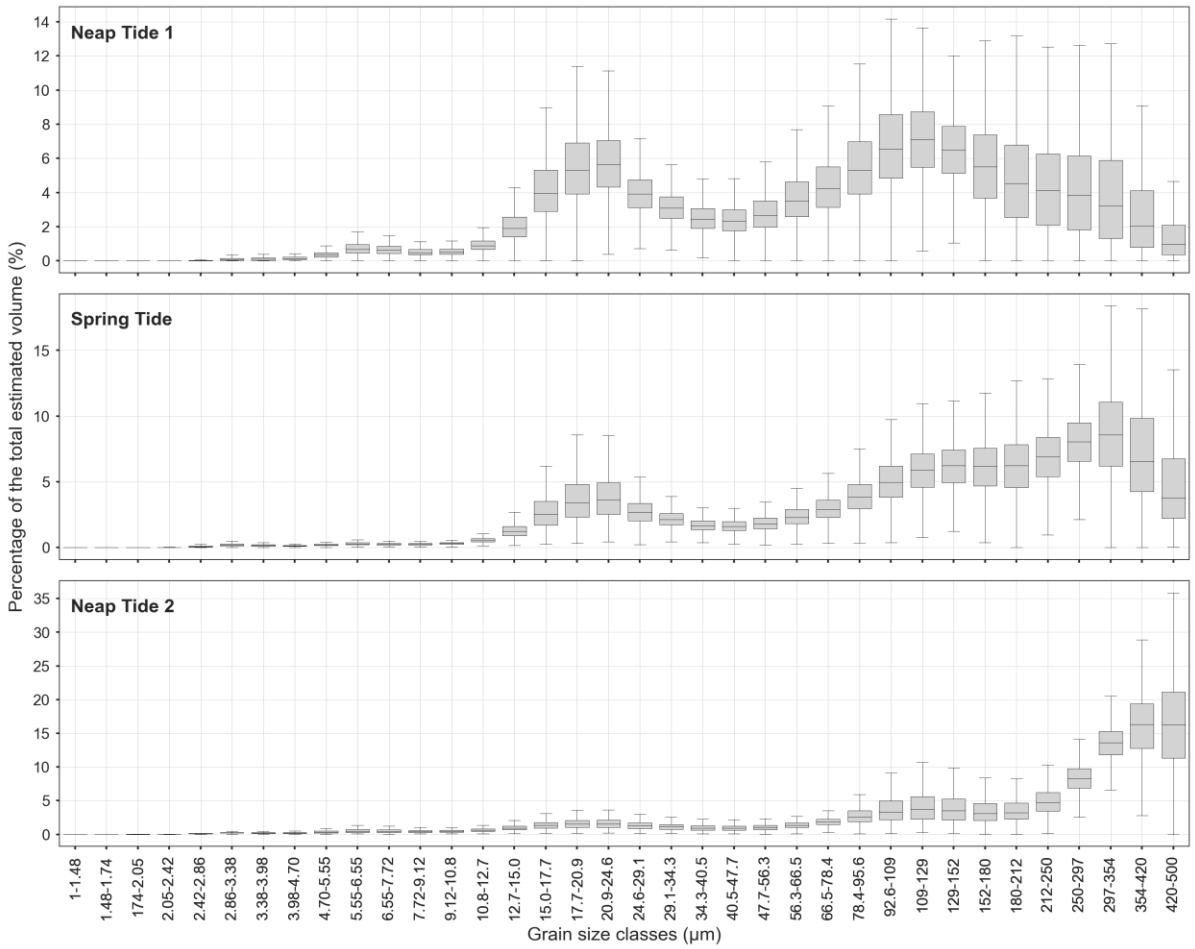

Figure 3.35. Particle size distributions for the three distinct periods recorded by the LISST-200x on tripod T001.

As expected, the two traps placed on the tripod collected different amounts of sediment, with the 10mm trap containing twice as much as the 5mm trap (Figure 2.22). Over a period of 48 days, the former collected about 2119 cm³ of sediments compared to 1060 cm³ for the later. These sediments are mainly composed of clay and very fine silt, the latter being particularly important towards the middle of each of the traps (slices of 4 to 7 cm for the 10 mm trap and 4 to 5 cm for the 5 mm trap) (Figure 3.36). However, it is difficult to estimate exactly what period this corresponds to, partly because it is difficult to rule out the possibility that, although the traps were kept as straight as possible, no movement disturbed the layering of the sediments. In the absence of Geotek measurements, the level of resolution does not allow for such precise analysis.

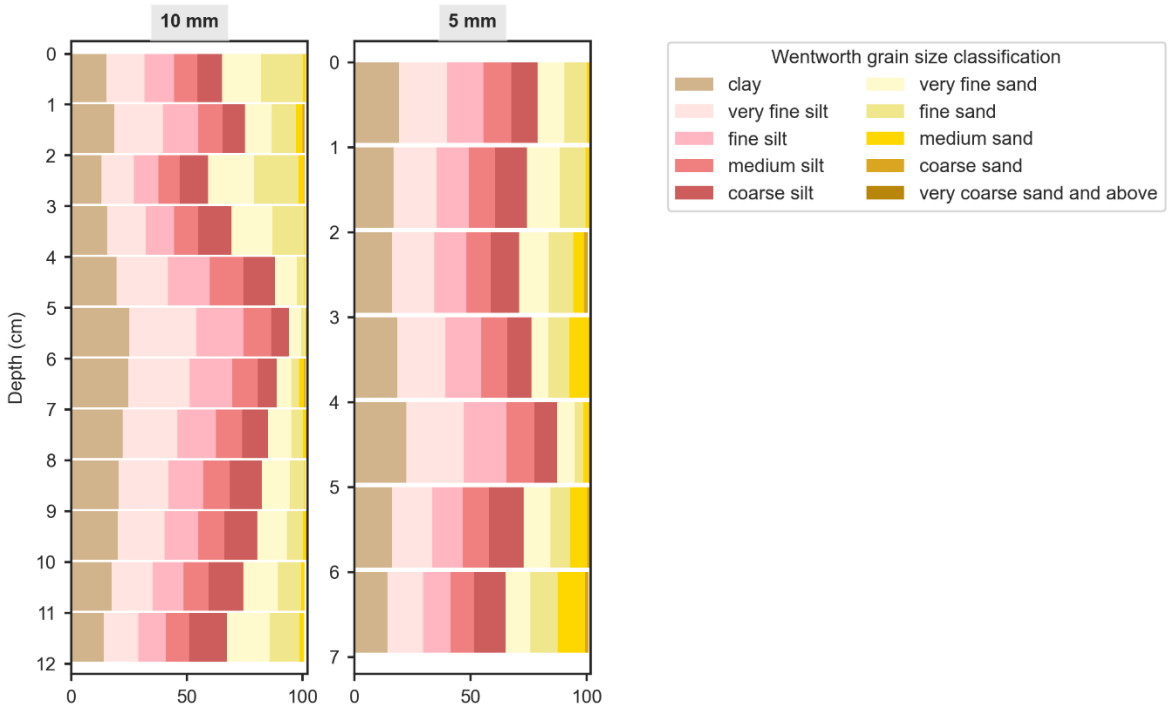

Figure 3.36. Percentage of each grain size class for each centimeter slice of the two sediment traps collected on tripod T001.

Comparatively, the trap with 5 mm holes shows a greater relative importance of larger particles (medium sand) than the one with 10 mm holes. The two distributions show two peaks around 5 µm (very fine silt) and 145 µm (very fine to fine sand) as well as a third, although less strong, around 0.67 µm (clay). The presence of fine to very fine sand is also visible in the distributions obtained by the LISST-200x (see section 2.4.2.2),, but the latter does not detect the peaks found here in the very fine silt or clay particles, which could indicate that these flocculate in the water (Figure 3.37).

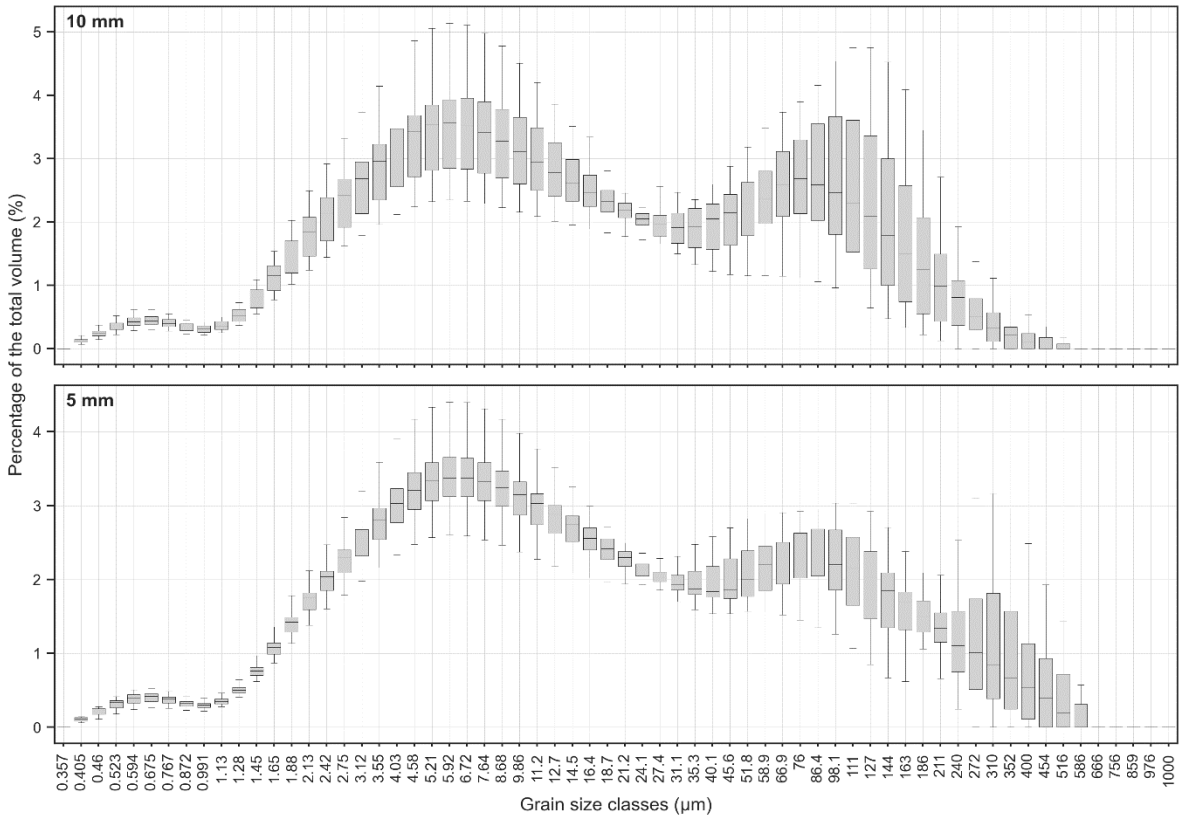

Figure 3.37. Particle size distribution as measured samples from the sediment traps mounted on tripod T001.

3.2.3.8. Size and volume of the particles during campaign ST2022/32

Unlike what was observed in August, the data from both the LISST-100x and LISST-Holo2 show an unimodal distribution with a peak between 300 and 400 µm (medium sand size range) although the first instrument shows a much higher relative importance of this size class (Figure 3.38). It can be observed with both instruments that these large particles are relatively less important at low tide compared to high or slack tides. The LISST-Holo2 (and the LISST-100x in a minor measure) shows an increase in the relative importance of particles between 150 and 200 µm at low tide (when the current comes from the East, so from the aquaculture). While peaks were also found at 25, 60 and 90 µm in summer, they seem to have disappeared in December, shifting the particle size distribution towards larger particles. The lowest total volume is found in cast C (just before high tide) while the highest is found in cast E (just before slack tide) (Figure 3.39, upper graph). Interestingly, cast A shows particularly high values for the total volume measured by the LISST-100x but it also shows a high variability. This observation is confirmed by the high number of particles found in holograms of this cast by the LISST-Holo2 (Figure 3.40). When compared on their overlapping measuring size range (12-500 µm), the two instruments show a generally good correlation (Figure 3.39, middle graph), except for cast A where they show opposite results. When looking at the volumes of the particles larger than 500 µm, they appear to be negligible for most casts (values between 0 and 0.5 µl/l) except for cast A where it goes a little over 1 µl/l but also shows a higher variability (Figure 3.39, lower graph). The total volume of particles smaller than 12 µm tends to be higher just before low tide (cast G) as well as in cast A (with, again, a higher variability) and lower at high tide (cast D). This latter observation was already made in August. The highest amount of particles in holograms are found from slack to low tide (Figure 3.40), as it was already the cast during summer.

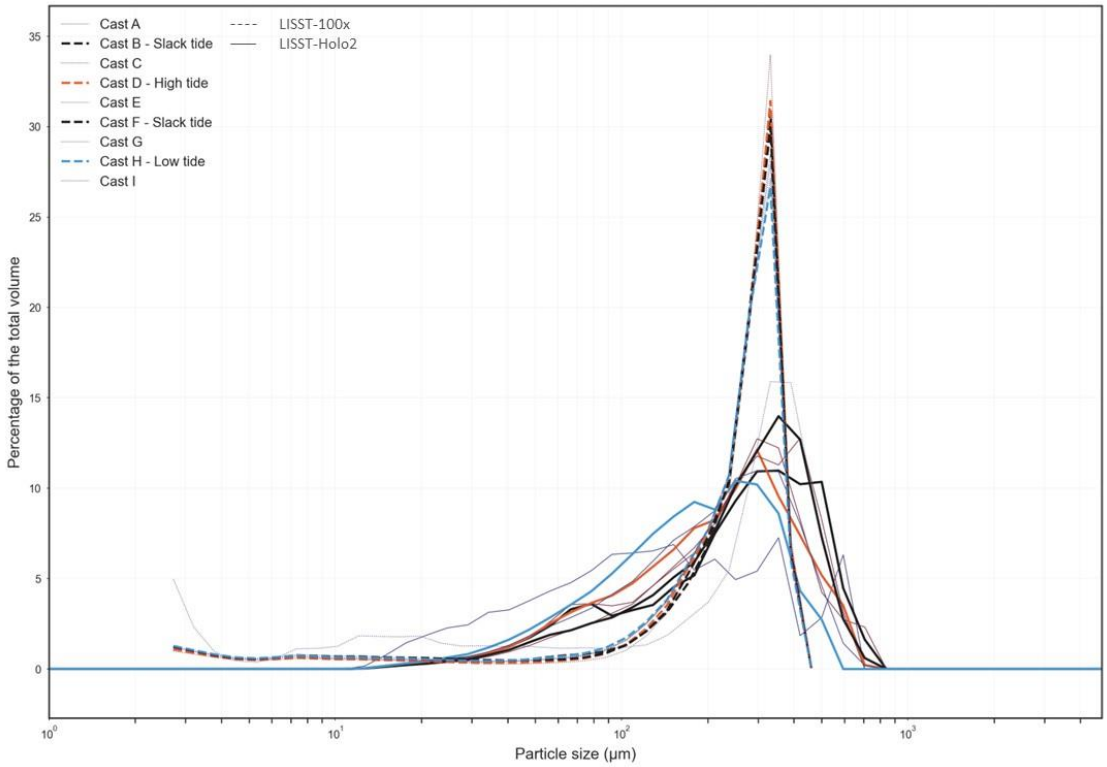

Figure 3.38. Particle size distributions for each cast during campaign ST2022/32 as measured with the LISST-Holo2 (full lines) and with the LISST-100x (dotted lines).

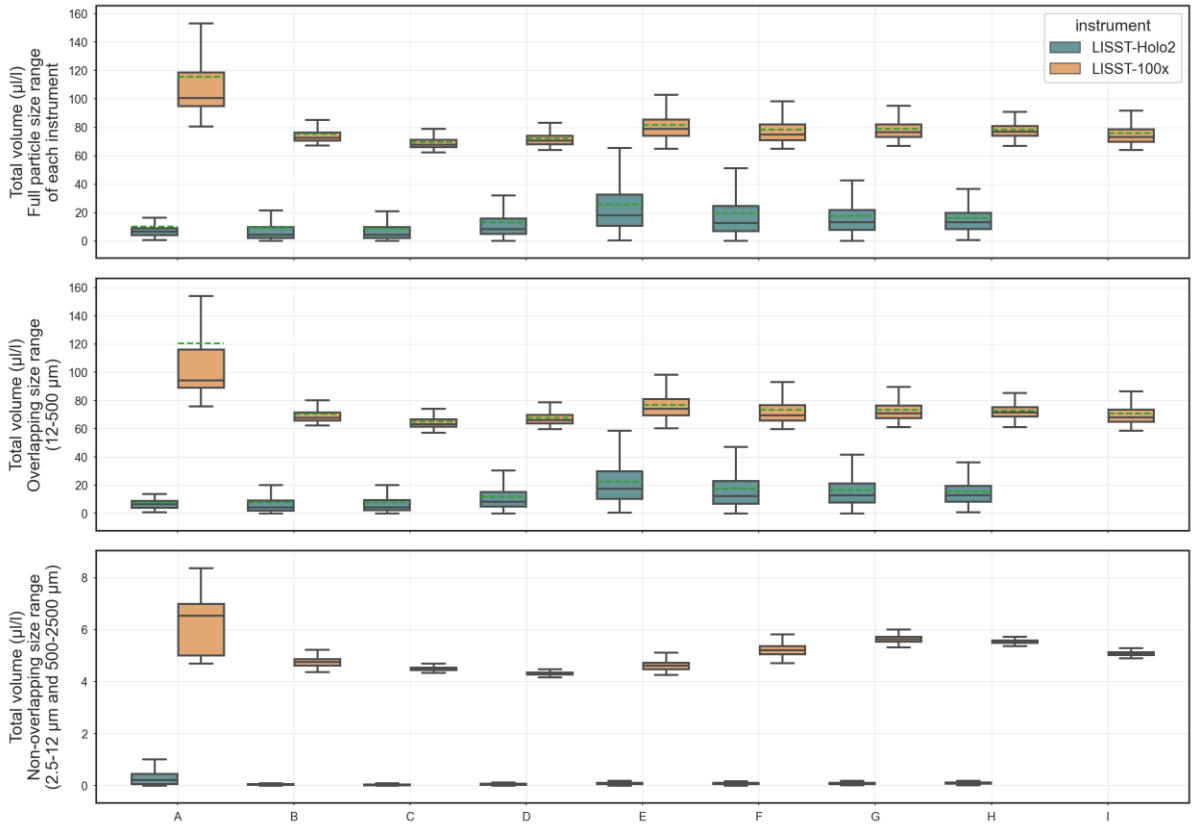

Figure 3.39. Box plots of the total volume of particles measured with the LISST-Holo2 and the LISST-100x for each cast during campaign ST2022/32. The upper graph represents the data containing the full size ranges of each instrument, the middle graph represents only the data in the overlapping size range and the lower graph represents the data outside the overlapping size range (2.5-12 µm for the LISST-100x and 500-2500 µm for the LISST-Holo2).

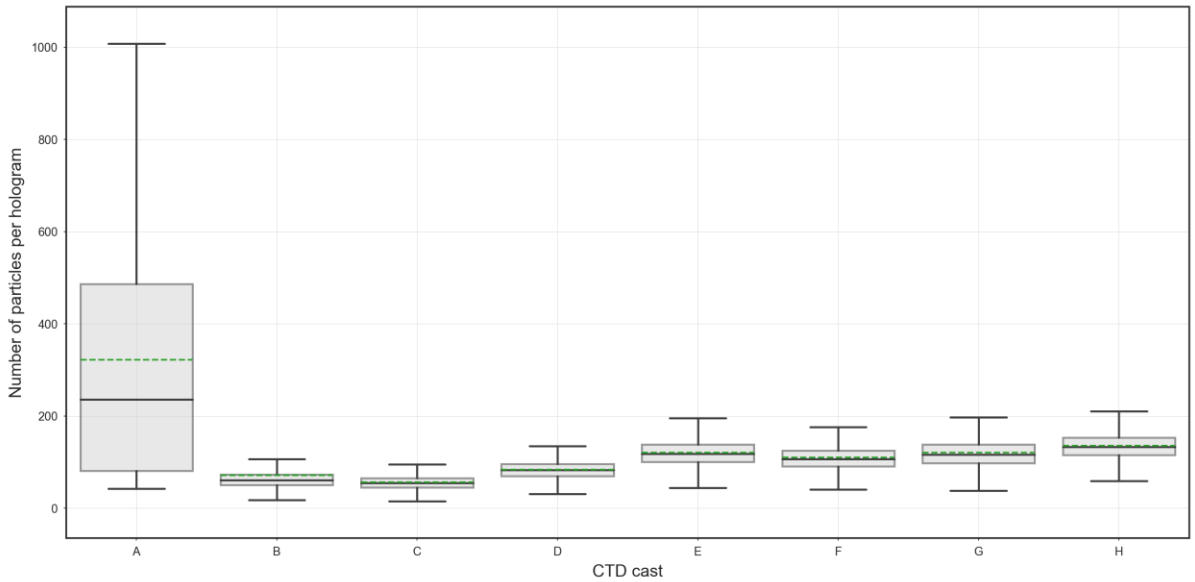

Figure 3.40. Boxplots of the number of particles found per hologram for each cast during campaign ST2022/32.

3.2.3.9. Composition of the particles in suspension during campaign ST2022/19

The analysis of the holograms from two casts (B and C) reveals the presence of numerous species of phytoplankton and zooplankton with a predominance of organisms of type P 1.1, P 1.3 and P1.6 (Figure 3.41, Figure 3.42). Several larvae could also be observed (Figure 3.43). In addition to that, the holograms show an abundance of flocs of all sizes, ranging from a few tens of µm up to more than 1200 µm and sometimes aggregating with phytoplankton (see F 1.1 and F2.5 for instance) (Figure 3.44).

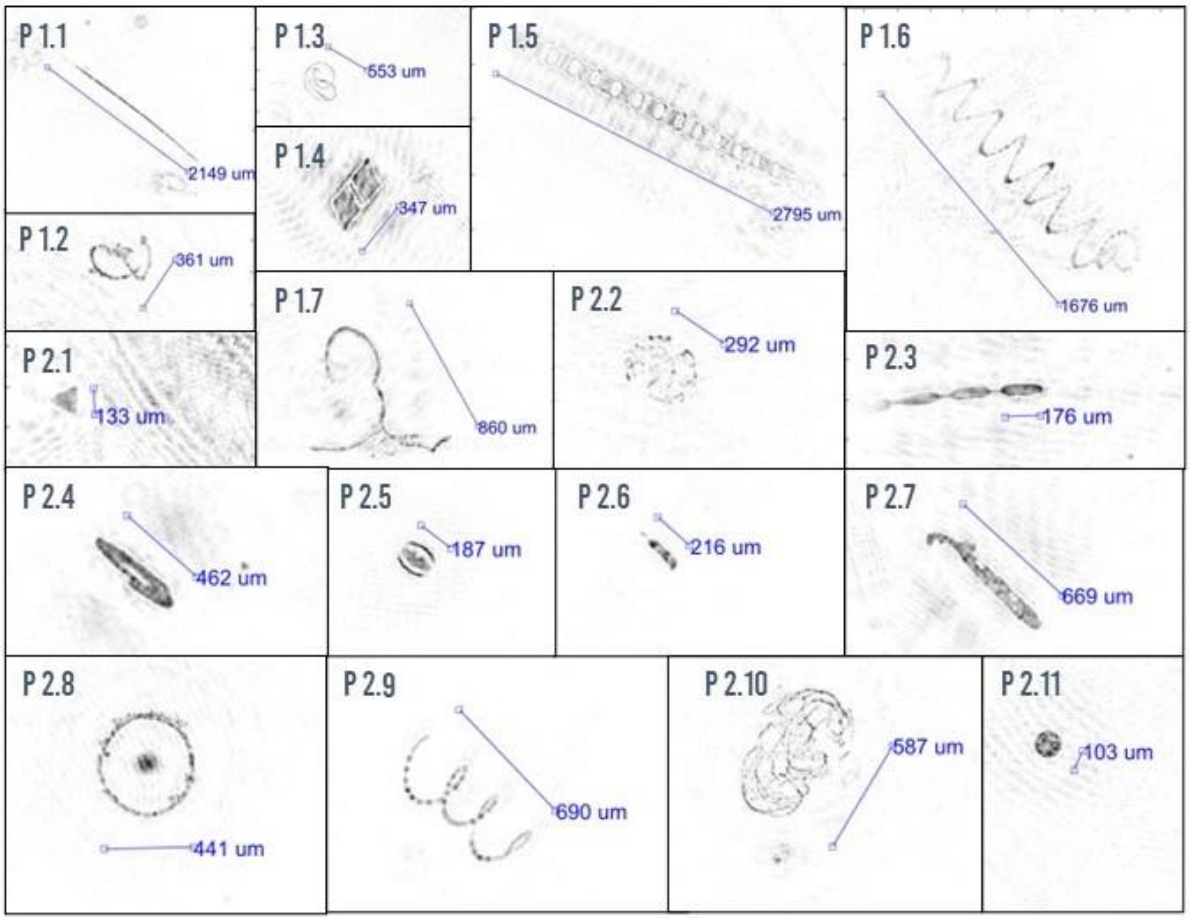

Figure 3.41. Selection of reconstructed holographic images representative of the phytoplankton community observed with the LISST-Holo2 at Codevco-TC-E during the first two casts of campaign ST2022/19. P1.1, P1.4, P1.5, P1.6, P2.3, P2.9: diatoms. diatom chains.

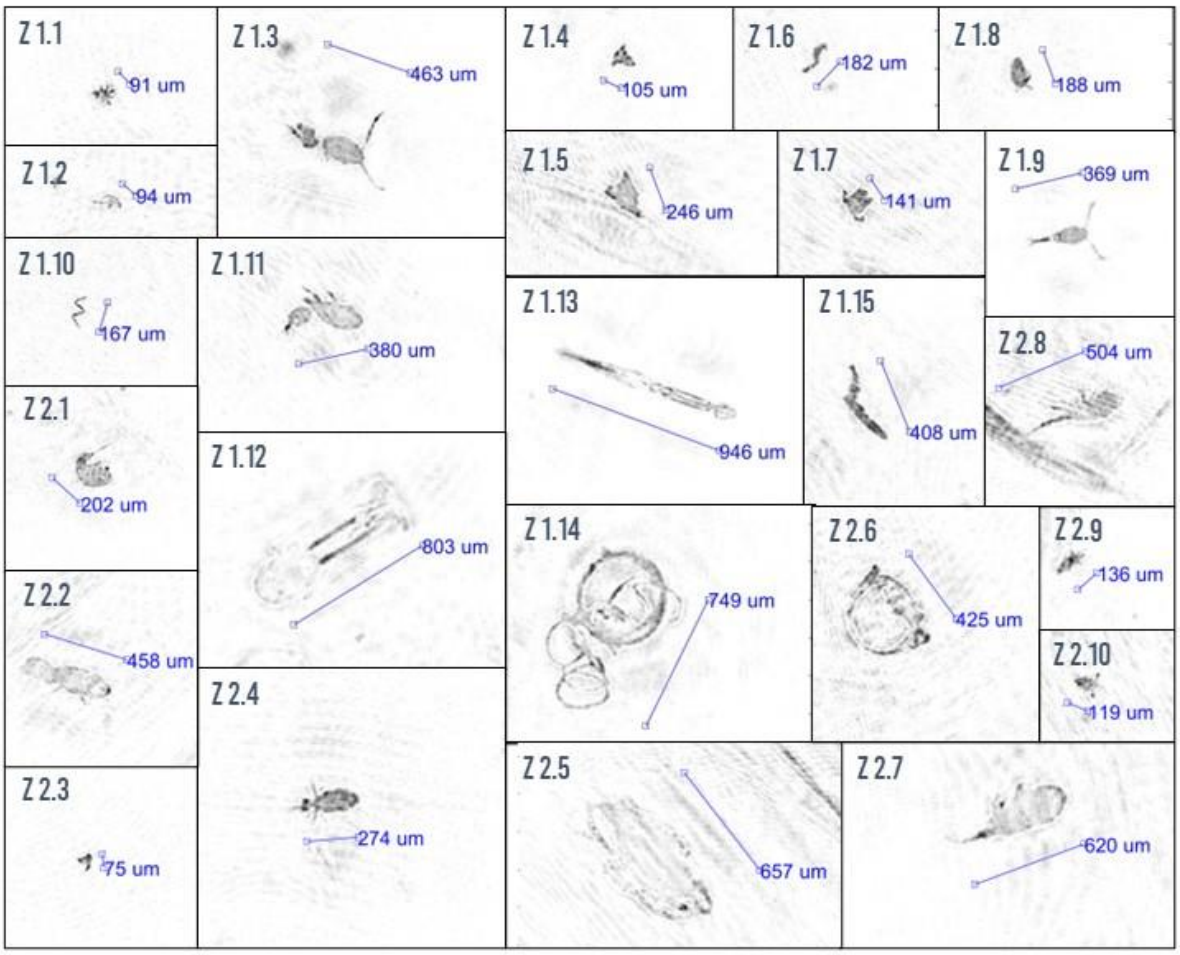

Figure 3.42. Selection of reconstructed holographic images representative of the zooplankton community observed with the LISST-Holo2 at Codevco-TC-E during the first two casts of campaign ST2022/19. Z1.1: nauplius. Z1.3, Z1.9: calanoid copepods. Z1.13: chaetognatha. Z2.8, Z2.7: harpacticoid copepods.

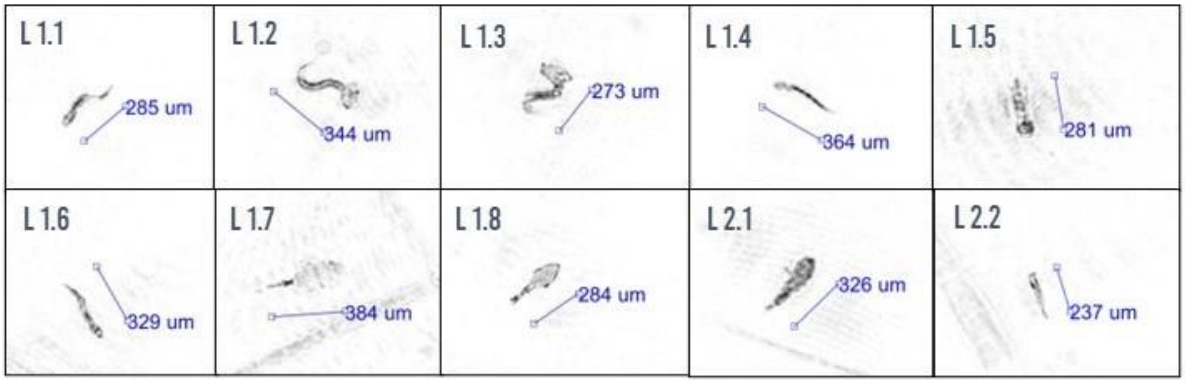

Figure 3.43. Selection of reconstructed holographic images representative of the larvae community observed with the LISST-Holo2 at Codevco-TC-E during the first two casts of campaign ST2022/19.

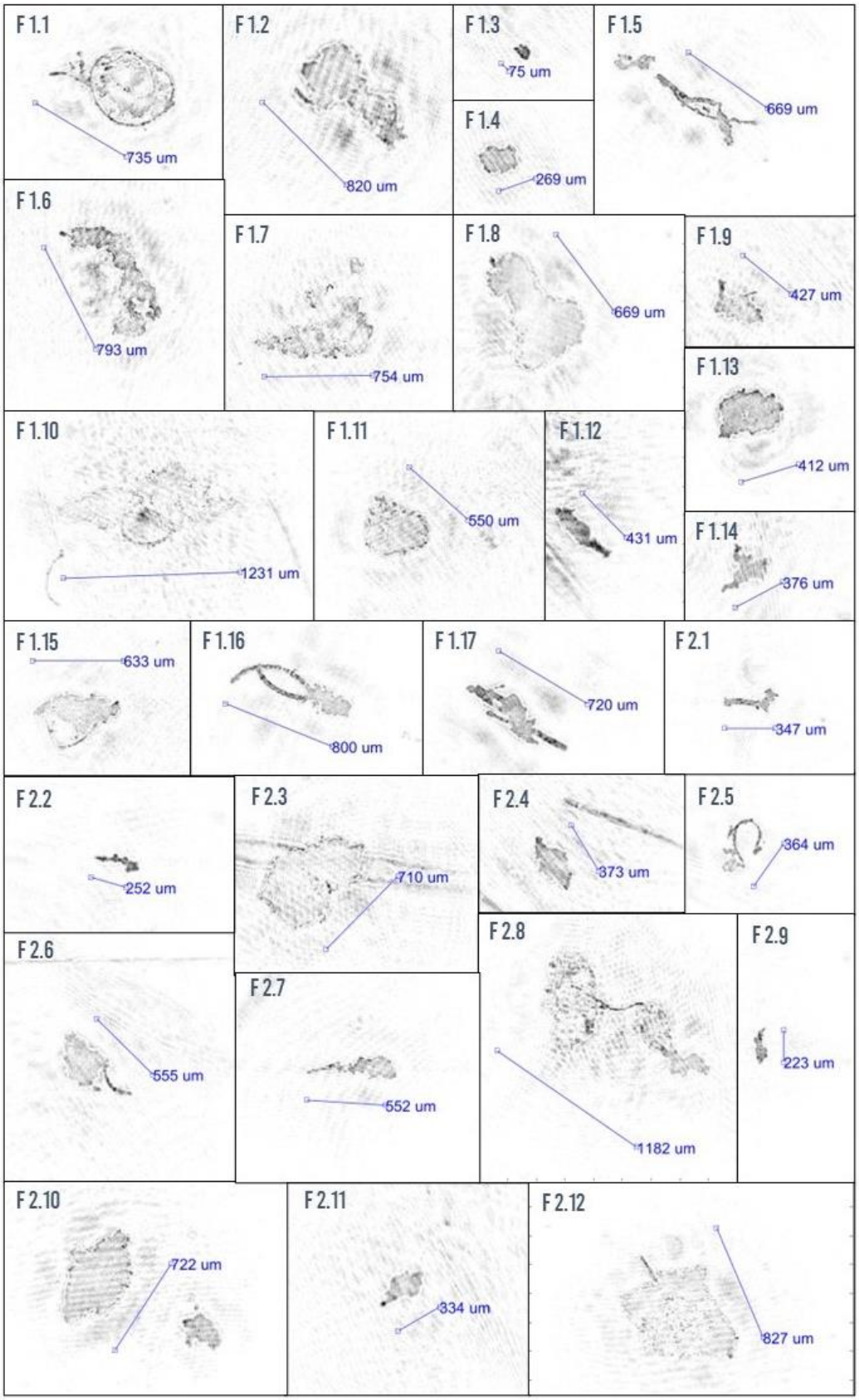

Figure 3.44. Selection of reconstructed holographic images showing flocs observed with the LISST-Holo2 at Codevco-TC-E during the first two casts of campaign ST2022/19.

3.2.3.10. Composition of the particles in suspension during campaign ST2022/32

The analysis of the holograms from two casts (A and B) reveals the presence of numerous species of phytoplankton and zooplankton with a predominance of organisms of type P 34 between many flocs ranging from a few tens of µm up to more than 2300 µm (Figure 3.45). In comparison with August, there seems to be a relatively higher diversity of phytoplankton species compared to the zooplankton community (Figure 3.46).

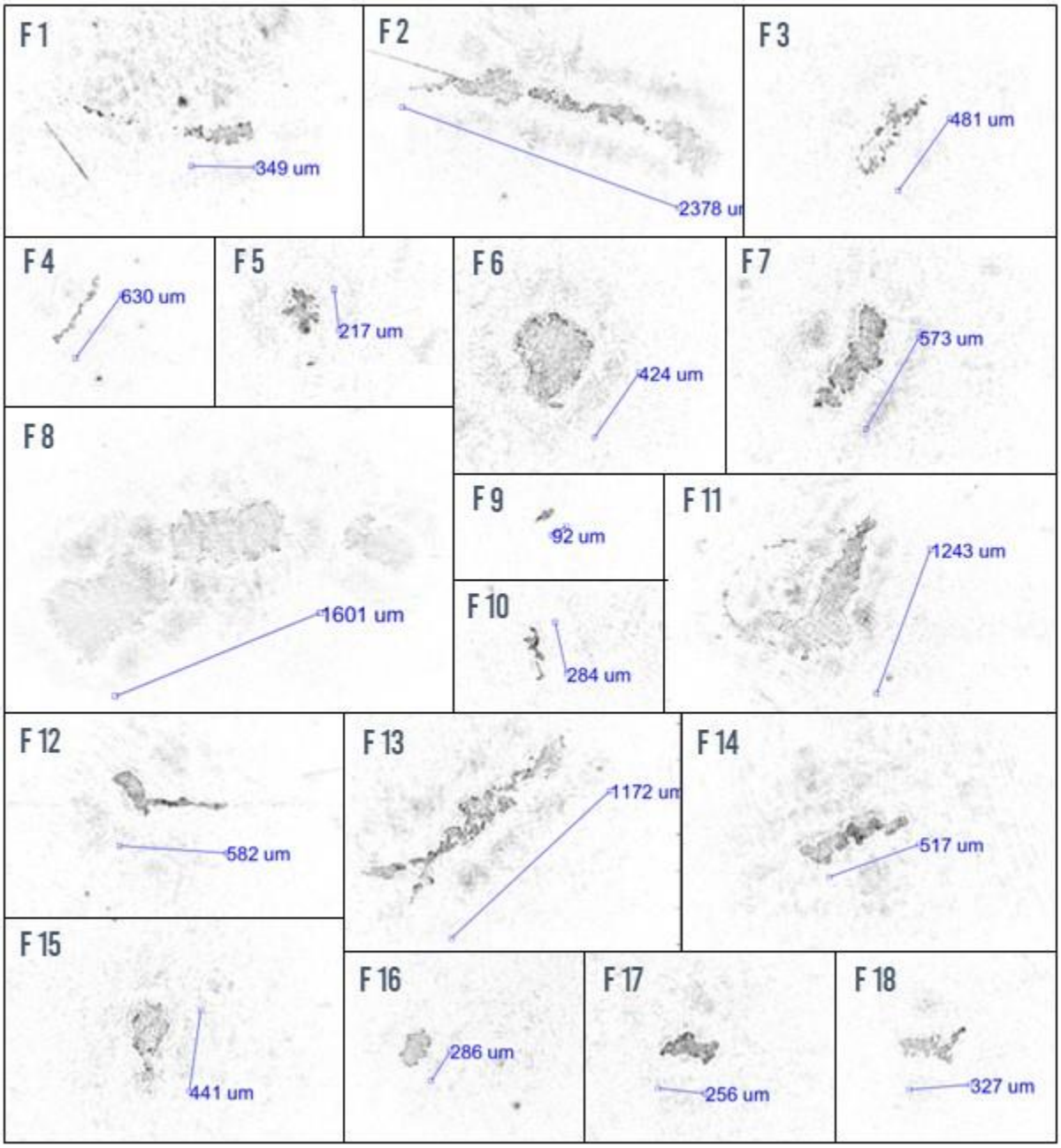

Figure 3.45. Selection of reconstructed holographic images showing flocs observed with the LISST-Holo2 at Codevco-TC-W during the first two casts of campaign ST2022/32.

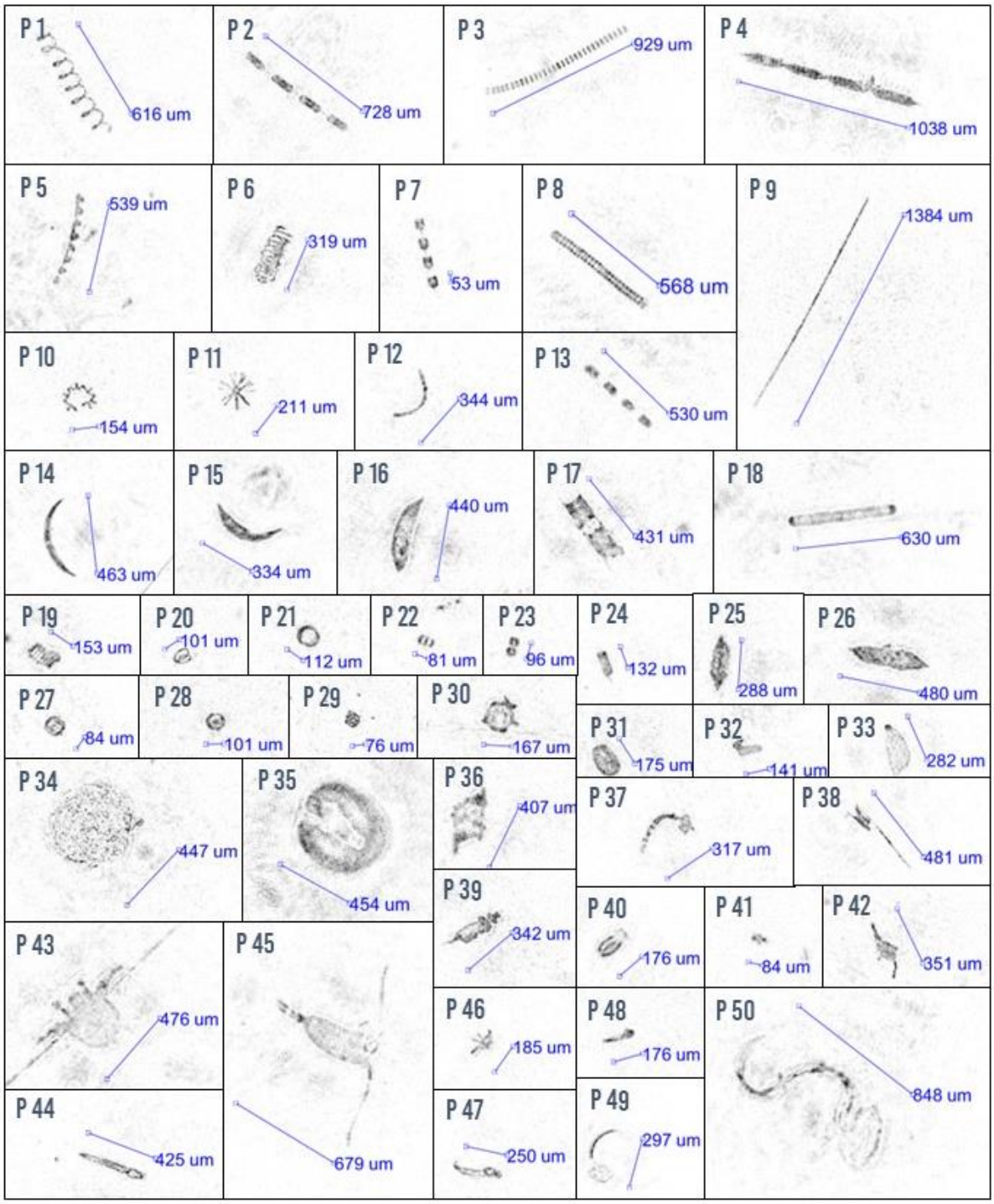

Figure 3.46. Selection of reconstructed holographic images representative of the plankton community observed with the LISST-Holo2 at Codevco-TC-W during the first two casts of campaign ST2022/32. P1-9, P13, P17: diatom chains.

4. CONCLUSIONS & FUTURE PROSPECTS

The development of a mussel, oyster and seaweed aquaculture project is being undertaken by the Colruyt Group a few kilometres offshore of Nieuwpoort, in a small depression known as Westdiep. Once fully constructed, the seafarm will extend over 4.5 km². Like all other activities in the Belgian territorial waters, its development must be accompanied by an environmental study to ensure that it will not have any significant impact on the marine ecosystem. To this end, a monitoring programme has been developed around a number of environmental aspects. This report covers the sedimentological part, and aims to present the activities carried out in this regard in 2022 as well as some preliminary results. Given the scarcity of data dating from before the installation of the first long lines, this report also serves as a description of the environment in which they were installed, as observed by the SUMO team in 2022, in order to facilitate future monitoring.

Following the descriptors of the Marine Strategy Framework Directive, the sedimentological monitoring is developed around two axes: the conservation of (1) the seabed integrity and of (2) the hydrographic conditions. In 2022, this consisted in the deployment of the first tripod from August until October, two cycles of water measurements, one in August and one in December, a multibeam survey and sediment samples taken with a box core at six locations at different distances on the eastern side of the farm. This was accompanied by a first analysis of 64 satellite images taken in 2022, to mitigate the sporadic nature (both spatially and temporally) of our data acquisition.

The first research target, i.e. maintaining the integrity of the seabed, is subdivided into three tasks consisting in ensuring that (1.A) there is no major bathymetric change, (1.B) there is no change in the composition of the seabed and (1.C) the latter preserves its roughness and substrate type.
The bathymetric survey conducted in August 2022 did not indicate any significant morphological changes to the seabed compared to the surveys conducted by the Flemish Hydrography in 2017 and 2018. The few differences observed can be explained by natural dynamics and seem to show that the section surveyed in 2022 is a rather stable environment, as previously described in the literature.
The scarcity of data on the organic matter and CaCO3 contents in the sediments in 2021 did not allow us to assess any possible impact of the aquaculture on the composition of the seabed at this stage.
Finally, between 2021 and 2022, clay, silt and coarse sand contents appear comparable for all stations, with the exception of COD-3275 and COD-4275, which have much lower coarse sand contents in 2022 than in 2021. On the contrary, the content of fine to very fine sand appears to be higher in 2022 and the content of medium sand lower than the values measured in 2021. However, given the variability between replicates as well as between sampling methods, it is not yet possible to determine whether these observed differences are related to the development of the aquaculture or whether they are simply the result of natural spatio-temporal variability.

The second research target, i.e. conserving hydrographic conditions, is also subdivided into three tasks which consist in assessing changes in (2.A) water currents and sediment transport, (2.B) turbidity and suspended particulate matter concentration and (2.C) particle size and composition in the water column.
Given the absence of data dating from before the construction of the farm, it is not yet possible to determine whether changes in hydrodynamics, temperature, salinity and oxygen concentration in the water column have occurred as a result of the construction of the aquaculture farm. Current velocities and direction were generally consistent with the model predictions in the study area, with maximum values of 0.6 to 1 m/s at low and high tides and minimum values at slack tide (0 to 0.2 m/s).

Predominant current directions were towards the NE at high tide and shifting at slack tide to reach a WSW direction during low tide.
Around the aquaculture farm, the concentration of suspended particulate matter in August 2022 ranged from 2.07 mg/l to 5.9 mg/l with generally higher concentrations at low tide. These values were higher during the December sampling, ranging from 3.47 to 12.8 mg/l. For the latter period, the water column seemed to be well-mixed while bottom samples tended to show higher values in August compared to those taken at the surface. The satellite-derived and in situ observed SPM concentrations were rather consistent and seemed to show that a maximum SPM concentration is reached in February and September with a minimum in June. Generally, there was a higher concentrations of both SPM and chlorophyll a towards the coast as well as on the Eastern side of the seafarm. A more thorough analysis of the satellite images over the past ten years would be required in order to detect any change in SPM or chlorophyll a concentration in the study area. The satellite images also showed that, in a few occasions, the Yser river plume extended far enough offshore to reach the aquaculture site but the hydrological and meteorological parameters influencing the occurrence of these events still need to be studied. Regarding the turbidity, values ranged between 0.27 and 1.59 FTU during the water cycle measurements in August but were considerably higher during the tripod deployment with average values of 15.62 FTU at 2 mab and 23.23 FTU at 1 mab.
In terms of composition of the water column, POC and PON values ranges were respectively 0.41 to 0.61 mg/l and 0.05 to 0.08 mg/l in August against 0.17 to 0.31 mg/l and 0.03 to 0.05 mg/l in December. Compared with values recorded at different locations in the Belgian part of the North Sea, the ratios of POC:SPM, PON:SPM and TEP:SPM reported here are well within the trends and show no deviation from the values observed at W05, W08 and Nieuwpoort, suggesting that no major changes in POC, PON, TEP or SPM caused by the aquaculture have been detected at this time. In August, the LISST-100x showed a trimodal particle size distribution with peaks at 25, 60 and 300 µm while the LISST-Holo2 showed a bimodal distribution with peaks at 90 and 500 µm. In December however, the data from both the LISST-100x and LISST-Holo2 showed an unimodal distribution with a peak between 300 and 400 µm. The highest total volume of particles was found around low tide. In general, the mean diameter of the particles was found to be higher at high tide during the tripod deployment but the particle size distribution varied greatly from one neap tide cycle to another. Based on a preliminary analysis of the LISST-Holo2 data, plankton communities seem to be different between August and December, but a more in-depth analysis is still required.

In the next steps, a more extensive analysis of satellite images over the last ten years will be carried out to gain a better understanding of the spatial and temporal variability in the study area. Cross-referencing hydrological and meteorological data with satellite images should allow a better understanding of when and why the plume of the Yser river has an influence on the study site. Seabed and water sampling data will be compiled to gain a better understanding of the variations and evolutions of the seabed and hydrographic conditions at Westdiep. In addition to that, a few data collected in 2022 still need to be analyzed in more details (i.e. the holograms from the last casts of the two water sampling cycles) and a more thorough identification of the species observed is foreseen. The samples and data collected in 2023 will be processed and compared with the results presented in this report.

OUTPUTS

The sediment and benthos monitoring plan was presented as a poster at the Aquaculture Europe conference held in Rimini, Italy, from 27 to 30 September 2022.

Delhaye, L. D. Van den Eynde, U. Braeckman, K. De Cauwer, C. Van Colen and L. Vigin, 2022. From long-established consumer to responsible producer: monitoring benthic and sediment impacts of a shellfish offshore aquaculture project in one of Europe's favorite mussel markets. Abstract + Poster for Aquaculture Europe 2022, Rimini (IT), 27-30/9/2022.

ACKNOWLEDGEMENTS

With special thanks to the ECOCHEM team for the chemical analysis of the water samples, to the MSO team for managing the instruments deployed, to Genavir and the officers from the Belgian Navy on board the RV Belgica for the successful completion of the operations at sea, to the SUMO team for proofreading and supervising, to Quinten Vanhellemont for providing the satellite images as well as Francis Kerkhof and Thomas Kerkhove for their help with the identification of phytoplankton on the holograms.

REFERENCES

Avdelas L., Avdic-Mravlje E., Marques A.C.B., Cano S., Capelle J.J., Carvalho N., Cozzolino M., Dennis J., Ellis T., Fernández Polanco J.M., Guillen J. et al., 2021. "The decline of mussel aquaculture in the European Union: causes, economic impacts and opportunities", Reviews in Aquaculture 13, 91-118.

Bergström P., 2014. "Blue Oceans with Blue Mussels – Management and planning of mussel farming in coastal ecosystems", University of Gothenburg, Department of Biological and Environmental Sciences.

BMM, 2005. Milieueffectenbeoordeling van het project ingediend door de AG Haven Oostende. Annex 2: Verspreiding van mosseluitwerpselen in de Belgische mariene wateren. Beheerseenheid van het Mathematisch Model van de Noordzee, Brussel, 10 p.

Cabre L.M., Hosegood P., Attrill M.J., Bridger D. and Sheehan E.V., 2021. "Offshore longline mussel farms: a review of oceanographic and ecological interactions to inform future research needs, policy and management", Reviews in Aquaculture 13, 1864-1887.

Deines, K.L., 1999. "Backscatter Estimation Using Broadband Acoustic Doppler Current Profilers".

Duarte C.M., Holmer M., Olsen Y., Soto D., Marbà N., Guiu J. et al., 2009. "Will the oceans helps feed humanity?", BioScience 59, 967-976.

FAO, 2014. "The European market for mussels", Food and Agriculture Organization of the United Nations.

FAO, 2016. "The state of the world's fisheries and aquaculture 2016 – Contributing to food security and nutrition for all", Food and Agriculture Organization of the United Nations.

FAO, 2018. "The state of the world's fisheries and aquaculture 2018 – Meeting the Sustainable Development Goals", Food and Agriculture Organization of the United Nations.

Fettweis M., Baeye M. and Francken F., 2015. "MOnitoring en MOdellering van het cohesieve sedimenttransport en evaluatie van de effecten op het mariene ecosysteem ten gevolge van bagger- en stortoperatie (MOMO)". MOMO/7/MF/201501/NL/AR/2.

Franz, B.A., Bailey, S.W., Kuring, N., Werdell, P.J., 2015. Ocean color measurements with the Operational Land Imager on Landsat-8: implementation and evaluation in SeaDAS. J. Appl. Remote Sens. 9, 096070–096070.

International Marine & Dredging Consultants (IMDC), 2020. "Zeeboerderij Westdiep", milieueffectenrapport, 3 April 2020.

Janssens, J., Reyns, J., Verwaest, T. & Mostaert, F., 2011. "Morfologische evolutie van het Belgisch Continentaal plat gedurende de laatste 150 jaar". Deelrapport in het kader van het Quest4D-project. Rapport WL2011R814_02rev2_0. Waterbouwkundig Laboratorium Borgerhout, 98 pp.

Kint L., Hademenos V., De Mol R., Stafleu J., van Heteren S. and Van Lancker V., 2020. "Uncertainty assessment applied to marine subsurface datasets", Quarterly Journal of Engineering Geology and Hydrogeology, vol. 45. https://doi.org/10.1144/qjegh2020-028.

Lanckneus J., Van Lancker V., Moerkerke G., Van Den Eynde D., Fettweis M., De Batist M. & Jacobs P., 2001. "Investigation of the natural sand transport on the Belgian continental shelf (BUDGET)". Federal Office for Scientific, Technical and Cultural Affairs (OSTC).

Lapaty, A., Héquette, A., Pouvreau, N., Weber, N. & Robin-Chanteloup, J.P., 2019. "Mesoscale morphological changes of nearshore sand Banks since the early 19th century, and their influence on coastal dynamics, northern France". Journal of Marine Science and Engineering 7: 73. doi:10.3390/jmse7030073

Lauwaert B., De Witte B., Devriese L., Fettweis M., Martens C., Timmermans S., Van Hoey G. and Vanlede J., 2016. "Synthesis report on the effects of dredged material dumping on the marine environment (licensing period 2012-2016)". RBINS-ILVO-AMT-AMCS-FHR report BL/2016/09, 107pp.

Le Bot, S., Van Lancker V., Deleu M., De Batists M. and Henriet J.P., 2003. "Tertiary and quaternary geology of the Belgian continental shelf", scientific support plan for a sustainable development policy (SPSD II), PPS Science policy.

Mathys M., 2010. "Het onderwaterreliëf van het Belgisch deel van de Noordzee". De Grote Rede 26: 16-26.

Montereale-Gavazzi G., Roche M., Degrendele K., Lurton X., Terseleer X., Baeye M., Francken F. and Van Lancker V., 2019. "Insights into the Short-Term Tidal Variability of Multibeam Backscatter from Field Experiments on Different Seafloor Types", Geosciences 9, 34.

Mullison, J., 2017. “Backscatter Estimation Using Broadband Acoustic Doppler Current Profilers – Updated”, presented at ASCE Hydraulic Measurements & Experimental Methods Conference, Durham, NH. July 9-12, 2017.

Nechad, B., Ruddick K., and Neukermans G., 2009. “Calibration and validation of a generic multisensor algorithm for mapping of turbidity in coastal waters”. SPIE “Remote Sensing of the Ocean, Sea Ice, and Large Water Regions” Conference held in Berlin (Germany), 31 August 2009. Proc. SPIE Vol. 7473, 74730H.

Nechad, B., Ruddick K., and Park Y., 2010. “Calibration and validation of a generic multisensor algorithm for mapping of total suspended matter in turbid waters”. Remote Sens. Environ. 114: 854–866.

O’Donncha F, James S.C. and Ragnoli E., 2017. “Modelling study of the effects of suspended aquaculture installations on tidal stream generation in Cobscook Bay”, Renewable Energy 102, 65-76.

SARF, 2012. “Carbon Footprint of Scottish Suspended Mussels and Intertidal Oysters”. Scottish Aquaculture Research Forum: http://www.sarf.org.uk

Van Cauwenberghe, C., 1971. “Hydrografische analyse van de Vlaamse banken langsheen de Belgisch-Franse kust”. Ingenieurstijdingen 20(4): 141-149.

Vanhellemont Q. & Ruddick K. 2016. ACOLITE For Sentinel-2: Aquatic Applications of MSI imagery. Submitted for the proceedings of the 2016 ESA Living Planet Symposium held in Prague, Czech Republic, 9-13 May 2016, ESA Special Publication SP-740.

Van Lancker V., Deleu S., Bellec V., Le Bot S., Verfaillie E., Schelfaut K., Fettweis M., Van den Eynde D., Francken F., Monbaliu J., Giardino A., Portilla J., Lanckneus J., Moerkerke G. & Degraer S., 2007. “Management, research and budgetting of aggregates in shelf seas related to end-users (Marebasse)”. Final Scientific Report. Belgian Science Policy, SPSDII North Sea.

Van Lancker, V., Kint, L. and Montereale Gavazzi, G. 2023. Seabed substrate map, surficial sediments Belgian part of the North Sea - 1:250.000. Royal Belgian Institute of Natural Sciences, Brussels. https://doi.org/10.24417/bmdc.be:dataset:2762